2023-09-20

The negative BOLD response as a marker of the seizure onset zone

Dykens, Perry Everett

UNIVERSITY OF CALGARY

The negative BOLD response as a marker of the seizure onset zone

by

Perry Dykens

A THESIS

SUBMITTED TO THE FACULTY OF GRADUATE STUDIES

IN PARTIAL FULFILMENT OF THE REQUIREMENT FOR THE

DEGREE OF MASTER OF SCIENCE

GRADUATE PROGRAM IN NEUROSCIENCE

CALGARY, ALBERTA

SEPTEMBER, 2023

Abstract

Epilepsy is a neurological disease affecting 70 million people worldwide. For most individuals, these seizures can be controlled using medications, however nearly 1 in 3 people may need surgery to achieve seizure freedom. For this surgery to be successful, the brain region generating the seizures, which contains the critical seizure onset zone (SOZ), must be accurately identified and removed. Unfortunately, the surgical success rate is low likely due to imprecise determination of the SOZ. As a novel approach to SOZ identification, the collection of intracranial electroencephalography and functional magnetic resonance imaging (iEEG-fMRI) has been proposed as a novel method of identifying the SOZ. However, iEEG-fMRI faces the methodological challenge of artifact introduced from MR scanning which completely obscures the physiological EEG signal. Therefore, the first step towards bringing iEEG-fMRI into the clinical realm is to improve methods for extracting the physiological EEG signal from the iEEG-fMRI data. To this end, the first study in this thesis validated a set of methods aimed at removing fMRI artifact from iEEG, culminating in the creation of the first automatic iEEG pre-processing pipeline. The next step towards clinical utility for iEEG-fMRI is improving our interpretation of iEEG-fMRI results. Traditionally, only positive IED-related fMRI activation maps were considered in relation to SOZ localization, and the negative response was ignored. It has been suggested that both positive and negative activation maps should be considered, and the maximal cluster of these two maps, regardless of polarity, should be used to localize the SOZ. In the second study, the concept was tested using iEEG-fMRI and it was found that the use of the maximal negative cluster had limited utility for SOZ localization. The results of this thesis provide a new method for preparing EEG data from iEEG-fMRI experiments and it shows that the bulk of maximal negative fMRI clusters have limited reliability for clinical applications.

Preface

This thesis is the original, unpublished, independent work of the author, P E Dykens. The research reported in Chapters 2 and 3 were covered by ethics certificate REB13-0571 issued by the University of Calgary Conjoint Health Ethics Board for the project “Superior Seizure Focus Localization: Implications for Surgical Outcome” on August 13, 2013.

Acknowledgements

I have to start by continuing a tradition I started many years ago and mention my sincerest gratitude to Drs. Rowe and Gordon. It is likely no exaggeration that without them I would not be where I am today — alive, seizure-free (or epilepsy resolved), and still not allergic to milk.

Jess, my partner in life, soul, and on paper, thank you for keeping me grounded and stable through this journey. I'm so grateful that I found you and that your family has come to accept me as their own.

To my parents Phyllis and Darryl, your unwavering and unconditional love and support no matter the distance has been a comfort that has help me carry on.

To my supervisor, Dr. Federico, thank you for your patience and understanding in what has been one of the more interesting times in my life. I've appreciated your guidance and support through this process.

To my office mate, Dr. Mosher, thank you for always being there to provide levity, clarity, and support no matter the issue. If not for your guidance and willingness to work through ideas and complexities, large portions of this document would make far less sense. One that same note, thank you for editing well over 100 drafts of various parts of this thesis and other documents, presentations, posters, and abstracts that I have produced.

To Dan Pittman, thank you for putting up with me starting sentences mid-thought, teaching me volumes worth on signal processing, helping me clarify and distil my thoughts and ideals, and being a sounding board when I needed to talk an issue through. I believe you have also edited a very large number of documents for me which is greatly appreciated.

To Will Wilson, we had so much fun together, beta testing FiPP until the wee hours of the morning and rushing to generate various figures multiple times. Thank you for being there to listen to me complain and for splitting the shared data prep.

To Drs. Goodyear and Klein, thank you for taking the time to work through my documents and provide insight and clarity to my projects.

Dr. Goodyear, thank you for going well out of your way to find, and ensure I understood, statistical solutions that better suited my data and for your guidance when our lab developed the fMRI pipeline that was used in chapter 3 of this thesis.

To Dr. George, you came in towards the end of my time, but despite not being fully versed in the topic you were always willing to offer suggestions, support, and if all else failed a much-needed chat.

Dedication

This work is dedicated to all those living with epilepsy. May we seize the day and have hope for a seizure-free tomorrow.

Table of Contents

List of Tables

List of Figures

List of Equations

List of Symbols and Abbreviations

Abbreviations	Full Description
σ	Standard Deviation
x	Single Sample Value
$\bar{x}$	Sample Mean
n	Sample Size
3T	Three Tesla
AAS	Average Artifact Subtraction
AC	Alternating Current
BOLD	Blood Oxygen Level Dependent
CPU	Central Processing Unit
CSF	Cerebrospinal Fluid
DC	Direct Current
DMN	Default Mode Network
EEG	Electroencephalography
EPSP	Excitatory Post-Synaptic Potentials
FiPP	Federico Lab iEEG Processing Pipeline
FEAT	FSL Expert Analysis Tool
FIR	Finite Impulse Response (Filter)
FLAME	FMRIB Local Analysis of Mixed Effects
FLIM	FMRIB Improved Linear Model
FSL	FMRIB Software Library
FMRIB	Functional Magnetic Resonance Imaging of the Brain
EZ	Epileptogenic Zone
GABA	Gamma-Aminobutyric Acid
GE	General Electric
GSA	Gradient Switching Artifact
^{1}H	Hydrogen Atom
HRF	Hemodynamic Response Function
Hz	Hertz
IBM	International Business Machines
ICA	Independent Component Analysis
IED	Interictal Epileptiform Discharge
ILAE	International League Against Epilepsy
kHz	Kilohertz
LeGARE	LeVan Gradient Artifact Remover
mm	Millimeter
MRI	Magnetic Resonance Imaging
ms	Millisecond
NO	Nitric Oxide
PCA	Principal Components Analysis
PET	Positron Emission Tomography
RAM	Random Access Memory

RF	Radiofrequency
s	Second
SOZ	Seizure Onset Zone
SPECT	Single-Photon Emission Computerized Tomography
SPSS	Statistical Package for the Social Sciences
T1	Longitudinal Relaxation
T2	Transverse Relaxation
T2*	Transverse Relaxation with Inhomogeneities
TE	Echo Time
TR	Repetition Time

1.0 Introduction

1.1 Epilepsy

Nearly 1 in 100 Canadians are living with epilepsy, a neurological disease characterized by spontaneous, recurrent seizures or ictal episodes[1]. The concepts of epilepsy and seizures can be traced back as far as the Paleolithic period[2], but it was not until more recent history that the understanding of epilepsy as a complex disorder involving both medical and social implications began to emerge. As the understanding of epilepsy evolved, so too did the understanding of uncontrolled seizures. Notwithstanding the social and biological impact of seizures, 1 in 1000 individuals with uncontrolled seizures die due to sudden unexpected death in epilepsy (SUDEP) which ranks second among neurological diseases for potential years of life lost[3]. Adequate control of seizures is thus of paramount importance when treating epilepsy with the ultimate treatment goal being seizure freedom.

1.1.1 Defining seizures

With the advent of human electroencephalography (EEG) by Berger in the 1920s, it became possible to verify and confirm the electrical basis of seizures[4]. In 2017, the International League Against Epilepsy (ILAE) characterized seizures as a sudden onset of increased, uncontrolled neuronal discharges[5]. In order to be considered an epileptic seizure, the seizure must be 'unprovoked' meaning it cannot be the result of another disorder or infirmity such as concussion[6]. Seizures are grouped into two broad categories: focal seizures (originating in one brain region) or generalized seizures (originating from widespread brain regions)[5]. Both of these categories are broken down into more specific seizure types based on clinical manifestations, electrographic features, and in the case of focal seizures, level of consciousness (Figure 1.1). Some seizures, however, have an unknown onset and cannot be classified.

The use of EEG has also led to the discovery of brief seizure-like discharges that occur during the interictal period, or the time between ictal events. These brief bursts of abnormal brain activity, called interictal epileptiform discharges (IEDs), often occur without any associated clinical symptoms or signs and tend to originate from the same regions of the brain where seizures

originate. IEDs can therefore sometimes be used to identify the brain regions where seizures originate[7]. Thus, both IEDs and seizures can be useful electrographic markers in the treatment of epilepsy.

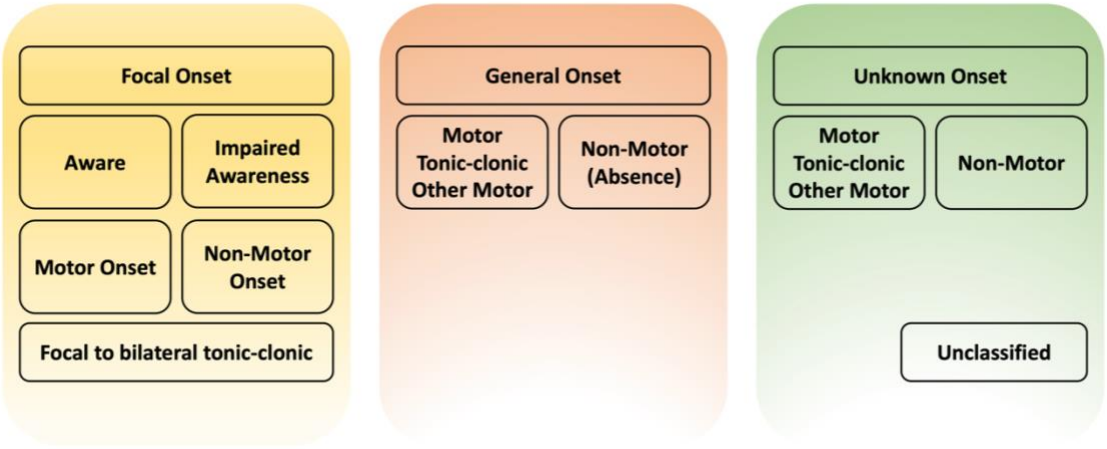

Figure 1.1: ILAE 2017 Summarized Classification of Seizures[5].

1.1.2 Defining epilepsy

In order to be diagnosed with epilepsy, an individual must meet one of the following three criteria: i) two unproved seizures separated by at least 24 hours, ii) one unprovoked seizure and a probability of further seizures similar to the general recurrence risk (at least 60%) after two unprovoked seizures, occurring over the next 10 years or iii) the diagnosis of an epilepsy syndrome[6] such as SeLECTS[8]. The key feature of each of these criteria is that the seizures cannot be attributed to a different medical cause. In the 2014 ILAE definition of epilepsy, the concept of 'resolved' epilepsy was introduced. Individuals who have not had a seizure in 10 years and have been off anti-seizure medications for 5 years and individuals who had an age-dependent epilepsy syndrome are said to have resolved epilepsy as they are unlikely to experience seizure recurrence[6]. This addition was added to help alleviate the burden of living with an epilepsy diagnosis due to the stigma that still surrounds epilepsy.

Once a diagnosis of epilepsy occurs, it is classified by etiology (e.g. genetic mutations, cortical malformations, infections, etc.), seizure type, comorbidities, and disease manifestation (Figure 1.2)[9]. Despite the heterogeneity of epilepsy, it is well controlled for approximately 68% of individuals living with epilepsy[10] using medications[11], lifestyle changes, or a combination of the two[12–14].

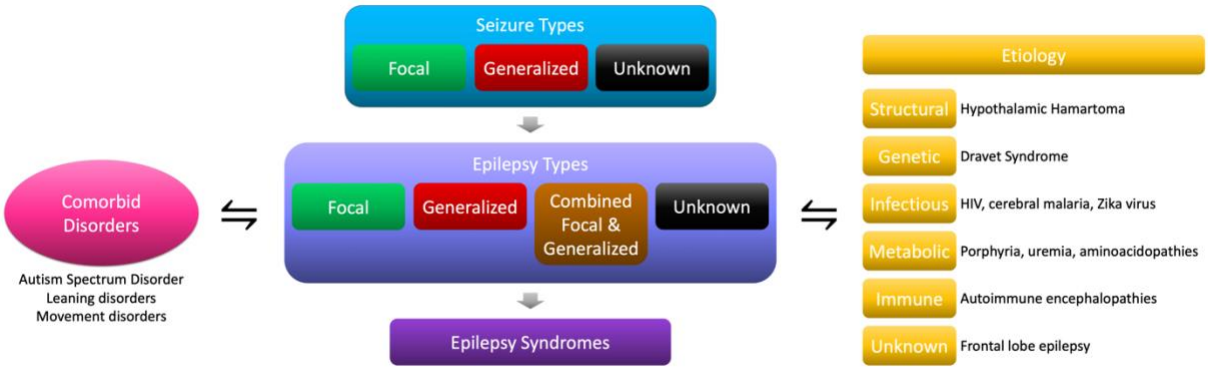

Figure 1.2: ILAE 2017 Classification of Epilepsies[8].

1.1.3 Interictal epileptiform discharges

The use of EEG has also led to the discovery of brief seizure-like discharges that occur during the interictal period[15], or the time between ictal events. These brief bursts of abnormal brain activity, called interictal epileptiform discharges, often occur without any associated clinical symptoms or signs[16] and tend to originate from the same regions of the brain as seizures[7,17–19], and are highly related to ictal activity[19,20], and may be useful in determining to where ictal activity may propagate[21,22]. Given that IEDs often have the same origin as seizures without the associated symptoms of seizures, IEDs can be useful and safer electrographic markers in the treatment of epilepsy.

1.1.4 Treating epilepsy

The primary method of treating epilepsy is anti-seizure medications[23]. These medications aim to reduce abnormal neuronal hyperexcitability or hypersynchronous activity[24]. Common mechanisms of action for these medications are: modulation of voltage-gated ion channels, such

as carbamazepine; GABA receptor agonists, such as gabapentin; or glutamate receptor antagonists, such as topiramate[25].

Beyond the traditional pharmaceutical route, there has been increased interest in treating epilepsy using alternative therapies. A more common alternative therapy is the ketogenic diet which has been shown effective in treating drug-resistant and other forms of epilepsy should the individual tolerate the diet[26]. New trends in the treatment of epilepsy have also began looking for holistic and organic supplements that may help control seizures[27]. Alternative medicines are particularly common in developing regions where there is very limited access to healthcare and anti-seizure medications[28]. Some alternative medicines have shown particular promise such as Shihogyejitang, an herbal medicine, which resulted in a >50% seizure frequency reduction in just over 44% of participants and seizure freedom in 24% of participants in a study of pediatric drug resistant epilepsy in Korea[29]. Another traditional treatment is *Paeonia officinalis* an herb with anticonvulsant properties the use of which resulted in a >50% seizure reduction for over 60% of participants after 4 weeks of use[30]. Promising results have also been shown for the effectiveness of cannabinoids in treating specific forms of epilepsy such as Dravet syndrome[31], traditional Chinese medicine in treatment of drug-resistant epilepsy, and several other alternative treatments[27]. This is not to say that traditional, holistic, or alternative medications should be used by everyone. Some common supplements can induce seizures[32,33], have high levels of heavy metals which could induce seizures[27], or interact with anti-seizure medications[32,34]. All epilepsy treatment should only be considered in consultation with clinicians.

1.1.5 Drug-resistant epilepsy

Despite seizures being well controlled for many individuals living with epilepsy, more than 54,000 Canadians live with seizures that cannot be readily controlled by anti-seizure medications[35]. An individual is defined as having drug resistant epilepsy if two well-chosen and tolerated anti-seizure medications have failed to control their seizures[36]. For some of these individuals, seizure freedom may be possible through epilepsy surgery.

1.1.5.1 Epilepsy surgery

For those individuals who have drug resistant epilepsy, the next treatment considered for seizure freedom is the removal of the region of the brain generating seizures. While more than 50% of epilepsy surgeries are unsuccessful, meaning many individuals living with drug-resistant epilepsy experience seizure recurrence[35], the consideration of epilepsy surgery is based on factors beyond seizure freedom alone. Recurrent and frequent seizures could lead to further increases in seizure frequency and/or severity[37], thus early intervention and seizure freedom are crucial for individuals living with epilepsy. Another consideration is the quality of life of the individual living with epilepsy. Epilepsy is known to be correlated with increased risk of comorbid anxiety[38–40], depression[39,41–44], and suicide[42,44]. Additionally, individuals living with epilepsy face stigma[43,45,46], and self-reported unfair treatment as a result of experiencing seizures[47]. In fact, this stigma and other social implications of the diagnosis of epilepsy was the impetus for the ILAE's inclusion of the concept of "resolved epilepsy" in the 2014 definition of epilpesy[6]. Despite potential negative neurocognitive and physiological risks[35], epilepsy surgery is a widely used intervention. This is likely because total seizure freedom is not needed to have a positive impact on a patient's life. Having a decrease in seizure burden after epilepsy surgery has been shown to be correlated with increased self-reported quality of life and/or depression and anxiety measures[48–50]. In fact, 27% of individuals surveyed reported higher quality of life despite persistent seizures[51]. While the ultimate goal of epilepsy surgery is complete seizure freedom, reducing seizures to increase quality of life and decrease risk of increased disease severity also demonstrates the utility of epilepsy surgery.

1.1.5.2 Clinically relevant brain regions

In epilepsy surgery, the goal is to resect the brain region generating the seizures. This region is known as the epileptogenic zone (EZ)[52]. The EZ is defined as the area of cortex that is necessary and sufficient for initiating seizures and whose removal (or disconnection) is necessary for complete abolition of seizures. Given this definition, the EZ can only be determined postoperatively. Using the data gathered from EEG, MRI, SPECT, PET, neuropsychological testing,

and other clinically relevant sources (such as symptomology), clinicians try to identify the location the EZ preoperatively using different markers as illustrated in Figure 1.3.

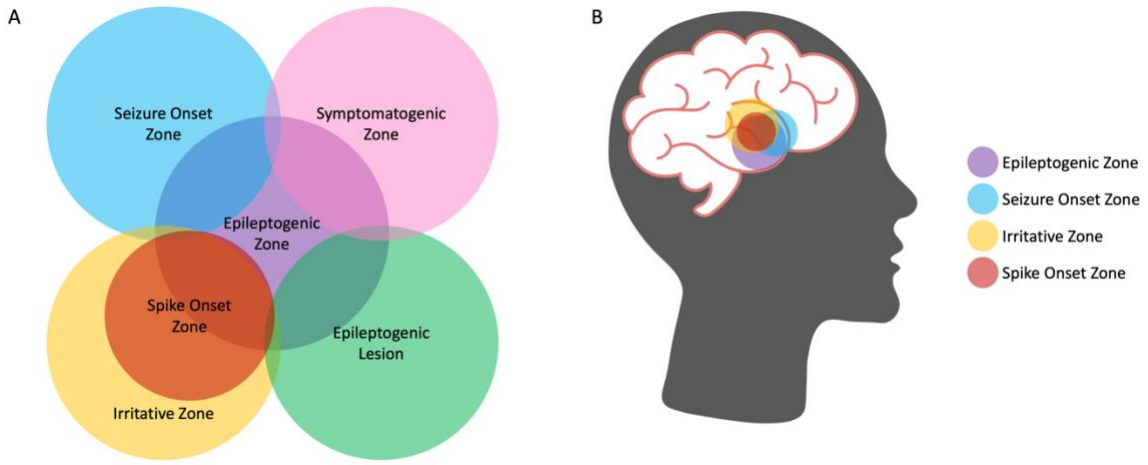

Figure 1.3: Cortical zones relevant to seizure generation and propagate. A) Graphical representation of the relationship between the epileptogenic zone and the other relevant zones. B) Demonstration of the overlap that is likely to occur for the zones examined in this thesis.

Arguably, the most important preoperative marker of the EZ is the seizure onset zone (SOZ), which is the region of the brain from which seizures are generated[52]. This is identified by scalp or intracranial EEG recordings of seizures, typically in a seizure monitoring unit. Lesions are also potential markers of the EZ, being identified in MRI or other imaging modalities. While the lesion may be related to seizure generation, not all lesions will be, thus EEG will be needed to verify the lesion's relationship to seizure generation and in some cases, such as tuberous sclerosis or other malformations of cortical development, intracranial EEG may be warranted[53]. Other zones are identified as well. The symptomatogenic zone – the region of the brain from which symptoms arise when activated by ictal activity; the irritative zone – the region of the brain from which IEDs originate; the functional deficit zone – the region of the brain where epilepsy-related deficits arise[52]. A new consideration of the irritative zone has subdivided the category into the spike onset zone, the specific region of IED origination, and the irritative zone as the regions to which IEDs may propagate[54]. This refinement was purposed as the irritative zone is often widespread making it unlikely to be a reliable marker of the EZ. Given that the spike onset zone often overlaps with the SOZ, it is often considered and reported with the EEG findings as both may be able to localize the EZ.

Should there be no clear structural abnormalities, the current gold standard is to use the SOZ as a presurgical marker of the EZ and the surgical target of epilepsy surgery. To identify the SOZ, clinicians use several imaging techniques with a primary focus on EEG. Other modalities such as SPECT, PET and MRI are often used to improve the delineation of the SOZ. Using the results of these investigations, clinicians will come to a consensus about the suspected location of the SOZ, however, the results from these modalities may be conflicting, may provide inconclusive results, or give the appearance of multiple SOZs. In addition, most of these modalities require the recording of actual seizures, which can be taxing to the patient. Imprecise presurgical identification of the SOZ is in part responsible for the poor surgical outcomes observed from epilepsy surgery. Thus, the critical need remains to presurgically identify the EZ more accurately and completely.

1.1.6 Epilepsy as a network disorder

Over the past decade, epilepsy has been reconceptualized: it is no longer thought of as a disruption of a particular brain region, but as a brain network prone to disruptions[55–57]. When an interictal or ictal event occurs within the primary node of the network, this activity can spread (or propagate) to the other regions of the network [58]. The assumption is that the primary node of an epilepsy network is the SOZ, and its removal will halt activity within the epilepsy network[59,60]. However, it is possible that multiple nodes may generate interictal and ictal activity, as other nodes of an epilepsy network may become more likely to generate interictal and ictal activity over time[61]. This could explain why epilepsy surgery has a low success rate when only one seizure-generating node is removed[59,60,62]. Additionally, it is not uncommon for activity to re-emerge after a seizure-free period following epilepsy surgery, suggesting that other nodes of the epilepsy network become the primary seizure-generating region of the brain if the network is not disconnected as a result of the surgery[63]. Hence, current research is attempting to estimate the interconnectedness of the epilepsy network as a means to predict the success of epilepsy surgery[64]. This approach, however, still requires accurate identification of the SOZ as the origin of epileptogenic activity within the epilepsy network.

1.2 EEG and Imaging in epilepsy

1.2.1 EEG

EEG is an electrophysiological technique that uses electrode sensors to record voltage changes from various areas of the brain relative to a defined ground. The technology underlying EEG was first applied to humans in 1929 by German psychiatrist Hans Berger[4]. While it was suggested that seizures may be related to electrical activity before the advent of EEG, in his early work, Berger found evidence that confirmed the theory that seizures are related to abnormal electrical brain activity through observational studies[4]. Today, EEG is divided into 7 frequency bands, the first 5 of which are considered the clinical EEG range. These bands are delta (0.1-3.9 Hz), theta (4-7.9 Hz), alpha (8-12.9 Hz), beta (13-29.9 Hz), gamma (30-79.9 Hz), ripple (80-249.9 Hz) and fast ripples (250-500 Hz)[65]. Ripples and fast ripples are known together as high frequency oscillations and have found limited use in clinical settings due to the limited ability of recording these frequencies using scalp EEG[66]. As technology advances however, more accurate recordings are being captured and these frequencies can be accurately recorded using intracranial EEG.

EEG primarily represents the summed total of post-synaptic potentials of groups of pyramidal neurons[67]. As currents propagate down the axons of the excited neurons, a primary current is generated, which can induce current in the surrounding tissue. When sufficient neurons are excited, the region becomes polarized creating a diploe. Dipoles can be transverse (parallel to the scalp and thus originating from the walls of the sulci) or radial (perpendicular to the scalp and thus originating from the gyri or bottom of the sulci). Radial dipoles will have the greatest recording on the EEG trace as the full voltage potential will align with the sensor[68]. Transverse dipoles will be recorded as well, however since the voltage potential is parallel to the sensor less of the potential will be captured[68]. This said, the large numbers of activated neurons enable meaningful results.

Scalp EEG is collected using sensors that are arranged according to a standard known as the 10-20 system and placed in reference to the measurements from an individual's nasion to inion (for anterior and posterior) and tragus to tragus (for left and right). This defined pattern helps

researchers and clinicians compare the results of various EEG studies and increases the spatial resolution of EEG by standardizing electrode locations and allowing for accurate source localization. While this may help, the spatial resolution of EEG is low compared to other imaging modalities.

EEG is the current clinical gold standard for diagnosing epilepsy and determining the SOZ. Most commonly, scalp recordings of seizures and IEDs are used to identity the SOZ. Scalp EEG can only record seizures and IEDs from superficial cortical regions. If the origin of the seizure is subcortical, or deep in the cortical tissue, the electrographic activity may be recorded on several electrodes and thus not provide a clear indication of the location of the SOZ. In these cases, where the SOZ cannot be identified by scalp EEG, intracranial EEG (iEEG) may be performed. In iEEG, EEG electrodes are surgically implanted into an individual's brain. There are three types of intracranial electrodes. Depth electrodes (Figure 1.4 A) are thin wire like electrodes that are implanted into the brain tissue. Strip electrodes (Figure 1.4 B) are a $1 \times n$ array of contact placed under the dura mater onto the surface of the brain tissue. Finally, grid electrodes (Figure 1.4 C) are a $n \times n$ matrix of contacts placed under the dura matter onto the surface of the brain tissue. Rather than following a standard layout, electrodes are placed according to where the suspected SOZ is located. Data gathered from scalp EEG and other clinical sources are used to help determine the placement of these electrodes and often wide and bilateral distribution of iEEG electrodes are used. The implantation of intracranial electrodes increases the spatial resolution of the EEG recordings, but only in the area surrounding the electrodes.

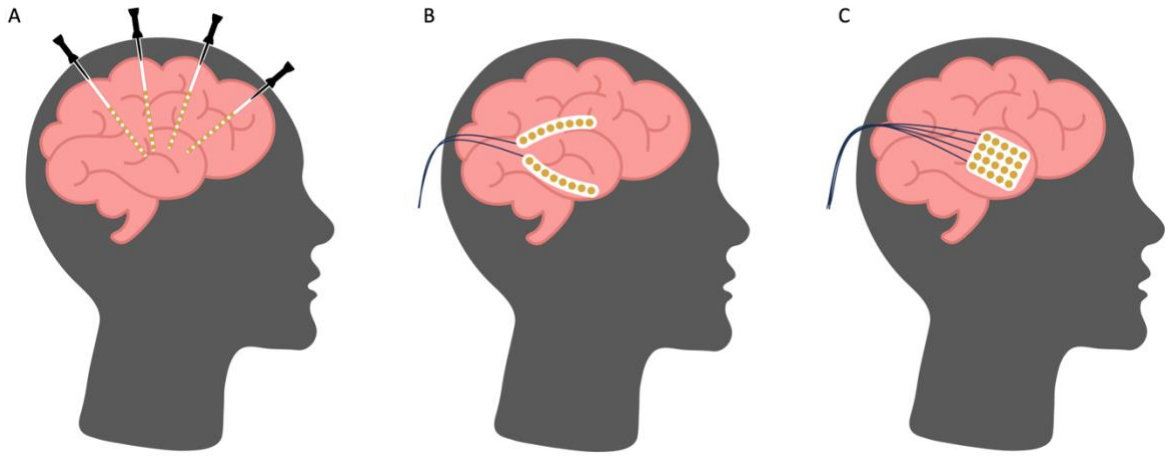

Figure 1.4: Types of intracranial electrodes. A) Depth electrodes which are implanted directly into the brain tissue. B) Subdural strip electrodes which are 1 x n strips placed on the surface of the brain. C) Subdural grid electrode which are n x n grids of electrodes placed on the surface of the brain.

1.2.2 SPECT and PET

Due to the lack of spatial specificity of EEG, it can be difficult to determine the extent of the SOZ. To better identify the extent of the SOZ, single photon emission computerized tomography (SPECT) and/or positron emission tomography (PET) scans are often added to the pre-surgical workup. PET and SPECT scans can also help identify the pathology, propagation, and neurochemical correlates of seizures[69]. A SPECT scan is used to investigate blood flow in the brain during and between seizures. For an ictal SPECT, a radioactive tracer is injected into the bloodstream within 30 seconds of the onset of a seizure. Due to the increase in neuronal activity that occurs during ictal events, vasodilators are released to ensure adequate oxygen and nutrients are delivered to these neurons, a process mediated by astrocytes[70]. The radioactive tracer is taken up with the nutrients, allowing clinicians to approximate the area of the brain in which the seizure originated. An interictal SPECT, performed when the patient has been seizure-free for at least 24 hours, is also obtained. The interictal SPECT is subtracted from the ictal SPECT in order to highlight the regions of the brain that may be key to seizure generation[71]. Typically, SPECT shows hyper-perfusion during seizures and hypoperfusion at the SOZ interictally, however it has been shown that SPECT may not a reliable indicator of the SOZ in seizures originating outside the temporal lobe[72]. PET uses [^{18}F] fluorodeoxyglucose, a glucose analog, to determine brain metabolism levels at the time of injection. Seizure generating tissue usually exhibits

decreased metabolism, as the increased demand in oxygen produces a localized hypoxic environment ultimately leading to a decrease in aerobic metabolism at that location[73]. This decrease in metabolism can be identified using PET, thus providing information about the potential location of the SOZ. The downside of PET is that [^{18}F]fluorodeoxyglucososse uptake typically extends beyond the SOZ, making accurate delineation of the SOZ difficult[71]. Despite the potential drawbacks of SPECT and PET, they can be used to corroborate and verify the results of other pre-surgical investigations and are an integral part of the pre-surgical work-up for epilepsy surgery.

1.2.3 MRI

A critical step in investigating patients with epilepsy is structural magnetic resonance imaging (MRI), which can be used to identify abnormalities in the brain that are potentially epileptogenic. MRI is becoming more commonly used in medical imaging due to its high spatial resolution, non-invasive nature, and lack of ionizing radiation[74]. MRI is based on the concept of nuclear magnetic resonance, which states that when nuclei are in a strong constant magnetic field, a small perturbation to these nuclei will cause them to resonate to a nuclei-specific frequency. One nucleus that is particularly susceptible to NMR is hydrogen [^{1}H], commonly referred to as a proton. Given the abundance of ^{1}H in the human body in the form of water, it is an ideal candidate for MRI. MRI uses a strong magnetic field to force protons within the body to align either in parallel or anti-parallel to the field. Radiofrequency pulses (brief magnetic field changes) are then applied to the region which disturbs the equilibrium of these protons. As the protons return to their equilibrium when the pulse ends, they release energy which is recorded in the form of a signal, the frequency of which is dependent on the magnetic field applied to the protons. The signal that is returned is used to determine the number of protons in the region. Since different tissues have distinct water contents, this signal can be used to identify the tissue [e.g., grey matter, white matter, cerebrospinal fluid, (CSF)]. In order to determine the location of these tissues, graded magnetic fields in the x, y, and z planes are generated, resulting in each coordinate (x,y,z), or voxel (a three dimensional pixel), having a unique magnetic field[75].

MR images are captured by changing the scanning parameters to create sequences that highlight different tissue types. The most common MRI sequences are T1- and T2-weighted scans. In a T1-weighted image, gray matter appears bright, and CSF appears dark providing a clear differentiation between gray and white matter. For this reason, T1-weighted images are often used as the primary anatomical image[76]. In a T2-weighted image, CSF appears bright, and gray matter dark highlighting regions with high water content. T2-weighted images are often used to detect disease and abnormalities since pathologic tissue usually has a higher water content than non-pathological tissue[76]. By examining MR images, clinicians can determine if a patient has epileptogenic structural abnormalities that are causing ictal activity such as a tumor or cortical dysplasia.

1.3 EEG-fMRI and the SOZ

Recently, alternative methods for identifying the SOZ have been developed to combat the low success rate of epilepsy surgery. One of these methods is simultaneous EEG and functional magnetic resonance imaging (EEG-fMRI), which allows for the determination of areas of the brain that exhibit metabolic changes in response to electrical activity in the brain.

1.3.1 Functional MRI

fMRI follows the same basic principles as MRI, but images are captured continually for the length of the sequence, producing a 4D image. By collecting these images over time, it is possible to determine signal changes that occur within the brain. fMRI uses T2*-weighted images that are sensitive to inhomogeneities in the magnetic field. These inhomogeneities in the magnetic field arise when materials with magnetic properties – such as hemoglobin – are present in the field. Oxygenated hemoglobin is non-polar and thus does not respond strongly to magnetic fields. Deoxygenated hemoglobin, however, is quasi-polar and thus produces a strong response to changes in magnetic fields and this response can be identified in T2* images. The specific contrast between deoxygenated and oxygenated hemoglobin is known as the blood oxygen level dependent (BOLD) signal[77], and is suggested to be indicative of synaptic activity[78]. Increased synaptic activity results in a decrease in deoxygenated hemoglobin concentration, as increases

in neuronal firing are metabolically demanding and thus require oxygen, resulting in a characteristic increase in blood flow and relative concentration of oxygenated hemoglobin known as the hemodynamic response[78]. In order to detect changes in the BOLD signal that are related to specific events, the signals are compared to a hemodynamic response which is modeled by a hemodynamic response function (HRF, Figure 1.5)[79]. The polarity of a BOLD signal refers to whether it is positively or negatively correlated with the HRF.

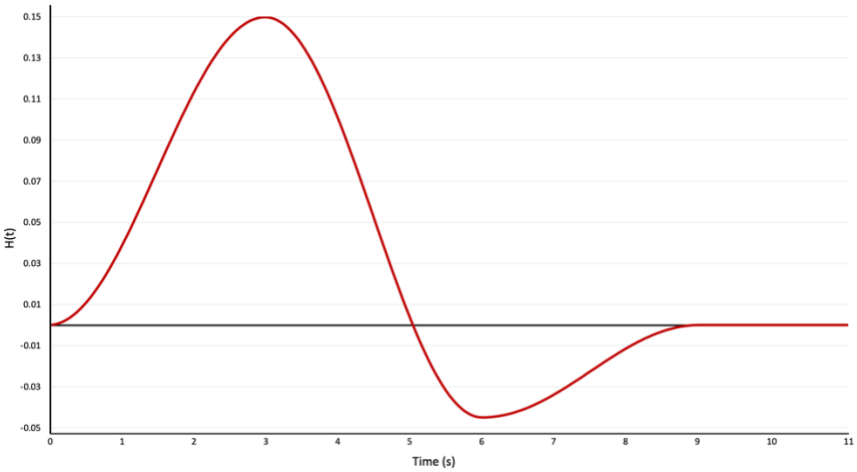

Figure 1.5: Example of a hemodynamic response function[78].

The exact physiological underpinnings of positive BOLD signals are still debated, but a cellular study has suggested that excitatory post-synaptic potentials (EPSPs) account for approximately 46% of oxygen usage due to postsynaptic glutamate-gated currents[80]. EPSPs cause the activation of voltage gated calcium channels which initiate a cascade resulting in the production of vasodilators such as nitric oxide[81], leading to the canonical hemodynamic response. The connection between positive BOLD signal and increased synaptic activity has been well established[82] and is often used to investigate various brain disorders[83–85].

The negative BOLD signal is not as well understood. Traditionally, it was thought that the negative BOLD signal was vascular in nature and not reflective of function. Recent studies, however, have begun positing neuronal-based theories of the negative BOLD response, suggesting that negative BOLD signals reflect an inhibition or reduction of brain activity[86–90]. In the neurotypical population, negative BOLD signals are suggested to represent suppression of neuronal activity.

For example, recent research has shown that during a visual task, the negative BOLD signal was correlated with the suppression of neuronal activity in task irrelevant areas[91].

1.3.2 The BOLD signal and neuronal activity

The assertion that the BOLD signal is representative of increases or decreases in neuronal activity originates from the idea that excitatory action potentials are metabolically demanding. When a physiological process is metabolically demanding, the body has homeostatic mechanisms to ensure that there is a large enough supply of oxyhemoglobin to meet the metabolic demand[92]. Thus, if an increase in the BOLD signal represents an increase in neuronal activity, a decrease in the BOLD signal should represent a decrease in neuronal activity. Recent evidence, however, demonstrated that increases in the BOLD signal were correlated with higher glucose consumption but decreases in the BOLD signal were not significantly correlated with lower glucose consumption, suggesting that some metabolic activity is still occurring[93]. If only the positive aspect of BOLD signal is correlated with metabolic activity, interpreting negative BOLD signal as a decrease in neuronal activity should be done with caution.

The focus on excitatory action potentials as the driving force of BOLD signal overlooks the role of inhibitory interneurons in the brain and neuronal activity. Interneurons are more metabolically efficient than excitatory neurons and therefore are unlikely to increase the metabolic demand of a brain region in any significant way[92]. Interneuron activity is typically manifested in one of two ways: tonic inhibition, where all action potentials are stopped, or in a rhythmic manner whereby the frequency of action potentials for a given set of excitatory neurons is regulated[94,95]. Beyond controlling action potentials, a study using a mouse model has found evidence that interneurons may play a role in increasing the supply of oxyhemoglobin[96]. When action potentials in interneurons are increased, they release nitric oxide (NO), a known vasodilator[96]. It is possible that the vasodilative actions of interneuron activity are an endogenous mechanism designed to ensure an increase oxyhemoglobin that is matched to an increase in the frequency of action potentials. This suggests that the BOLD signal may not be correlated to neuronal activity as a whole, but rather to the frequency at which the neurons are firing as mediated by interneurons.

Indeed EEG-fMRI studies have shown that positive BOLD is most often correlated with higher frequency oscillation bands (i.e., gamma and above) of EEG data[97]. This fits with the idea that the BOLD signal represents an increase in action potential frequency. Conversely, negative BOLD is typically found to correlate with lower frequencies[98,99] or tonic inhibition[100]. Given that vasodilation is a result of interneuron-released NO, fewer interneuron action potentials would occur at lower frequencies, resulting in lower levels of NO release and thus less vasodilation. It should be noted however, that both low frequency oscillations and tonic inhibition are still metabolic processes[92]. Thus, because these areas are still metabolically active, increases in low frequency excitatory action potentials or tonic inhibition would still use oxyhemoglobin despite the lower level of vasodilation in comparison to higher frequency action potentials. It is possible that the metabolic demand of low frequency activity or tonic inhibition paired with relatively lower levels of vasodilation is what is represented by negative BOLD signal meaning the negative BOLD signal may also be neuronally driven.

1.3.3 Collecting EEG-fMRI

Simultaneous EEG-fMRI has been shown to be an effective method to explore the connections between neuronal activation and metabolic activity in greater detail. As previously indicated, EEG is known to have a high temporal resolution and low spatial resolution, thus making claims of the origin of the electrographic activity captured using EEG should be done with caution. Unlike EEG, fMRI has high spatial resolution as measured voxels (with sizes in the order of mm^3) have clear coordinates that correspond to specific brain regions. Despite this high spatial resolution, fMRI is limited by the signal it measures: the BOLD response is dependent on hemodynamic changes which are believed to result from neuronal activity and thus occur at a delay from the originating activity. If the timing of neuronal activity is known however, this delay can be modeled using the HRF as previously described. By combining the collection of EEG and fMRI researchers can identify when specific events occur (EEG) and, by using HRFs, where the specific events occur (fMRI).

Simultaneous EEG-fMRI can be collected using either scalp or intracranial EEG. Simultaneous scalp EEG-fMRI is still limited by the fact that scalp EEG can only measure discharges from surface cortical brain areas or discharges from deep sources that propagate or have electrical fields that can be measured on the scalp. In the context of epilepsy, this means that simultaneous scalp EEG-fMRI may still not be able to identify the SOZ if the seizures are being generated in subcortical or in deep cortical tissues. While the use of intracranial EEG does increase the likelihood that IEDs and seizures generated in deeper brain tissues will be recorded, simultaneous intracranial EEG-fMRI does introduce its own set of challenges. The primary issue with simultaneous intracranial EEG-fMRI is that the electrodes placed in or on the brain cause susceptibility artifact. This decreased resolution in the brain areas around the electrodes may decrease sensitivity to BOLD changes immediately surrounding the electrodes. Given that electrodes are implanted where clinicians believe the SOZ to be located, this could produce issues trying to capture BOLD changes at the SOZ. This is a consideration researchers must have in mind when analyzing their results.

1.3.3.1 Gradient switching artifact

Despite the advantage of having high temporal and spatial resolution, simultaneous EEG-fMRI is not without its complications. The recording of EEG during fMRI induces artifact in the EEG trace recording[101]. At its core, EEG measures changes in electrical field potentials, and fMRI collects data by using electronic magnets to create magnetic gradients in the x, y, and z planes which are switched in a semi-continuous fashion throughout the fMRI recording. When two electrodes are placed in a magnetic field, as per Faraday's law, a current is induced between these electrodes[102]. Further, by Ampere's law, a magnetic field is also created between these electrodes[103]. As more electrodes are added, the current is induced between the two most distal electrodes[104]. It should be stressed that these currents are small and safe[103–106]. It is the induced currents from the electromagnets switching which creates a characteristic "sawtooth" artifact (Figure 1.6) known as the gradient switch artifact (GSA)[107–110]. GSA is repeated each slice and can be up to 400 times the size of the physiological signal[109,111]. The removal of GSA from EEG data is essential for downstream analyses such as event-related BOLD analysis.

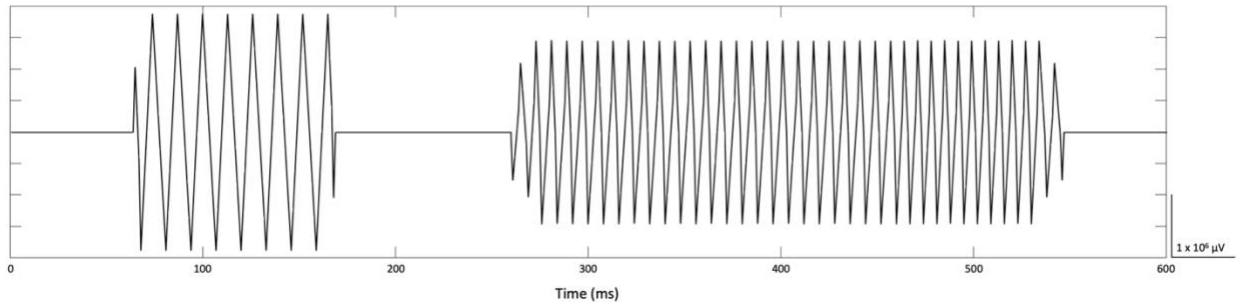

Figure 1.6: Example of gradient switch artifact.

Early studies utilizing EEG-fMRI often avoided recording EEG and fMRI at the exact same time[112]. One format the studies followed was an event evoked model wherein after an event was recorded on the EEG, the fMRI was recorded to capture the BOLD response[113]. Another process used to avoid GSA was the "stepping stone sampling" method which allows for the collection of EEG data with limited residual GSA by altering the fMRI pulse sequence[108]. A final method used was spacing the recording of fMRI TRs such that there are artifact free sections of EEG between each TR. Using frequency decomposition, the frequencies unique to the GSA can be identified and removed from the EEG signal thereby removing most of the GSA[110]. These methods, however, did not allow for true simultaneous EEG-fMRI data collection.

The initial interest in concurrent EEG-fMRI was for its applicability in epilepsy[113,114]. These studies suggested that with this new multi-modal approach it may be possible to identify the brain region generating IEDs, but also highlight the issue posed by what we now know is GSA[113,114]. Since IEDs are not evoked, predictable, or always isolated, using data collection methods that rely on events occurring in specific intervals or in isolation such as those in the previous paragraph are not ideal. This led to the use of "template" methods of artifact removal as a way to allow for continuous and truly simultaneous EEG-fMRI data collection. A common method used is known as average artifact subtraction (AAS). GSA is considered to be a highly reliable and repetitive artifact; thus, it should be the same throughout a TR. If enough TRs are averaged, for example 7 TRs, a template of the true artifact is created and can be subtracted from one TR. This process would be repeated for all TRs. First applied to EEG-fMRI data in 1998[115], AAS came to become a key part of GSA removal in many EEG-fMRI studies to this day[102]. It was determined, however, that AAS alone

does not remove all GSA[101,102,109,116,117]. Residual GSA can arise from temporal jitter as a result of temporal dyssynchronization between the MR scanner and the EEG clocks[101], head movement[117,118], ballistocardiogram artifact[101,116,117,119], or equipment vibrations such as the helium pump artifact[107,120]. In attempts to remove residual artifact, methods such as adaptive noise cancellation[109], independent component analysis[121], principal component analysis[122], and optimal basis sets[123], all of which are added after data has been undergone artifact removal using AAS.

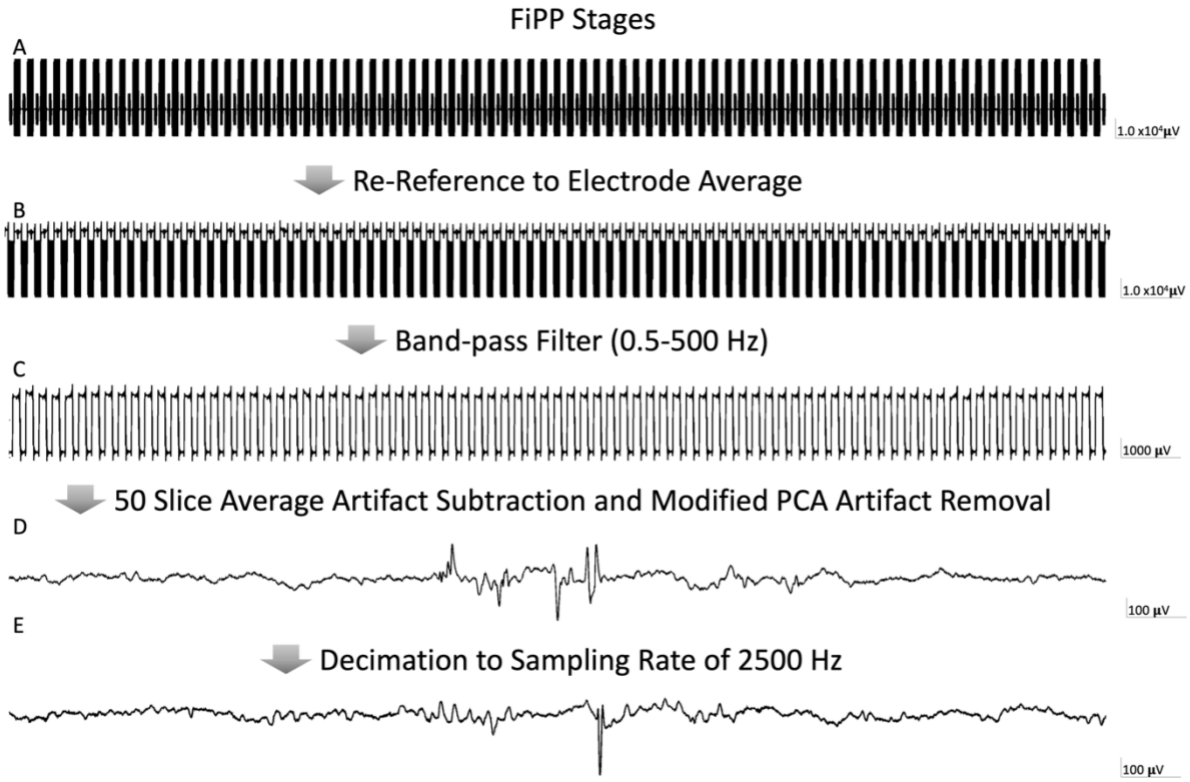

Figure 1.7: Methods included in new artifact removal pipeline. A) Raw artifact laden iEEG. B) iEEG after re-referencing to an electrode average. C) iEEG after previous step and band-pass filter 0.1-500 Hz. D) iEEG after previous steps and average artifact subtraction and modified PCA artifact removal algorithm. E) Decimated cleaned iEEG data.

The development and testing of a new processing pipeline centered around a modification of the AAS plus optimal basis sets GSA removal will described in this thesis. This artifact removal process also includes re-referencing to an electrode average, a band-pass filter of 0.1-500 Hz, average

artifact subtraction with a modified principal components analysis, and decimation to a sampling rate of 2500 Hz (Figure 1.7).

1.3.4 Using EEG-fMRI to determine the SOZ

Using interictal EEG activity as a temporal marker to guide fMRI analysis has permitted the identification of areas of the brain that exhibit changes in metabolic activity following IEDs. In these analyses, it is assumed that the maximal positive BOLD response will indicate the origin of the IEDs. In previous research using EEG-fMRI, the maximal positive BOLD response to IEDs has been used to identify the SOZ[124], epileptogenic irritative zones[125], brain structures involved in the generation of IEDs[126], and epileptic networks[127]. By using positive BOLD signals to identify where IEDs are originating, it is possible to determine the SOZ for treatments such as epilepsy surgery[128]. While more research is needed to increase the reliability of the positive BOLD response in localizing the SOZ, this line of research suggests that the positive BOLD signal in response to IEDs has potential as a localizing measure in the treatment of epilepsy.

In addition to the SOZ, research has suggested that the spike onset zone may also be a reliable indicator of the EZ[54], which is in line with research that suggests that IED originate from the same brain region as ictal activity[7]. In fact, one study demonstrated that the electrode from which IEDs originated was the exact SOZ contact or within 20 mm of the SOZ contact for 84% of patients[129]. Regardless of concordance with the SOZ, the spike onset zone itself has been proposed as a separate proxy of the EZ for decades. In 1961 Jasper and others presented evidence that the region producing “primary spikes”, or the spike onset zone, may localize the pathogenic region and the removal of this region is related to good surgical outcomes (defined as “no attacks since operation” or “rare auras/not more than 2 attacks since operation”)[130]. Similar results were observed in a study which used interoperative electrocorticography to determine the region showing “earliest peak" – the spike onset zone. Post-operative follow-up indicated that 25/27 patients with temporal lobe epilepsy whose resection cavity included the spike onset zone had good post-surgical outcomes (Engel I or II)[131]. In the modern interpretation of epilepsy as a network disorder, it has been suggested that the IED network is what should be considered as

the removal of the spike onset zone, the primary node of this network, is correlated with seizure freedom[132]. Further to this, a recent study has suggested that it is the spike onset zone that should be the presurgical proxy of the EZ[133]. In this study, it was determined that the inclusion of the SOZ in the resection was not sufficient for a good surgical outcome (Engel I), but for individuals with good surgical outcomes, the spike onset zone and the resection cavity had an average percent overlap of 96%[133]. These results indicate that the spike onset zone should be considered during pre-surgical localization of the EZ.

A developing theory in the field suggests that it is not the maximal *positive* BOLD response that identifies the SOZ, but rather it is the maximal BOLD response *regardless of its polarity*[54]. However, this suggestion should be interpreted with caution as the underlying mechanisms of negative BOLD signals in the context of epilepsy are not clear. Negative BOLD signals can be found in regions of the brain that are often distal, ipsilateral, or even unrelated to the SOZ. Additionally, negative BOLD signals are commonly observed in regions of the default mode network (DMN) during active brain processing and thus, not surprisingly, the negative BOLD response to IEDs is often concordant with the DMN[89,99,134–142]. Thus, there remains much speculation about SOZs and the polarity of the maximal BOLD signal.

The IED-related maximal positive BOLD response has been shown to be of prospective value in pre-surgical planning[128,143], suggesting clinical utility. Despite the promising results from these studies, EEG-fMRI is not considered in clinical setting. One of the reasons for doubt in EEG-fMRI is the low capture of IEDs during data acquisition[143,144]. This limitation is overcome with the use of iEEG which captures far more IEDs[145] and is the focus of this thesis. Another concern is the lack of standardized methods amongst the research centers that utilized EEG-fMRI[146]. Steps within this thesis have aimed to address this concern with the development of both a pipeline to remove artifact from the iEEG and to standardize a pipeline to standardize the statistical analysis of fMRI data. Another concern is the low concordance rate of the maximal BOLD response and the presumed SOZ[128,145,147,148]. In an attempt to address this low concordance rate, researchers have suggested the use of additional inclusion criteria before a BOLD response can be considered

localizing the SOZ[125,149]. The use of inclusion criteria is meant to increase researcher and clinician confidence that the selected cluster in reflective of the SOZ, further strengthening the arguments for the inclusion of EEG-fMRI in clinical settings.

1.4 Summary

Better pre-surgical localization of the SOZ is of critical importance in increasing the success rate of epilepsy surgery. Initial results from simultaneous iEEG-fMRI studies have shown promise, however, some limitations still exist.

One of potential area for improvement relates to methods of removing gradient switching artifact from the iEEG. Standard methods are known to leave residual GSA in the EEG trace, thus increasing the likelihood of identifying incorrect events as IEDs. Alternative methods of removing GSA could reduce this error. A new EEG processing pipeline to remove GSA will be described and assessed in this thesis.

A second area for improvement is in cluster selection. Typically, the maximal positive cluster is selected as the cluster that is more likely to represent the SOZ. Recent studies, however, suggest that the absolute maximal BOLD response to IEDs, positive or negative, can be useful in determining the SOZ, and that this absolute maximal cluster should be tested for significance before being selected. These studies, however, were limited by their use of scalp EEG. By using intracranial EEG, epileptiform activity can be measured with greater precision and closer to deep tissue electrophysiological generators. Thus, this thesis will investigate the absolute maximal BOLD response to IEDs and the confidence testing of these responses using iEEG and determine the utility of these methods for SOZ determination in iEEG-fMRI.

1.5 Thesis overview

This thesis contains two separate studies which have the hypotheses and aims listed below. The first study outlines the development and assessment of an EEG processing pipeline that may better remove gradient switching artifact than conventional methods. The second study aims to

determine if the maximal positive BOLD response to IEDs should be used to identify the SOZ instead of the absolute maximum BOLD response.

Hypothesis 1: iEEG data after artifact removal using the Federico Lab iEEG Processing Pipeline will be more similar to the original clinical iEEG than iEEG data after artifact removal using average artifact subtraction alone.

Aim 1: *Determine whether the Federico Lab iEEG Processing Pipeline results in a meaningful decrease in residual gradient switching artifact compared to average artifact subtraction alone.*

Ten subjects with drug-resistant epilepsy undergoing inpatient intracranial video-EEG monitoring will be included in the test cohort. Samples of each subject's clinical iEEG will be collected and five different artifact conditions will be added to the EEG data: no artifact, a sinusoidal chirp artifact, true scanner artifact, a generated 'realistic' gradient switching artifact, and a generated 'noisy' artifact. These artifacts will be subjected to both average artifact subtraction alone and the Federico Lab iEEG Processing Pipeline for artifact removal. Differences between the two cleaning methods will be assessed.

Hypothesis 2: The SOZ will be more spatially concordant with the maximal positive BOLD response to IEDs than the maximal negative BOLD response.

Aim 2: *Measure and compare the distances between the maximal positive and negative BOLD response to IEDs and the SOZ.*

Seventy adult subjects with drug-resistant epilepsy undergoing inpatient intracranial video-EEG monitoring will be recruited. Patients will undergo a 60-minute iEEG-fMRI study from which BOLD activation maps will be generated and a maximal positive and negative BOLD response will be identified. The distance between clinically determined SOZ and the maximal positive and maximal negative BOLD responses will be measured and compared.

1.5.1 Significance

Accurate determination of the SOZ prior to epilepsy surgery is crucial for good surgical outcomes. By demonstrating that the negative BOLD response to IEDs is not a reliable indicator of the SOZ this study hopes to highlight the importance of the positive BOLD response to IEDs for SOZ localization and direct future studies to explore the meaning of the negative BOLD response to IEDs.

1.6 Statement of contributions

Chapter 2: Perry Dykens, Dan Pittman, and Paolo Federico conceptualized the project. Perry Dykens, Craig Beers, Laura Gill, Victoria Mosher, Dan Pittman, Joseph Peedicail, Negar Tehrani, Will Wilson, and Paolo Federico were involved in data acquisition. Pierre LeVan and Shuoyue Zhang conceptualized and developed LeGARE. Perry Dykens, Dan Pittman, Will Wilson, and Paolo Federico conceptualized FiPP. Perry Dykens, Dan Pittman, and Will Wilson developed FiPP. Perry Dykens coded, maintained, and curated FiPP. Perry Dykens performed the cleaning and preparation of iEEG data, the summary statistics, wrote the initial manuscript, and created all figures. All authors interpreted and discussed the results and contributed to the final manuscript. Paolo Federico supervised this project.

Chapter 3: Perry Dykens, Victoria Mosher, and Paolo Federico conceptualized the project. Perry Dykens, Craig Beers, Laura Gill, Victoria Mosher, Dan Pittman, Joseph Peedicail, Negar Tehrani, Will Wilson, and Paolo Federico were involved in data acquisition. Perry Dykens, Shuoyue Zhang, Will Wilson, Dan Pittman, Pierre LeVan, and Paolo Federico developed the EEG cleaning pipeline. Will Wilson prepared and cleaned the EEG data. Perry Dykens, Victoria Mosher, Dan Pittman, and Will Wilson conceptualized the fMRI processing pipeline. Perry Dykens developed the workable and fully automatic fMRI processing pipeline. Victoria Mosher and Will Wilson performed the preprocessing of the fMRI data. Laura Gill, Joseph Peedicail, Paolo Federico and the CEP collaborators performed the IED marking. Perry Dykens, Victoria Mosher, and Will Wilson performed the statistical analyses of the fMRI data. Perry Dykens performed summary statistics,

wrote the initial manuscript, and created all figures. All authors interpreted and discussed the results and contributed to the final manuscript. Paolo Federico supervised this project.

Chapter 2: The Federico Lab intracranial EEG processing pipeline

Perry Dykens[1,2], Shuoyue Zhang[7], William Wilson[1,2], Victoria Mosher[1,2,4], Daniel J. Pittman[1,2], Laura Gill[2,3], Joseph Peedicail[2,3], Antis G. George[1,2,3], Bradley Goodyear[1,2,4], Pierre LeVan[1,4,5,6], Paolo Federico[1-4] on behalf of the Calgary Comprehensive Epilepsy Program collaborators

The Calgary Comprehensive Epilepsy Program collaborators are: Yahya Aghakhani, Walter Hader, Nathalie Jetté, Colin Josephson, Karl Martin Klein, William Murphy, Neelan Pillay, Andrea Salmon, Yves Starreveld, Samuel Wiebe.

1 Hotchkiss Brain Institute, Cumming School of Medicine, University of Calgary, Canada.
2 Seaman Family MR Research Centre, Cumming School of Medicine, University of Calgary, Canada.
3 Department of Clinical Neurosciences, Cumming School of Medicine, University of Calgary, Canada.
4 Department of Radiology, Cumming School of Medicine, University of Calgary, Canada.
5 Alberta Children's Hospital Research Institute, Cumming School of Medicine, University of Calgary Canada.
6 Department of Pediatrics, Cummings School of Medicine, University of Calgary, Canada.
7 Department of Radiology, Medical Physics, Faculty of Medicine, University of Freiburg, Germany.

2.1 Abstract

Background

One challenge of intracranial electroencephalography-functional magnetic resonance imaging (iEEG-fMRI) is the gradient switching artifact imparted onto iEEG recorded in the fMRI environment. This artifact obscures the physiological signal, rendering the iEEG unreadable. To address this, an artifact removal pipeline was developed.

New Method

The Federico iEEG Process Pipeline (FiPP) includes channel rejection, re-referencing, 0.5 Hz high-pass filter, 500 Hz low-pass filter, 50-slice average artifact subtraction, and modified optimal basis sets wherein slices are pre-whitened and the component weights when reconstituting the signal are determined using generalized least squares.

Results

iEEG data processed using FiPP was more morphologically similar to clinical iEEG data than processed using average artifact subtraction alone. Specifically, there was less residual artifact across the frequency range of 0.5 – 500 Hz using FiPP. Additionally, FiPP cleaned datasets were more similar to clinical iEEG than average artifact subtraction alone cleaned datasets in the frequency domain.

Comparison with Existing Method(s)

FiPP represents the first self-contained and automatic artifact removal pipeline for iEEG recording during fMR image acquisition. The use of modified optimal basis sets is novel and increases artifact removal with the addition of pre-whitened slices, generalized least squares, and spectra comparison.

Conclusions

FiPP presents a contained, reliable, and standardized method for the removal of gradient switching artifact from iEEG, allowing for more accurate event identification for downstream analyses.

Keywords

Keywords: epilepsy; intracranial electroencephalography; interictal epileptiform discharges; gradient switching artifact; functional MRI, EEG-fMRI

2.2 Background

Epilepsy is a neurological disease characterized by spontaneous and recurrent seizures, affecting approximately 1 in 100 Canadians[1]. For most individuals living with epilepsy, their seizures are well controlled by anti-seizure medications. However, this is not the case for approximately 30% of individuals who are said to be drug-resistant [36]. For these patients, resective surgery is often the only option. The practical targets of this intervention are usually the seizure onset zone (SOZ), which is the region of the brain where seizures are thought to begin[52], or the spike onset zone, which is the region of the brain where interictal epileptiform discharges (IEDs) originate[150]. IEDs are brief pathological discharges unique to epilepsy which can only be recorded electrographically using EEG[16]. Importantly, IEDs commonly, but not always, originate from the same brain region as seizures[7,17–19,129]. Thus, the SOZ and spike onset zones often overlap. In recent years, a body of research has been developed around the use of IEDs as temporal events in the analysis of simultaneous EEG-fMRI[89,90,99,118,124–128,134–139,142,144,145,147,149–160]. Simultaneous EEG-fMRI allows researchers to identify localized changes in the blood oxygen dependent (BOLD) signal which occur in response to a specific event. When applied to IEDs, the associated BOLD signal changes may identify the SOZ or IED generator, thus localizing the surgical target.

The advantage of using EEG-fMRI to localize the SOZ is that the patient would not need to experience additional seizures for this localization to occur. Typically, to localize the SOZ, patients are monitored in hospital where their medications are decreased with the intent to record multiple seizures. With EEG-fMRI, IEDs could be used to localize the SOZ, reducing or eliminating the need for patients to experience seizures.

Despite the advantages of EEG-fMRI, there are methodological challenges to analyzing the data. EEG measures changes in electrical field potentials associated with brain activity[161]. MRI imaging uses gradient magnetic fields to collect data from each voxel in the field of view[75]. These gradients are modified, or switched, for each slice. Given that changes in magnetic fields induce changes in electrical field potentials, MR images acquisition imparts gradient switching artifact (GSA) onto the EEG recording which is several magnitudes larger than the physiological EEG

signals and completely obscures the EEG signal of interest[101]. The magnitude of the artifact makes removal of GSA both difficult and necessary before IEDs can be identified in EEG for a simultaneous EEG-fMRI analysis.

Traditionally, removal of the GSA is performed using filtering and average artifact subtraction (AAS)[109,115], however it has been shown that AAS alone leaves residual artifact[109,112,116,123]. For simultaneous EEG-fMRI to be used as a reliable indicator of the SOZ, better methods of artifact removal must be developed. In this report, we present a novel EEG pre-processing pipeline for GSA removal known as the Federico Lab Intracranial-EEG Processing Pipeline (FiPP). We also aimed to determine whether FiPP could adequately remove GSA from contaminated iEEG data and compared its performance to AAS.

2.3 Theory

An EEG signal from simultaneous EEG-fMRI data collection contains both the physiological signal and the GSA. Artifact removal methods must find a balance between the maximal removal of artifact and the maximal retention of true physiological signal. Our signal of interest, the physiological EEG, is an unknown signal unlikely to follow a predictable pattern and is in constant flux. During EEG-fMRI acquisition, this physiological signal is obscured by the GSA which is several magnitudes larger. In contrast, the GSA is highly predictable: the artifact is the same in each fMRI volume acquired. Using the precise timings of the GSA and the fMRI settings used during acquisition, it is possible to fully characterize the GSA. By leveraging the consistent nature of the GSA, one can devise an algorithmic approach to identify and remove this artifact.

2.3.1 EEG Acquisition

While the methods described herein could be adapted for all EEG-fMRI data, they were developed using intracranial EEG-fMRI. Unlike scalp EEG, each iEEG electrode is placed either on the surface of the brain or implanted directly into brain tissue in regions of clinical interest. Most often, iEEG depth electrodes, a linear array of 4-10 electrical contacts, are used, each of which is the source for recording an EEG channel. These electrodes use specialized clamping headbox

connectors which connect all contacts at the same time. Intracranial electrodes can be placed anywhere in the brain, but all EEG contacts are subject to the introduction of GSA, which has slightly different morphology at each contact due to the slightly different magnetic field strength and behavior at each location in the brain. Therefore, each electrode must be treated as an independent source.

2.3.2 FiPP process 1: Channel selection

While not directly aimed at removing gradient-switching artifact, channel selection is an important first step in EEG pre-processing. This involves removal of all channels with poor data quality where the signal is either flat or pure GSA. This could be caused by a damaged electrode contact or incomplete connection between the electrode and the connector harness. If left in the dataset these channels would skew the cleaning process.

2.3.3 FiPP process 2: Re-referencing

During EEG data acquisition, each signal records the changes in a differential electrical potential: this difference is measured between the recording contact and a reference channel. Although the signal is recorded as a difference between these two electrodes, the data can be arithmetically "re-referenced" to reflect the difference between the recording contact and any other channel. This re-referencing can be particularly useful if a subset of channels is more likely to be similar to each other than to other channels in the dataset in terms of artifact. This is the case with EEG data collected during a simultaneous iEEG-fMRI study, where there are different magnetic field strengths and gradient switching behaviors at each electrode contact location. The differences in magnetic fields, however, differ less over short distances, and iEEG electrode contacts are spaced between 4-10mm apart[162]. Thus, an electrode's closely grouped contacts will have similar GSAs. Given this, for each electrode contact, the second processing step involves subtracting an average of all the electrode contacts across the same electrode, which will remove a large portion of the "common" GSA.

2.3.4 FiPP process 3: Filtering

In EEG recordings there are typical artifacts inherent to data collection which can be digitally filtered out of the signal. In EEG, data are typically high-pass filtered to remove any low frequency drifting artifact that may have been caused by imperfections in the hardware or from slow changes in DC potential[163]. The cutoff frequency is typically between 0-1 Hz, so as to not remove any meaningful physiological signal. In addition to a high-pass filter, low-pass filters can be used in EEG data processing to attenuate unwanted higher frequencies caused by irrelevant fluctuations in artifact, for easier interpretation or better visual presentation, or to ensure that the Nyquist condition is enforced when decimating or resampling[164]. In FiPP, the high-pass filter is 0.5 Hz and the low-pass filter 500 Hz.

2.3.5 LeVan gradient artifact remover

The final processing stage in FiPP is the LeVan Gradient Artifact Remover (LeGARE). LeGARE is a combinations of average artifact subtraction and a modified principal component analysis.

2.3.5.1 FiPP process 4A: Average artifact subtraction

AAS is a noise removal process[115] which begins with the signal being sub-divided into many smaller identical timespans, or epochs. When a sufficient number of epochs are averaged together, the relatively random physiological signal is cancelled out, and the average should contain only, or dominantly, the commonly occurring artifact[115]. This average can then be subtracted from the average's constituent epochs, leaving only the physiological signal. However, given the random nature of the physiological signal, it is unlikely that the physiological signal in a given epoch will be similar to the physiological signal in another epoch several epochs away. For this reason, this process is performed repeatedly using a sufficient number of epochs immediately surrounding each given epoch being cleaned, in a sliding window manner[109]. During EEG-fMRI processing, the epoch length is typically set to the span of 1 TR (1.5 s) but is reduced to 1 slice (600 ms) in the FiPP method.

While AAS will remove much of the GSA, some residual artifact often remains[112]. GSA will theoretically be the same across the entire dataset, but there are factors, such as the magnetic gradients, which can influence the morphology and timing of the artifact enough to cause changes and errors in the average[123]. The instability in the GSA is created by micromovement in the electrodes, drift in the EEG, and larger movement of the individual being scanned[112]. These factors cannot be accounted for in AAS which is why the method is not used in isolation.

2.3.5.2 FiPP process 4B: Principal component analysis

To help remove remaining artifact, a modified principal component analysis (PCA) was developed in collaboration with Dr. LeVan and Dr. Zhang[165]. In essence, a PCA decomposes a long complex signal into a set of shorter simpler components, or sub-signals, each of which represent a portion of the variance in the signal. Each component represents a portion of the signal that accounts for some of the variability in the original signal and are usually ordered according to this measure[122]. One drawback to the decomposition process is that generally no single component visually resembles the original signal, which makes the classification of each as signal or noise an interesting challenge. Typically, the largest components in an EEG signal's PCA will represent artifact, and removing an appropriate number of these components will remove the artifact from the original signal[122]. The removal of these components must be done with caution because if too many are removed it is possible that true signal may be removed as well.

To mitigate this possibility, rather than applying the PCA directly to the signal, in the modified PCA, it was applied to pre-whitened epochs. Pre-whitening is the process of adding random noise to a signal to make the contributions of the sub-signals or frequencies that constitute the signal more similar[166]. When performing a PCA on pre-whitened data, the standard deviations of the artifact components are increased, making these components larger and more distinct from the components representing the underlying physiological signal.

In a typical PCA reconstitution, the original eigenvalues are used to create the transformation matrix which is then used to create the modified signal[123]. Rather than use these eigenvalues,

this method built off work using optimal basis sets[123]. A generalized least squares method is used to generate a weight value, representing an estimate of each component's contribution to the variance relative to the other identified artifact components, rather than to the variance within the signal as a whole[167]. The transformation matrix is composed of these weight values, rather than the original eigenvectors. After PCA reconstitution, the resultant signal is a representation of the residual GSA artifact and was subtracted from the epoch being cleaned.

The initial modified PCA removed 30 components, using the modified PCA method just described. When the results were was reviewed, it was discovered that in some cases a portion of the physiological signal was being removed, and in others the GSA was not being adequately removed. To account for these discrepancies, two additional processes were added to the procedure.

First, the algorithm was modified to accept a sample of uncontaminated EEG data collected outside of MRI scanning, thus there would be no GSA. By comparing the spectral composition of the uncontaminated EEG data to EEG data contaminated with GSA, the performance of the PCA algorithm could be evaluated. This evaluation entailed removing a component from the contaminated EEG and calculating the spectral signature of this data. The spectral signature of the contaminated data was then subtracted from the spectral signature of the uncontaminated EEG data. This process is repeated, with an additional component being removed each time, until the difference between the spectral signature of the uncontaminated data and the spectral signature of the data that was contaminated with GSA was 0 or was unchanged for 20 consecutive components removals.

Secondly, the algorithm was modified so that the user could specify the number of PCA components to remove. This second modification forced the modified PCA to remove the exact number of components specified, in cases where the uncontaminated EEG data may not have been representative of the EEG data contaminated with GSA. The application of this modified

PCA is poised to remove any residual artifact should the automatic method not perform artifact removal adequately.

2.4 Methods

2.4.1 Participants

Ten patients were recruited from among those admitted for inpatient intracranial video-EEG monitoring as part of their pre-surgical workup for drug-resistant epilepsy. Inclusion criteria were focal epilepsy, at least 18 years of age, and no severe post electrode implantation complications (e.g., subdural hematoma, infection, intracranial hemorrhage). This study was approved by the Conjoint Health Research Ethics board of the University of Calgary. Written, informed consent was provided by all participants prior to participation.

2.4.2 Clinical iEEG data

Clinical iEEG data were collected from the patients while they were in the Seizure Monitoring Unit undergoing intracranial video-EEG monitoring as part of a pre-surgical investigation. The iEEG data were collected continuously using a 128-channel Natus Quantum headbox and Brain Monitor Amplifier (Natus Xltek, Oakville, Ontario) at a sampling rate of 1000 or 2000 Hz. iEEG samples were selected that were 5 or 10 minutes in length, recorded more than 3 days after electrode implantation, not within 24 hours of a seizure, and with minimal movement artifact.

In preparation for processing using FiPP, the clinical iEEG data were modified to be more closely comparable in its parameters to the data for which FiPP is designed (e.g., iEEG-fMRI data). To accomplish this, the clinical iEEG data were resampled to 10 kHz which is the native sampling rate of FiPP. Resampling was performed using the default Matab resample function. A linear nearest neighbour interpolation was used during resampling. Interpolating in this manner maintains the original samples as limits and creates smooth lines between any two original samples to maintain the original morphology of the signal. As part of resampling, a FIR antialiasing filter was applied. Interpolating data is typically avoided, however, for this particular purpose the process was needed. In order to validate FiPP as it would be used, the validation data needs to meet the same

parameters as the data collected during an iEEG-fMRI study. More importantly however, LeGARE processes data at the slice level. For data sampled at 10 kHz a slice is 600 samples, at 2000 Hz a slice is 120 samples which is not a sufficient sampling of the GSA for a complete removal. Following resampling, a 60 Hz notch filter was applied, to remove RF artifact from AC electrical supply.

The electrodes included in the datasets were culled so that they contained only those channels that were included in the iEEG-fMRI study for the same patient. The clinical iEEG data were then visually inspected and the most actively spiking channel was identified. From this spiking channel, a 5.0-second epoch which contained a prominent IED(s) was selected as a test EEG epoch.

2.4.3 Test datasets

To validate FiPP, 5 datasets were prepared by adding artifact to the clinical iEEG described in section 2.3.2: No GSA Added, Gaussian pulse (Chirp) Artifact, True GSA, Realistic GSA, and Noisy GSA. The datasets were created to facilitate evaluation of FiPP's ability to remove these different GSA forms from a test signal which was a known ground truth, namely the clinical iEEG signal. Validating FiPP by adding artifact to a known ground truth is essential to be certain that the cleaned EEG represents the true underlying clinical iEEG signal.

2.4.3.1 No GSA Added

Before testing FiPP's ability to remove GSA, it first had to be confirmed that an artifact free dataset can be passed through the processing pipeline without altering the original data. Thus, the first test dataset had no additional noise added to it.

2.4.3.2 Chirp Artifact

One of the deviations from traditional artifact removal in FiPP is the use of slice-wise AAS. To ensure this new method sufficiently removed artifact, an ideal test dataset would have identical slice to slice artifact. To ensure a uniform dataset, an artifact was generated that had 4 sinusoidal pulses (truncated 10 kHz Gaussian) centered within the span of 1 slice and repeated for the length

of the sample. The Chirp GSA was recentered to the mean of the channels to which the GSA was added.

2.4.3.2 True GSA

To determine if FiPP could remove real GSA, an iEEG-fMRI scan was performed using a phantom to ensure that only GSA would be captured in the EEG recording. This was accomplished using a custom 8-tailed (64 contact) intracranial electrode connector connected to a phantom in the MR scanner while conducting an fMRI scan (Neuroscan, Compumedics, Charlotte NC, USA). EEG was recorded at 10 kHz. Data collection was performed using a SynAmpsRT amplification/digitalization system and Curry 8 software (Neuroscan, Compumedics, Charlotte NC, USA), with the EEG system and MRI scanner clocks synchronized. GSA was generated from a fMRI protocol (gradient-recalled echo planar imaging: TE = 30 ms, TR = 1500 ms, flip angle = 65°, 24 cm field of view, 64 x 64 matrix, 25 slices, 3.75 · 3.75 · 5 mm) using a 3.0 T GE Discovery MR750 whole body scanner equipped with a 12-channel receive-only phased array head coil (GE Healthcare, Waukesha, WI). True GSA was mean subtracted and recentered to the mean of the channels to which it was added.

2.4.3.3 Synthetic GSAs, Realistic GSA and Noisy GSA

The True GSA dataset may not be able to account for other variables of a GSA occurring during an iEEG-fMRI acquisition. At any given location in the magnetic field, the summed magnetic vectors may not directly line up with the z-axis producing an altered total field potential for that location changing the recorded GSA. This alteration could be due to head position, imperfections innate to the scanner, the iEEG electrodes themselves, or factors innate to the individual being scanned. To test whether FiPP can adequately clean EEG from an iEEG-fMRI dataset, these imperfections need to be approximated and the GSA modified.

To test this aspect of GSA, the EEG from the iEEG-fMRI acquisition of the subjects was examined to define these inconsistencies based on slice-wise variability across the cohort. Slice-wise GSA varies along three primary dimensions: within the TR, between TRs, and between locations within

the magnetic field. The primary difference across these three dimensions was the amplitude of each peak of the GSA. The standard deviation of the amplitude was calculated across these three variables and averaged across all subjects. It was also noted that the morphology of the peak was subject to change as was the sample at which the peak occurred, although most GSA peaks had the same morphology.

Synthetic GSA was first created by making a slice template that included common changes within the GSA (such as a suppression of peak). Each peak was initially given the same amplitude before being multiplied by random values within the range of the standard deviation described above. This process was repeated until a GSA the size of the test dataset was generated.

From this concept, two GSA datasets were generated: one Realistic GSA, and one Noisy GSA. To create the Realistic GSA, limits were placed on how much the amplitude of each peak could vary and all peaks had the same morphology. In the Noisy GSA dataset, the peak morphology for each peak was randomized and a random scalar between 0-1 was multiplied with the peak amplitude before standard deviations were added. The inclusion of the Noisy GSA dataset was to test the ability of FiPP to remove complex artifact which is occasionally observed in our data. In both test datasets, the peak timing is randomized for a few peaks in some as this was common to all subjects. Both datasets were recentered on the mean of channels to which the GSA was added.

2.4.4 Pipeline validation

Unprocessed clinical iEEG data were reviewed, and a channel containing IED events (the “spiking channel”) was selected for further analyses and validation purposes. Each of the test GSA datasets described in 2.3.3 were subjected to both FiPP as well as a 7-epoch AAS to determine whether FiPP can remove the GSA and furthermore also remove the GSA better than AAS alone.

2.4.4.1 Analysis - IED channel comparison

In order to evaluate morphological changes to the signal, direct comparisons of the clinical iEEG trace and trace of the test datasets after artifact removal by each of the two cleaning methods,

AAS alone or FiPP, Pearson's r was calculated. The use of Pearson's r allowed for a determination of whether the cleaning method allowed residual GSA to significantly alter the morphology of the signal relative to the clinical iEEG. The calculated r values will provide an indication at the individual level regarding whether the trace cleaned using AAS alone or the trace cleaned using FiPP is more similar to the clinical iEEG, an additional step must be taken to determine if one of these two methods performs a superior artifact removal at the group level. Through the use of a t-test of the r values from AAS alone and FiPP for all participants such a comparison is possible in an indirect manner. If it is determined that the means of the r values are significantly different, it is likely that the use of FiPP more accurately removes GSA and results in cleaned iEEG data more similar to the clinical iEEG.

2.4.4.2 Analysis - IED spectral comparison

A 5-second epoch was created around one IED from the pre-selected spiking channel. Using a short-time Fourier transform over the selected epoch, frequency power spectrograms were generated for each of the test datasets, as well as for the unaltered clinical iEEG dataset. Differences between the spectral power of the test datasets from each cleaning method and the clinical iEEG data were identified by subtracting the test epoch from the clinical iEEG epoch and maps were visually inspected for similarities.

To further interrogate the spectral differences of the datasets, the percent change in the average power in each of the frequency bands delta (0.5-4 Hz), theta (4-8 Hz), alpha (8-13 Hz), beta (13-30 Hz), gamma (30-80 Hz), ripples (80-250 Hz), fast ripples (250-500 Hz)[65] over the whole spiking channel between the clinical iEEG dataset and each of the test datasets was calculated (see Equation 2.1). Percent change values indicate how different a new value is from the original value with zero being ideal. The use of percent change will indicate either how much artifact remains in the signal after GSA removal (percent change is positive) or how much signal is erroneously removed with the GSA (percent change is negative). In order to determine if percent change is driven by the GSA removal method, a group level comparison must be made. By comparing the percent change values within each frequency band and test dataset pairing for the ten

participants using t-tests an indirect determination of which artifact removal method results in iEEG that is more similar to the original clinical iEEG in terms of each frequency band can be made, thereby indicating the superior GSA removal method.

Equation 2.1: Precent change equation.

$$Percent\_Change = \frac{x_2 - x_1}{x_1} \times 100$$

2.5 Results

2.5.1 Participants

All ten participants were included in this study. Three patients were female, all were right-handed, and the average age was 32.5 (range = 22-49). All participants had temporal lobe epilepsy with an average disease duration of 20.2 years (range = 10-34) and an average seizure frequency of 29.3 (range = 3-120) per month. Full participant demographics can be found in Table 2.1.

Table 2.1: Participant demographics. Abbreviations: bFLE bilateral frontal lobe epilepsy, bTLE bilateral temporal lobe epilepsy, FA focal aware, FIA focal impaired awareness, FTBTC focal to bilateral tonic clonic, GTC generalized tonic clonic, LHE left hemispheric epilepsy, LTLE left temporal lobe epilepsy, MO month, PID patient ID, RFLE right frontal lobe epilepsy, ROFTE right orbitofrontotemporal epilepsy, RTLE right temporal lobe epilepsy, SMA supplementary motor area.

PID	Age at Study	Sex	Handedness	Onset Age	Seizure Type	Seizure Frequency (MO)	Seizure Onset Zone	Diagnosis	Noted Lesion	Previous Surgery
1	49	Male	Right	25	FA, FIA, FTBTC	4	Left Temporal Lobe	LTLE	No	Yes
2	42	Male	Right	19	FTBTC	3	Left Insula	LTLE	No	No
3	24	Female	Right	11	FA, FIA, FTBTC	30	Bilateral SMAs	bFLE	No	No
4	23	Male	Right	11	Absence, GTC	15	Left Temporal Lobe	LHE	No	No
5	22	Male	Right	12	FA, FIA, FTBTC	50	Right Temporal Lobe	RTLE	No	No
6	30	Male	Right	0	FA, FIA, FTBTC	5	Left Temporal Lobe	LTLE	No	No
7	30	Female	Right	16	FIA, FTBTC	18	Right Frontotemporal Lobe	RFLE	No	No
8	31	Male	Right	15	FA, FIA, FTBTC	120	Right Temporal Lobe	ROFTE	Yes	No
9	40	Male	Right	6	FIA, FTBTC	6	Left Hippocampus	bTLE	Yes	No
10	34	Female	Right	8	FA	42	Right Orbitofrontal Lobe	RFLE	No	No

2.5.2 EEG epoch selection

Table 2.2 summarizes all parameters for epoch selection as well as the location of the spiking channel. The number study channels ranged from 46-60, study clip lengths were 10 min (400 TRs) for 7 subjects and 5 min (200 TRs) for three. Indicated in this table is the artifact free comparator, which is the epoch used by FiPP during GSA removal as well as the test epoch which is an epoch containing a spiking event used in the spectral analysis.

Table 2.2: Study dataset parameters. Abbreviations: LA left amygdala, LAH left anterior hippocampus, LMO left mesial occipital, LPTP left posterior temporal parietal, PID patient ID, RAI right anterior insula. RAST right anterior and superior temporal gyrus, RMC right middle cingulate, RMF right mesial frontal, RPM right premotor, RPM right premotor area, RSMA right supplementary motor area.

	Original Data Parameters			Test Parameters							
SID	Clinical Sampling Rate (Hz)	Number of Clinical Channels	Clinical Clip Length	Study Sample Rate (Hz)	Number of Study Channels	Study Clip Length	TR (s)	Number of TR	Artifact Free Comparator Span (s)	Spiking Channel	Test Epoch Span(s)
1	2000	90	10m13s	10000	46	10m00s	1.5	400	542-547	LA1	218-223
2	2000	91	6m24s	10000	46	5m00s	1.5	200	82-87	RSMA5	20-25
3	2000	95	10m02s	10000	57	10m00s	1.5	400	423-428	RPM4	356-361
4	2000	90	11m10s	10000	52	10m00s	1.5	400	127-132	LPTP5	514-519
5	2000	96	10m02s	10000	56	10m00s	1.5	400	112-117	RAST1	160-165
6	2000	53	10m45s	10000	53	10m00s	1.5	400	65-70	LAH2	404-409
7	2000	87	10m46s	10000	58	10m00s	1.5	400	250-255	RMF3	21-26
8	2000	123	10m25s	10000	60	10m00s	1.5	400	79-84	RAI6	193.5-198.5
9	1000	108	6m42s	10000	60	5m00s	1.5	200	29-34	LMO4	173-178
10	1000	112	9m05s	10000	52	5m00s	1.5	200	21-26	RMC1	103-108

2.5.3 Spiking channel correlations

For each spiking channel, Pearson's r was calculated to evaluate the similarity of the signal before and after GSA removal. Figure 2.1 shows an epoch of clinical iEEG data before and after the introduction of GSA, and its subsequent removal using AAS (top row) or FiPP (bottom row). Pearson's r correlation value calculations were made for each participant, for each of the five test datasets, and for both GSA removal methods. These correlation values can be seen in Table 2.3.

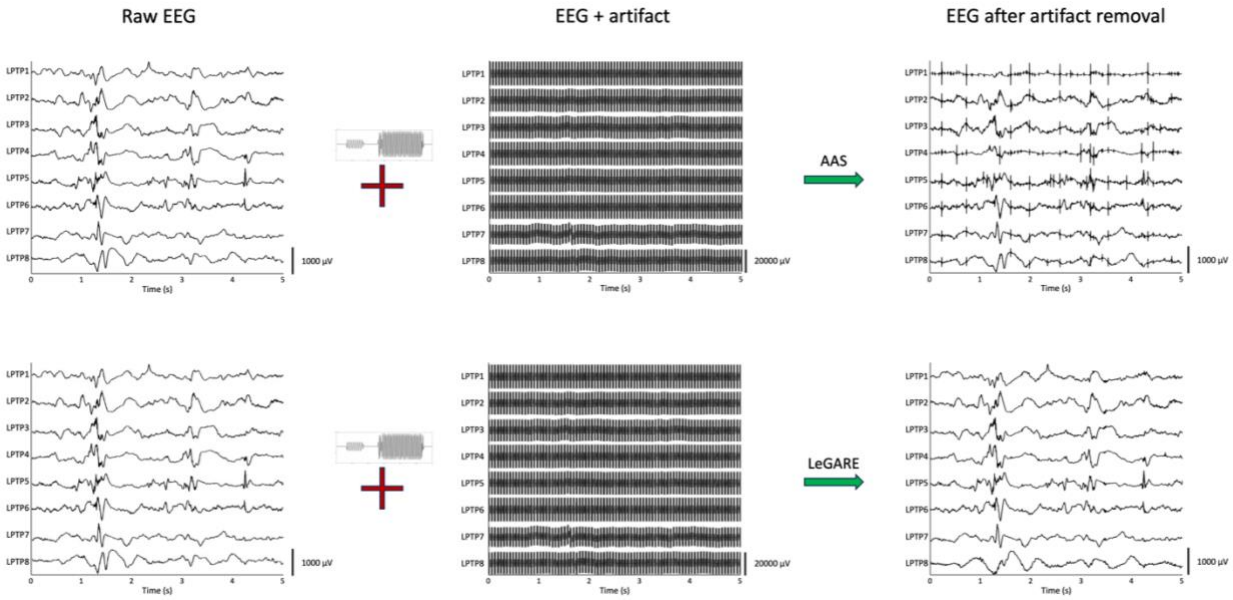

Figure 2.1: Artifact removal processing testing. Sample of artifact free clinical iEEG recorded during the patient's pre-surgical planning before and after introduction of GSA removal using AAS (top row) or LeGARE (bottom row). In both cases, realistic GSA was added to clinical iEEG.

To determine whether GSA is better removed by using AAS alone or by using FiPP, t-test comparisons of the correlation values were employed. At the participant level, there were no significant differences for all five datasets between the use of AAS or FiPP. At the group level, however, significant differences were found between the use of AAS and FiPP when considering each type of GSA separately. The largest significant differences were found between the AAS and FiPP cleaned No GSA Added datasets ($t(11) = 3.18$, $p < 0.01$) and the AAS and FiPP cleaned Chirp artifact datasets ($t(11) = 2.20$, $p < 0.01$). The difference found between No GSA Added datasets is particularly interesting: eight of the ten FiPP cleaned datasets had perfect correlations with the clinical iEEG, with two participants, 5 ($r = 0.99$) and 8 ($r = 0.97$), approaching a perfect correlation. This was the expected result for both GSA removal methods as there was no artifact to remove. Of the datasets cleaned with AAS alone however, only 1 (participant 1) had a perfect correlation, with participants 9 ($r = 0.98$) and 10 ($r = 0.98$) having near perfect correlations. While the remaining 7 correlations were high ($r > 0.90$), these results were lower than expected, suggesting that AAS alone may add artifact to the data. Significant differences were also found between the use of AAS and FiPP for artifact removal for the True GSA ($t(11) = 2.10$, $p < 0.05$) and the Noisy

GSA ($t(11) = 2.20$, $p < 0.05$) but not for the Realistic GSA ($t(11) = 2.10$, $p = 0.77$), although the correlation values for these datasets were low.

Table 2.3: Correlation values between the clinical iEEG and each test artifact dataset after GSA removal by either AAS alone or LeGARE. Abbreviation: PID patient ID.

PID	No GSA Added		Chirp Artifact		True GSA		Realistic GSA		Noisy GSA	
	AAS Cleaned	LeGARE Cleaned	AAS Cleaned	LeGARE Cleaned	AAS Cleaned	LeGARE Cleaned	AAS Cleaned	LeGARE Cleaned	AAS Cleaned	LeGARE Cleaned
1	1	1	0.92	1	0.01	0.08	0.23	0.26	0.04	0.04
2	0.93	1	0.93	1	0.02	0.68	0.92	1	0.23	0.67
3	0.95	1	0.94	1	-0.01	-0.04	0.16	0.19	0.03	0.11
4	0.92	1	0.92	1	0.02	0.59	0.32	0.36	0.09	0.18
5	0.93	0.99	0.93	0.99	0.03	0.26	0.92	0.99	0.3	0.6
6	0.92	1	0.92	1	0.02	0.77	0.61	0.68	0.16	0.43
7	0.92	1	0.92	1	0.06	0.64	0.46	0.51	0.17	0.2
8	0.92	0.97	0.92	0.97	0.01	0.13	0.25	0.21	0.04	0.16
9	0.98	1	0.98	1	0.02	0.9	0.89	0.99	0.12	0.71
10	0.98	1	0.98	1	-0.06	-0.68	0.96	0.99	0.14	0.78

2.5.4 Spectral analyses

Spectral analyses of the test epoch were generated for 0.1 – 50 Hz and 51 – 250 Hz from a FiPP cleaned Realistic GSA dataset (shown in Figure 2.2C and D) for one channel. Figure 2.2G and H show the difference between the spectral analyses of the FiPP cleaned dataset (shown in Figure 2.2C and D) and the clinical iEEG data (shown in Figure 2.2E and F). The spectral differences shown in Figure 2.2G and H indicate how different the FiPP cleaned dataset is from the clinical iEEG at each frequency and each point in time. Blue areas in Figure 2.2G suggest that FiPP has removed meaningful signal in the range of 0.5 – 30 Hz at ~ 3.15 and 4.25 s. The red area in Figure 2.2H suggests that FiPP failed to remove GSA in the range of 51 – 120 Hz range at ~ 4.25 s.

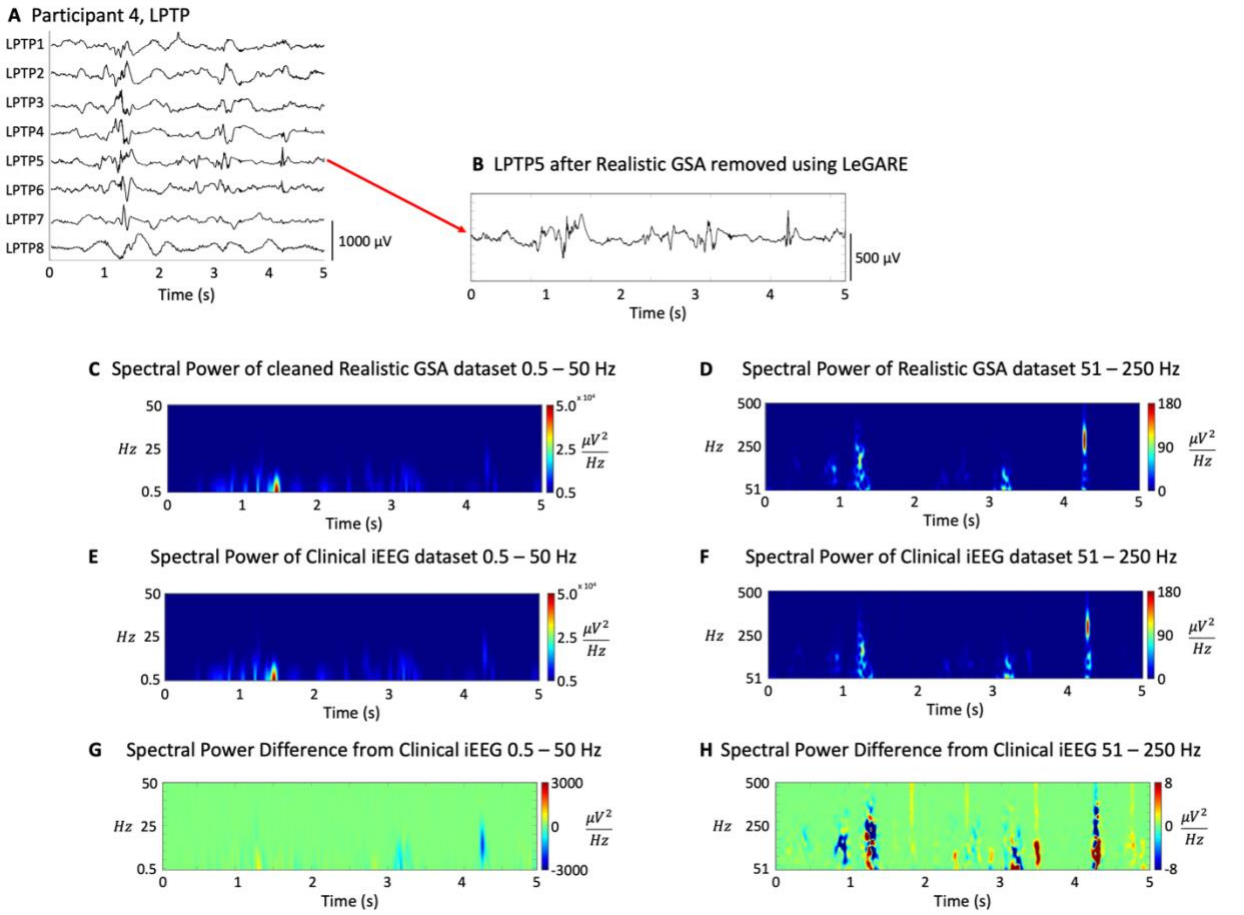

Figure 2.2: Spiking channel spectral analysis. A) Sample of iEEG electrode LPTP from realistic GSA dataset after cleaning with LeGARE. B) EEG trace of the test epoch of the selected spiking channel LPTP5. The spectral power of LPTP5 from 0.5 – 50 Hz (C) and 51-250 Hz (D) from the realistic GSA dataset cleaned using LeGARE over the test epoch. The difference between the spectral power of LPTP5 from 0.5 – 50 Hz (E) and 51-250 HZ (F) from the realistic GSA dataset cleaned using LeGARE and the clinical iEEG.

Figure 2.3 shows the spectral analysis for all datasets for the patient shown in Figure 2.2. Visual inspection of the spectral analyses, and the differences from these analyses and the clinical iEEG, show that the artifact removal using AAS is not as effective as artifact removal using FiPP (Figure 2.3 fourth and sixth columns). This is particularly notable in the higher frequency bands (ripples and fast ripples) where AAS leaves noise that could make it more difficult to reliably distinguish clinically relevant signal. In addition, the use of AAS increased spectral power throughout the epoch in the low frequency range (delta, alpha) and either removed spectral power or failed to remove GSA from the high frequency ranges (ripples, fast ripples). Using FiPP however, more noise was removed across all spectral bands, which would likely result in easier differentiation of

clinically relevant events. Similarly, another dataset from participant 10 had increased noise in lower frequencies using AAS alone (Figure 2.4, fourth column). In the higher frequencies AAS reduced spectral power about t = 1.5 s and it failed to fully remove the GSA (Figure 2.4, sixth column). On the other hand, artifact removal using FiPP showed decreased differences from clinical iEEG data in comparison to AAS alone with more noise being removed in the lower and higher frequencies (Figure 2.4, fourth and sixth column).

2.5.4.1 Spectral band comparison

Percent changes were calculated for each frequency band between the clinical iEEG data and the test datasets (Table 2.4). To determine whether AAS or FiPP produced datasets more similar to the original clinical iEEG datasets, these percent changes were compared using t-tests. Of the 35 comparisons shown in Table 2.3, FiPP cleaned EEG had smaller changes from the clinical iEEG than the AAS cleaned EEG in all but four cases. Furthermore, these changes were significant for 15/35 cases (42%).

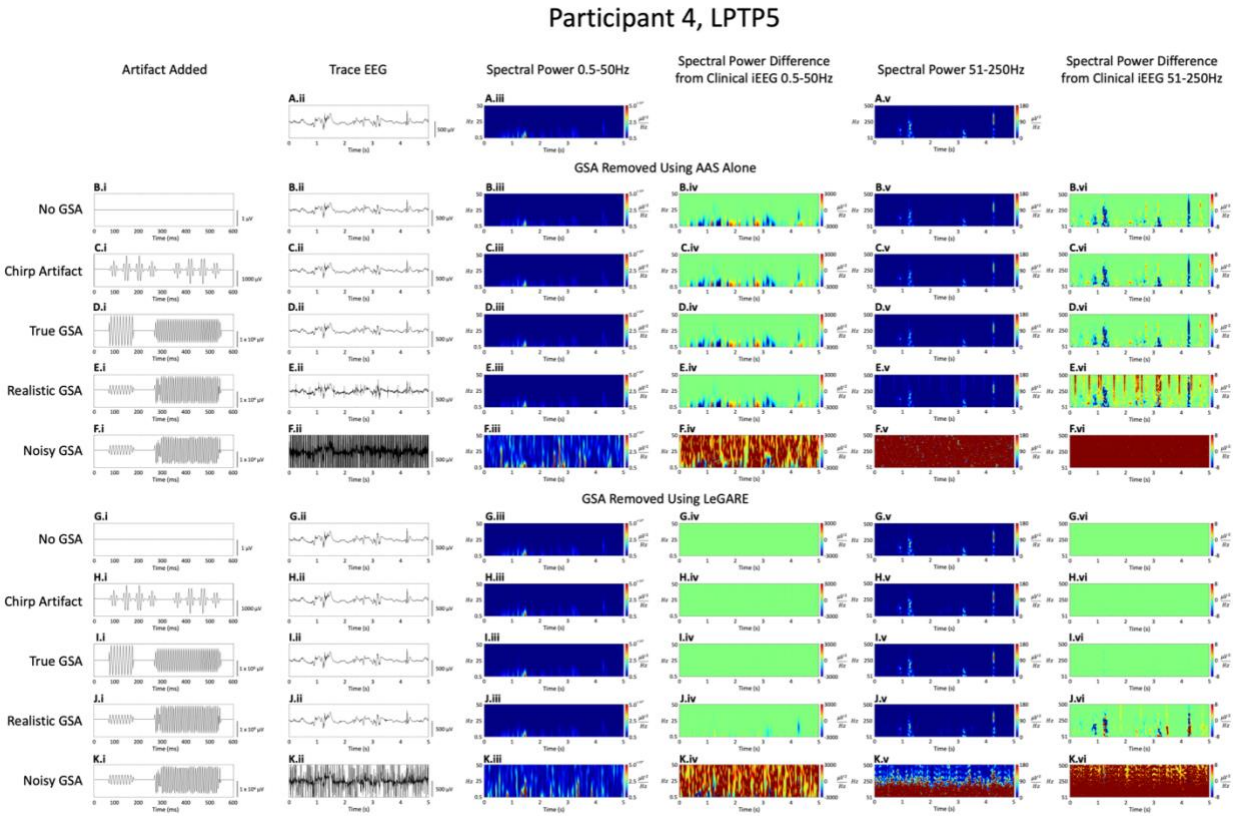

Figure 2.3: iEEG trace and spectral plots for Participant 4, electrode contact LPTP5. Plots: i, first column) Diagram of the artifact added to the clinical iEEG to create the testing condition for GSA removal method testing. ii, second column) EEG trace of the test epoch in the testing condition after artifact removal. iii, third column) The spectral analysis of LPTP5 from 0.5 – 50 Hz of the test epoch in the testing condition after artifact removal. iv, fourth column) The difference between the spectral power of LPTP5 from 0.5 – 50 Hz from the test epoch in the testing condition after artifact removal and the spectral power of the clinical iEEG. v, fifth column) The spectral power of LPTP5 from 51 – 250 Hz of the test epoch in the testing condition after artifact removal. vi, sixth column) The difference in spectral power of LPTP5 from 51 – 250 Hz from the test epoch in the testing condition after artifact removal and spectral power of the clinical iEEG. Testing Conditions: A) Clinical iEEG no testing; ground truth comparator. B) No GSA Added, AAS. C) Chirp Artifact Added, AAS. D) True GSA, AAS. E) Realistic GSA, AAS. F) Noisy GSA, AAS. G) No GSA Added, LeGARE. H) Chirp Artifact Added, LeGARE. I) True GSA, LeGARE. J) Realistic GSA, LeGARE. K) Noisy GSA, LeGARE.

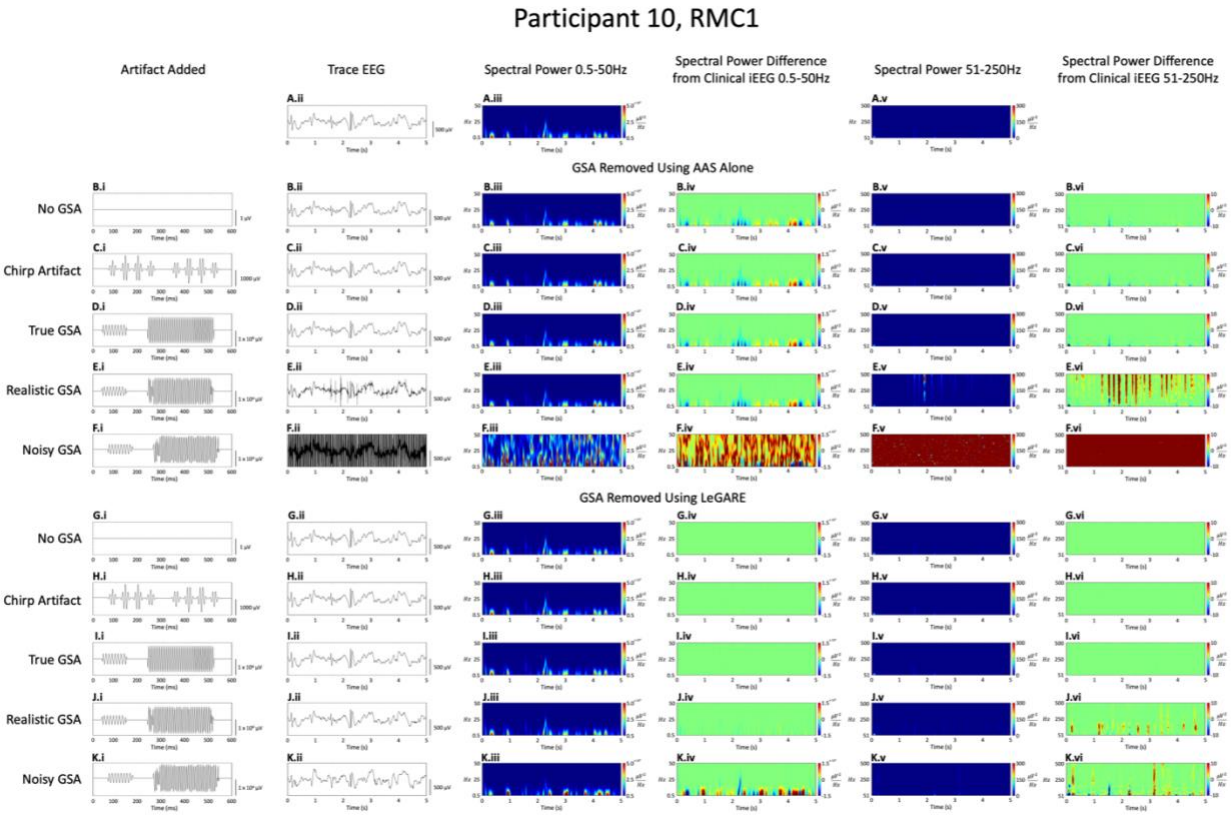

Figure 2.4: iEEG trace and spectral plots for Participant 10, electrode contact RMC1. Plots: i, first column) Diagram of the artifact added to the clinical iEEG to create the testing condition for GSA removal method testing. ii, second column) EEG trace of the test epoch in the testing condition after artifact removal. iii, third column) The spectral analysis of LPTP5 from 0.5 – 50 Hz of the test epoch in the testing condition after artifact removal. iv, fourth column) The difference between the spectral power of LPTP5 from 0.5 – 50 Hz from the test epoch in the testing condition after artifact removal and the spectral power of the clinical iEEG. v, fifth column) The spectral power of LPTP5 from 51 – 250 Hz of the test epoch in the testing condition after artifact removal. vi, sixth column) The difference in spectral power of LPTP5 from 51 – 250 Hz from the test epoch in the testing condition after artifact removal and spectral power of the clinical iEEG. Testing Conditions: A) Clinical iEEG no testing; ground truth comparator. B) No GSA Added, AAS. C) Chirp Artifact Added, AAS. D) True GSA, AAS. E) Realistic GSA, AAS. F) Noisy GSA, AAS. G) No GSA Added, LeGARE. H) Chirp Artifact Added, LeGARE. I) True GSA, LeGARE. J) Realistic GSA, LeGARE. K) Noisy GSA, LeGARE.

2.6 Discussion

The complete removal of the GSA is essential for the proper analysis of iEEG-fMRI data. Given the nature of this artifact, however, complete removal is challenging. Traditional methods of GSA removal rely on the use of AAS alone which often results in incomplete artifact removal, particularly in the higher frequency bands (ripples, fast ripples) making research or clinical

analyses at these bands difficult. The development of a new GSA removal process that does not rely solely on AAS is critical to help iEEG-fMRI evolve further.

Table 2.4: Percent changes in each of the spectra power bands between the clinical iEEG and each test artifact dataset after GSA removal by either AAS alone or LeGARE. Standard error in brackets.

Frequency Band		No GSA Added	Chirp Artifact	True GSA	Realistic GSA	Noisy GSA
Delta	AAS	-12.48 (1.40)	-13.89 (0.22)	20.03 (14.99)	-11.68 (0.88)	348.34 (123.24)
	LeGARE	3.14 (4.06)	-0.61 (0.57)	33.78 (14.46)	-0.39 (1.68)	366.59 (129.71)
	p-value $t(18) = 2.10$	< 0.05 *	< 0.001 ***	0.51	< 0.001 ***	0.92
Theta	AAS	-13.20 (1.49)	-14.76 (0.29)	77.18 (85.97)	-14.74 (0.28)	2104.52 (912.88)
	LeGARE	-4.89 (3.98)	-5.05 (3.96)	0.96 (0.48)	-15.21 (8.80)	1552.86 (682.63)
	p-value $t(18) = 2.10$	0.07	< 0.05 *	0.38	0.96	0.63
Alpha	AAS	-12.84 (1.44)	-14.24 (0.19)	134.93 (83.84)	-14.22 (0.19)	5804.67 (2042.10)
	LeGARE	-3.15 (8.54)	-3.36 (8.54)	0.37 (0.19)	-8.85 (10.46)	4203.31 (2080.01)
	p-value $t(18) = 2.10$	0.28	0.22	0.13	0.61	0.59
Beta	AAS	-2.93 (9.71)	-12.69 (1.42)	5.78×10^5 (2.41×10^5)	-12.63 (1.36)	2.25×10^4 (9488.34)
	LeGARE	1.58 (3.99)	1.46 (4.00)	0.67 (0.35)	-9.44 (9.56)	1.68×10^4 (9960.65)
	p-value $t(18) = 2.10$	0.67	< 0.05 *	< 0.05 *	0.74	0.68
Gamma	AAS	-10.65 (2.41)	-14.25 (0.14)	3.46×10^5 (1.85×10^5)	14.61 (12.33)	5.83×10^5 (3.30×10^5)
	LeGARE	0.01 (0.02)	-0.39 (0.30)	1.60 (0.73)	1.60 (7.37)	1.97×10^5 (1.57×10^5)
	p-value $t(18) = 2.10$	< 0.001 ***	< 0.001 ***	0.08	0.38	0.30
Ripples	AAS	-11.57 (1.61)	-13.10 (1.00)	6.27×10^6 (2.89×10^6)	5050.55 (2472.10)	1.66×10^7 (8.24×10^6)
	LeGARE	-0.01 (0.007)	-0.98 (0.73)	9.19 (3.92)	312.40 (162.46)	6.32×10^6 (5.35×10^6)
	p-value $t(18) = 2.10$	< 0.001 ***	< 0.001 ***	< 0.05 *	0.07	0.31
Fast Ripples	AAS	-12.49 (1.40)	-10.37 (1.11)	4.16×10^7 (1.39×10^7)	9.03×10^4 (3.83×10^4)	5.81×10^7 (2.39×10^7)
	LeGARE	-0.03 (0.03)	-2.19 (0.54)	266.66 (156.97)	39.64 (44.54)	1.53×10^7 (1.38×10^7)
	p-value $t(18) = 2.10$	< 0.001 ***	< 0.001 ***	< 0.01 **	< 0.05 *	0.14

2.6.1 Channel correlations

Across all datasets, signals cleaned by FiPP were more similar to the clinical iEEG data than those cleaned with AAS. Additionally, both AAS and FiPP removed more of the Chirp artifact and True GSA than Realistic or Noisy GSA. The test datasets that were particularly remarkable were the No GSA Added datasets. No artifact was added to these datasets before they were subjected to either AAS or FiPP. After FiPP processing, the datasets of 8 of 10 participants had perfect correlations with the clinical iEEG data, with the other datasets of the other two participants being near perfect correlations. For datasets cleaned with AAS alone however, only the signal

from participant 1 had a perfect correlation with the clinical iEEG data with the datasets from 2 participants approaching a perfect correlation. The datasets of 7 participants however had correlation values that, while still very high ($r > 0.90$), were a problematic deviation from a perfect correlation given there was no artifact to remove. In light of these results, it is possible that the use of AAS alone may add noise to signals in some cases. FiPP had superior artifact removal capabilities since it did not change the signal morphology at all for 8 of 10 participants and only minimally for the other 2. Furthermore, the overall FiPP-cleaned signals were more similar to the original clinical iEEG data than the AAS-cleaned data.

2.6.2 Spectral analyses

Visual inspection of the spectral decomposition of the signals showed that artifact removal using AAS alone leaves residual GSA in the signal data. It also modified the spectral power of the signal by removing power at spikes or prominent waveforms, or nonuniformly increase power, by either amplifying minor events or creating spurious events. The GSA residual after AAS was particularly notable in higher frequency bands, which is particularly troublesome as the field is moving towards the use of markers in these frequency bands for iEEG-fMRI studies (e.g., high frequency oscillations). However, FiPP does not have the same drawbacks, as there was less noise in the higher frequency bands. This affords easier detection of events or markers in these frequencies, such as can be seen in Figure 2.1.

While some spectral differences do occur between FiPP-cleaned signals and the clinical iEEG data, these differences are much smaller than the differences between AAS-cleaned signals and the clinical iEEG data. The differences between the AAS-cleaned signals and clinical iEEG was particularly stark in the ripples and fast ripples frequency bands. Percent changes in the magnitude of tens of thousands are not typical, and it was results such as these that indirectly prompted the use of a 50-slice AAS in LeGARE. When using a small number of epochs in AAS, such as 7, it is possible that the "average artifact" that will be subtracted will still contain variations which may introduce artifact into the EEG while removing the common artifact. This new artifact can be caused by large events around the epoch or be the result of the averaging

process. As the noise or nuisance signal increases, the "average artifact" calculated will include more variation which are likely to introduce more artifact. This is likely what is responsible for the large values for the percent change between the AAS alone datasets and the clinical iEEG reported in **Table 2.4**. By using a larger number of epochs, or a shorter epoch, these concerns can be mitigated. FiPP employs both of these methods which is likely why the majority of percent change values are much lower than the AAS alone counterparts. For the noisy GSA datasets however, the percent changes for the two methods are very similar which contrasts with the no GSA Added and the Chirp artifact datasets where the majority of comparisons were significant different. This contrast suggests that AAS has limits across all the datasets, but FiPP may have more difficulty cleaning signals as the complexity of the noise increases.

2.6.3 Limitations and future directions

The datasets included in the validation process have provided evidence of how well FiPP can remove GSA for a random dataset compared to AAS. GSA, however, is unique to each subject and electrode. The generated GSAs used in the analyses were relatively consistent despite steps being taken to insert variability into the artifact. A more in-depth analysis could be explored wherein the GSA from the subject's simultaneous iEEG-fMRI data acquisition is replicated in a more direct manner. This could be done by regressing out the FiPP-cleaned, assuming that FiPP is in fact removing the majority of the GSA. Alternatively, a custom GSA could be made for each electrode by mapping the maximal GSA to a template. However, it is possible that this method will fail to reproduce the true slice to slice variability seen in the GSA.

In the spectral analyses, FiPP-cleaned datasets were more similar to clinical iEEG than AAS-cleaned iEEG datasets (Table 2.4). Despite these promising results, limited (42% of cases) significant differences were found between the comparison of the AAS only cleaned and FiPP cleaned datasets and the clinical iEEG. This was likely due to the decision to reduce each EEG band to a single average spectral power. Having one value per frequency band resulted in very small sample sizes, which may have reduced statistical power. Future analyses should attempt to develop better means to verify how well FiPP maintains the spectral power of EEG signals. The

premise of this study, however, was aimed at determining if the trace iEEG was sufficiently similar pre and post artifact addition and removal, limiting direct concerns of the power density of the signal itself. Finally, these analyses were limited to investigating just the artifact removal, a critical step in the complete validation of FiPP, but only the first of many steps needed to make iEEG-fMRI readable for clinicians.

Future research should work to determine clinically relevant events in FiPP-cleaned data. For example, a double-blinded approach to event marking might be considered. This could be achieved by creating two versions of the data: one that was unadulterated and one that had artifact artificially induced and then removed using FiPP. These datasets could then be blinded and given to clinicians to identify IEDs. IED counts between these two datasets could then be compared to see if FiPP removed events (type 1 error) or induced non-existent events (type 2 error). Such an analysis would be an ideal next step in the FiPP validation process. The development and implementation of FiPP represents a novel self-contained iEEG preprocessing pipeline with superior cleaning to all processes previously developed.

2.7 Acknowledgements

This research would not have been possible without the kind, thoughtful, and selfless patients who generously agreed to participate in our research knowing it would help future generations. To them I extend my eternal gratitude. Further, research in healthcare simply is not possible without the dedication and diligent care of our health care allies, including porters, EEG technologists, 3T MR technologists, nurses, fellows, and clinical assistants Drs. Rey Avendano, Mabel Cruz-Bagadiong, Salma Hanna, and Alma Retuta.

2.8 Funding sources

This research was supported by the Canadian Institutes of Health Research (MOP-230809).

2.9 Disclosure

None of the authors have any conflicts of interest to disclose.

3.0 The BOLD response to intracranially recorded interictal discharges

Perry Dykens[1,2], Victoria Mosher[1,2,4], William Wilson[1,2], Daniel J. Pittman[1,2], Laura Gill[2,3], Joseph Peedicail[2,3], Antis G. George[1,2,3], Shuoyue Zhang[7], Bradley Goodyear[1,2,4], Pierre LeVan[1,4,5,6], Paolo Federico[1-4] on behalf of the Calgary Comprehensive Epilepsy Program collaborators

The Calgary Comprehensive Epilepsy Program collaborators are: Yahya Aghakhani, Walter Hader, Nathalie Jetté, Colin Josephson, Karl Martin Klein, William Murphy, Neelan Pillay, Andrea Salmon, Yves Starreveld, Samuel Wiebe.

1 Hotchkiss Brain Institute, Cumming School of Medicine, University of Calgary, Canada
2 Seaman Family MR Research Centre, Cumming School of Medicine, University of Calgary, Canada.
3 Department of Clinical Neurosciences, Cumming School of Medicine, University of Calgary, Canada.
4 Department of Radiology, Cumming School of Medicine, University of Calgary, Canada.
5 Alberta Children's Hospital Research Institute, Cumming School of Medicine, University of Calgary Canada.
6 Department of Pediatrics, Cummings School of Medicine, University of Calgary, Canada.
7 Department of Radiology, Medical Physics, Faculty of Medicine, University of Freiburg, Germany.

3.1 Abstract

Objective

EEG-fMRI uses the timings of interictal epileptiform discharges (IEDs) to create maps of the blood oxygen level dependent (BOLD) response. Typically, only positive IED-associated BOLD responses are considered in localizing the seizure onset zone (SOZ), while largely ignoring the negative response. Recently, it has been suggested that the maximal BOLD response, regardless of polarity, should be used to localize the SOZ. We therefore performed intracranial EEG-fMRI (iEEG-fMRI) to assess the ability of the absolute maximal BOLD response (positive or negative) to localize both IED origin and the SOZ. We also explored the use of additional confidence criteria to select maximal responses with a higher likelihood of being significant.

Methods

Fifty-eight patients underwent an iEEG-fMRI study. The maximal IED-associated BOLD clusters (positive or negative) were identified. Maximal clusters that had much higher z-scores compared to the second maximal clusters were deemed high confidence. The distances from the recorded IEDs or SOZ to the maximum positive and negative BOLD clusters were calculated and used in a linear mixed model to determine significant differences.

Results

From the 58 subjects, 104 Cluster-IED pairs and 82 Cluster-SOZ pairs were identified. Maximal negative clusters were significantly farther from both the IED ($p < .001$) and the SOZ ($p = .017$) than maximal positive clusters. Most absolute maximal clusters were positive (88%), but when the absolute maximal cluster was negative, it was significantly further from the IED generator or SOZ than the maximal positive cluster from the same IED. Additionally, the use of confidence criteria did select for more proximal clusters.

Conclusions

The use of the absolute maximal clusters provides no added benefit over considering just the maximal positive cluster in iEEG-fMRI. Utilizing confidence criteria to positive BOLD maps selects BOLD clusters closer to IED origin and the SOZ, thus increasing the potential clinical utility of iEEG-fMRI.

Key Points:

- Absolute maximal IED-related BOLD response of limited utility in iEEG-fMRI analyses.
- Maximal negative IED-related BOLD response may localize the SOZ or IED in limited cases.
- BOLD response inclusion criteria does select for clusters more proximal to the SOZ or IED in iEEG-fMRI.

Keywords: epilepsy; BOLD; intracranial electroencephalography; functional MRI; EEG-fMRI; interictal epileptiform discharges

3.2 Background

The goal of epilepsy treatment is seizure freedom and for roughly 30% of individuals living with epilepsy, this goal cannot be achieved using anti-seizure medications[10]. These individuals are said to have drug-resistant epilepsy[10], a classification of epilepsy wherein two well-chosen and tolerated medications have failed to control their seizures[36]. Epilepsy surgery may be considered for treatment in these patients; however, the success rate is less than 50%[35], with one of the primary factors being the incomplete resection of the epileptogenic zone (EZ) – the region of the brain necessary and sufficient to generate seizures[168]. The EZ can only be determined post-operatively[168], therefore the seizure onset zone (SOZ), or the region of the brain where seizures are thought to originate, is often used as the surgical target.

Although not currently used during the presurgical work-up, the use of simultaneous EEG and functional magnetic resonance imaging (EEG-fMRI) may be an effective tool in increasing the accuracy of identifying the SOZ. fMRI is commonly used to identify regions of increased neuronal activity through measuring relative changes in the blood oxygen level dependent (BOLD) signal[77]. Specifically, it is the positive BOLD response, or a relative increase in the BOLD signal, that is thought to indicate an increase in neuronal activity[78,82]. Unlike the positive BOLD response, it was thought that the negative BOLD response, a relative decrease in the BOLD signal, was vascular in nature and not reflective of function[169]. Recent studies, however, have begun positing neuronal-based theories of the negative BOLD response, suggesting that negative BOLD signals reflect an inhibition or reduction of brain activity[86,88–90].

Interictal epileptiform discharges (IEDs) can be used as a temporal marker to guide EEG-fMRI analyses allowing identification of brain regions that may be the SOZ [7]. Currently, the utility of the maximal positive BOLD response to IEDs in aiding clinical decisions has been shown in a limited series[128], demonstrating that the positive BOLD response to IEDs may have utility in clinical settings.

It has been suggested that it is not the maximal *positive* BOLD response that identifies the SOZ, but rather it is the *absolute* maximal BOLD response regardless of its polarity[54,149]. This contrasts with studies which have shown that negative BOLD responses can be found in regions of the brain that are often distant, ipsilateral, or even unrelated to the SOZ[89,99,135–142]. Notably, the aforementioned studies employed scalp EEG-fMRI. In the present study, we therefore used intracranial EEG-fMRI to determine whether the absolute maximal BOLD response to IEDs can be used to identify the SOZ. We hypothesized that the maximal positive BOLD responses to IEDs will consistently be closer to the SOZ than the maximal negative BOLD response.

3.3 Methods

3.3.1 Participants

Seventy adult participants with drug resistant focal epilepsy were recruited from patients admitted for pre-surgical inpatient intracranial video-EEG monitoring. Participants were recruited using the following criteria: focal epilepsy, at least 18 years of age, no MRI contraindications, and no severe post-electrode implantation complications (e.g., subdural hematoma, infection, intracranial hemorrhage). This study was approved by the Conjoint Health Research Ethics board of the University of Calgary. Written informed consent was obtained from all participants prior to participation.

3.3.2 Data acquisition

Each participant underwent a simultaneous iEEG-fMRI session which included two structural MRI sequences and up to three 20-minute functional MRI runs, during which EEG data were simultaneously recorded from the participant's implanted electrodes.

EEG data from impatient intracranial video-EEG monitoring were reviewed by two experienced epileptologists (two of P.F., L.G., J.S.P.) who selected up to eight electrodes for use during each participant's simultaneous iEEG-fMRI study. Electrodes were connected to either a custom 2 tailed (subjects 1-7) or 8-tailed intracranial electrode connector allowing up to 20 or 64 channels, respectively, of data collection (Neuroscan, Compumedics, Charlotte NC, USA). EEG data were

recorded at 10 or 20 kHz using a SynAmpsRT amplification/digitalization system and either Scan 4.4 (prior to 2020) or Curry 8 software (Neuroscan, Compumedics, Charlotte NC, USA). For subject 25 and above, the EEG system clock was synchronized to the MRI scanner clock, to ensure that the timing of the gradient switching artifact was at the same point along each transition in the EEG data.

MRI data were collected using either a 3T GE Sigma LX whole body scanner with a receive-only eight-channel phased-array head-receive/body transmit coil (subjects 1-7) or a 3T GE Discovery MR750 whole body scanner equipped with a 12-channel receive-only phased array head coil (GE Healthcare, Waukesha, WI).

The MRI protocol included multi-slice anatomical imaging (spoiled gradient-recalled two-dimensional multi-slice sequence: echo time [TE] = 2.1 ms, repetition time [TR] = 150 ms, flip angle = 18°, 128 × 128 matrix, 24 slices, 0.94 × 0.94 × 5 mm), anatomical three-dimensional T1-weighted imaging (TE = 3.8 ms, TR = 9.3 ms, flip angle = 12°, 24 cm field of view, 320 × 256 × 64 matrix, 0.47 × 0.47 × 2 mm), and fMRI (gradient-recalled echo planar imaging: TE = 30 ms, TR = 1500 ms, flip angle = 65°, 24 cm field of view, 64 × 64 matrix, with 24, 25, or 29 slices, 3.75 × 3.75 × 5 mm).

3.3.3 iEEG processing

Processing of iEEG data collected during the simultaneous iEEG-fMRI exam was performed using the Federico iEEG processing pipeline as described previously (chapter 2). Processes in this pipeline include channel rejection, within-electrode average re-referencing, a 2^{nd}-order Butterworth high-pass filter at 0.1 Hz and a 2000^{th}-order FIR low-pass filter at 500 Hz, a channel-by-channel slice-wise average artifact subtraction, and a modified PCA. Following artifact removal, channel data were decimated to a sampling rate of 2500 Hz.

3.3.4 IED marking and contact selection

Acquired iEEG data were reviewed by two qualified epileptologists (two of Y.A., P.F., L.G., C.J., K.M.K., J.S.P., A.S., S.S.) who identified the timing and morphology of the IEDs as well as the contact where they occurred. Discrepancies were reviewed and resolved in-person by both reviewers. IEDs were grouped according to location and morphology with each distinct group deemed a separate IED type.

For each IED type, the channel(s) with maximal amplitude in the referential montage and/or phase reversal in the bipolar montage were defined as the most active electrode contact(s). Up to three contacts were identified using these criteria, in some cases on separate electrodes. The anatomical coordinates of these contact(s) were determined visually using FSLView (3.2.0), and the geometric centre of those coordinates was calculated as a proxy.

3.3.5 fMRI data processing

All fMRI data processing was completed using the FMRIB Software Library (Functional Magnetic Resonance Imaging of the Brain Software Library, Oxford, England)[170–172]. Preprocessing steps included: standard brain extraction, motion correction, slice-timing correction, anatomical registration, high-pass temporal filtering (sigma = 50 s), and 6.0 mm Gaussian kernel spatial smoothing. Datasets with motion exceeding 1.5 mm were split in 2 segments after removing the frames containing the excessive motion. This process was performed recursively, and any segment less than 5-minutes was removed from analysis. To remove artifact, an ICA was used to decompose each dataset into 60 components. These components were visually inspected by 2 reviewers (VM, WW) who identified components attributed to noise or artifact and these signals were regressed from the data[173,174]. Discrepancies were reviewed and resolved in-person by both reviewers.

3.3.6 fMRI statistical analysis

For each IED type in each patient, four hemodynamic response functions (time to peak offsets of 3, 5, 7, and 9 seconds) were convolved with the onset timings of these events to create models

of the predicted fMRI time course for each of these hemodynamic delays. Statistical analyses of these models were performed using FEAT (FSL Expert Analysis Tool) and FILM (FMRIB Improved Linear Model) with local autocorrelation correction for each run[175]. A statistical average of each fMRI run was generated using FLAME (FMRIB Local Analysis of Mixed Effects), employing a fixed effects model, forcing the random effects variance to zero[176]. Maps of statistically significant BOLD signal changes (BOLD response maps) using cluster correction with a cluster z threshold of $z > \pm 3.1$ and a cluster *p* threshold of .01, were generated for each convolved hemodynamic response function. Similar to established methods in the literature[125,138,155,159,177,178], the four z-score threshold maps generated were amalgamated into a single cluster map. To create this map, the highest z-score for each voxel location from amongst the four z-score maps was selected as that voxel location's z-score. Cluster descriptive statistics (e.g., center of gravity, max z-score, extent) were generated for the final amalgamated cluster map using FSL cluster[170–172].

3.3.7 Electrode pairing and cluster selection

Some participants included in the study had multiple IED generating regions and multiple potential SOZs. Since both the IED generating regions and the clinically determined SOZs are potential markers of the epileptogenic zone, we measured the distances between the IED-associated BOLD clusters and i) IED contacts and ii) SOZ contacts as determined by ictal EEG recordings from video-iEEG monitoring. Additionally, for the SOZ studies, IED types and SOZs were paired based on their proximity to each other, pairing first based on shared electrodes and then on nearest electrode pairs. Importantly, each IED type and SOZ could not be included in more than one pair. All unpaired IEDs or SOZs were removed from further analysis.

For each analysis, the BOLD cluster with the highest positive and highest negative z-score were identified and deemed the maximal positive and maximal negative BOLD response, respectively. Of these clusters, the one with the largest absolute z-score was selected as the absolute maximal BOLD response. Clusters that were outside of the brain or in white matter were rejected as these clusters were not predictive of the SOZ.

3.3.8 Confidence testing

We stratified our fMRI data using the recent concept of confidence testing[125] which aims to identify maps where the maximal cluster has a much higher z-score than the second maximal cluster. Under this test, a cluster must have 5 contiguous voxels, a z-score $\geq$ 3.1, and satisfy the inequality in equation 3.1 (second max z-score assumed to be zero if there is no second significant cluster) [125,149]. Clusters that have a high confidence are suggested to have a higher chance of being concordant with the SOZ, potentially increasing the clinical yield of these maps. In order for an absolute maximal cluster to have high confidence, it had to meet an additional requirement: the absolute maximal cluster must have a much higher z-score than the other maximal z-score. Thus, the absolute maximal cluster was subjected to the test again with the alternative maximal cluster being used as the second maximal z-score.

Equation 3.1: Test of cluster high confidence

$$|z_1| \times 0.025 + (|z_1| - |z_2|) \times 0.080 > 0.302$$

z_1: z-score of the maximal cluster
z_2: z-score of the second maximal cluster

3.2.9 Distance measurements

The distance between the geometric centre of the most active contact(s) for each IED type and the maximal voxel of the identified BOLD clusters were calculated using the 3D geometric distance formula (see *Equation 3.2*). This calculation was repeated to measure the distance from the geometric centre of a clinically defined SOZ to the maximal voxel of the identified BOLD clusters. The SOZ was defined as those contacts involved in ictal onset during video-iEEG monitoring.

Equation 3.2: 3D distance equation

$$Distance_{12} = \sqrt{(x_2 - x_1)^2 + (y_2 - y_1)^2 + (z_2 - z_1)^2}$$

3.3.10 Statistical calculations

Statistical testing was performed using SPSS Statistics version 28.0.1.0 (IBM, Armonk, NY). The data were tested for normality using the Shapiro-Wilk test prior to performing any statistical

testing. While many subsets of the data were normally distributed, the variables within the full dataset were not normally distributed. Consideration, however, was given to the nature of the data as well. In simultaneous iEEG-fMRI studies it is common for a single participant to have multiple IED types and SOZs. Should a participant have two of each, there is a potential for four repeated measures from this participant. This problem is often resolved by considering each IED type and SOZ as independent. This however ignores any potential influence the models of these IED types might have on one another during the fMRI analyses. For this reason, a fixed effects linear mixed model with a post-hoc Sidak correction for multiple comparisons was used to test for significant differences between the maximal positive BOLD cluster to IED contacts distances and the maximal negative BOLD response to IED contact distances. In this model, the cluster polarity and the IED type or SOZ number were input as the factor of the model. In instances where the model could not converge due to low sample sizes (< 50), the IED or SOZ clinical ranking was removed to account for the decreased variance.

Differences between the distances from the BOLD clusters to IEDs were tested considering: (1) all maximal clusters, (2) only IEDs that generated both a positive and a negative BOLD response (paired clusters), (3) all absolute maximal BOLD clusters, and (4) only absolute maximal BOLD clusters from IEDs that generated both a maximal positive and a maximal negative BOLD cluster. These 4 groups were compared first using all clusters that met the group criteria, and then with only those clusters that met the criteria for high confidence. For the absolute maximal clusters, we were interested in the difference in z score between the absolute maximal cluster and its corresponding non-absolute, opposite polarity cluster. Thus, the dataset will be split into four categories: absolute maximal positive clusters, non-absolute maximal negative clusters, absolute maximal negative clusters, and non-absolute maximal positive clusters. The relationships between these four groups will be explored. All statistical tests were repeated for cluster-SOZ pairs.

3.4 Results

3.4.1 Participant characteristics

All seventy participants were monitored by a physician during simultaneous iEEG-fMRI data acquisition and no ictal or adverse events occurred. Of the 70 participants, 5 were excluded due to incomplete removal of gradient switching artifact from the iEEG, 5 were excluded from the analysis as they had < 5.0 minutes of fMRI data after artifact and motion correction, and 2 participants failed to produce statistically significant BOLD clusters ($z > 3.1$). Following these exclusions, 58 participants remained in the study, with the following demographics: female 46.6%, average age 35.30 years (range = 20-64 years), disease duration 2-53 years, seizure frequency 1-210 per month, temporal lobe epilepsy 69.0%, lesional MRI scans 39.7%. Full participant demographics are detailed in Supplementary Table 3.1.

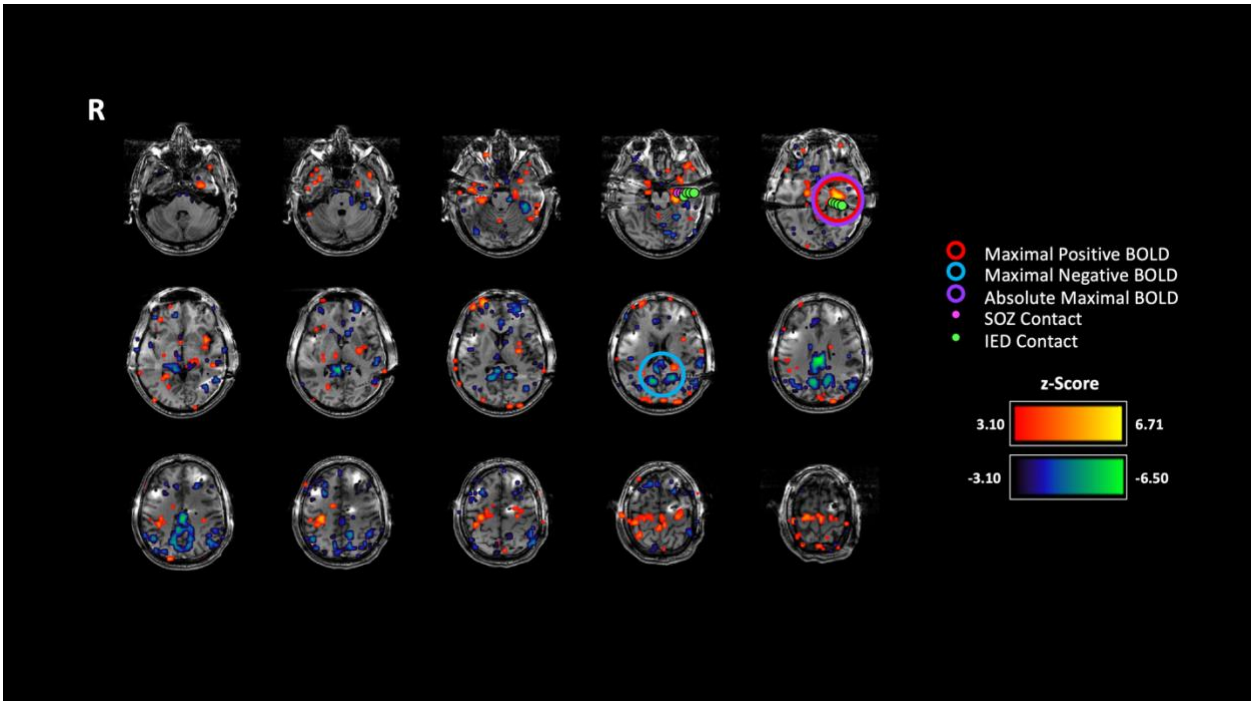

Figure 3.1: iEEG-fMRI results for participant 38. This exemplar demonstrates the typical finding of the maximal positive BOLD cluster being proximal to both the IED and SOZ EEG electrode contacts and the maximal negative BOLD cluster being distal to both. Additionally, for this subject, the maximal positive BOLD cluster was also the absolute maximal cluster which was the most common configuration in the cohort.

3.4.2 Cluster selection

The average number of IEDs identified per IED type was 468 (range = 5-2596) with participants having between 1-5 IED types and 1-4 SOZs. IED types 4 and 5 were excluded from analysis as the sample size was too small to reach statistical significance. With removal of these IED types, 104 Cluster-IED studies were identified comprising 54 which generated both positive and negative BOLD clusters, 47 studies that generated only positive BOLD clusters, and 3 that generated only negative BOLD clusters. After SOZ-IED pairing, 82 Cluster-SOZ studies were identified. 45 generated both positive and negative BOLD clusters, 35 of these studies generated only positive BOLD clusters, and 2 generated only negative BOLD clusters. A representative example of IED-associated BOLD activation maps can be found in Figure 3.1. A summary of data organization and parcellation for analysis is shown in Figure 3.2 and a summary of the EEG-fMRI data can be found in Supplementary Table 3.2.

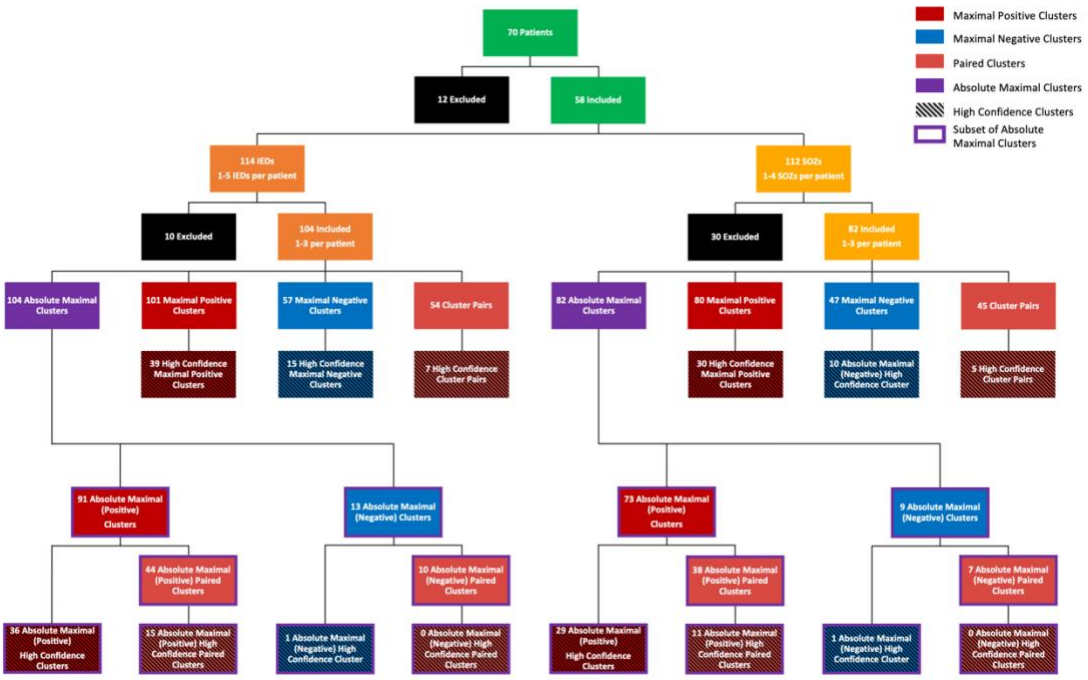

Figure 3.2: Hierarchy of data parcellation. This chart provides a breakdown of how data is grouped for statistical testing. The left side of the chart details BOLD clusters in relation to the EEG electrode contact that generated the IED and the right side of the chart details BOLD clusters in relation to the EEG electrode contact involved in the seizure onset.

3.4.2.1 Cluster-IED analyses

Figure 3.3 summarizes the results of the BOLD cluster-IED analysis. The polarity of the cluster was determined to be a significant main effect in the distance from cluster to IED contact ($p < .001$). Post-hoc pairwise testing using a Sidak correction revealed that the maximal positive clusters ($\bar{x}$ = 49.35 mm, σ = 34.87 mm, n = 101) were significantly closer to the IED ($p < .001$) than the maximal negative clusters ($\bar{x}$ = 75.21 mm, σ = 26.92 mm, n = 57, Figure 3.3A). Only 39 maximal positive clusters and 15 maximal negative clusters met the criteria for the high confidence. When considering only the high confidence clusters, the average distance from maximal positive cluster to the IED contact was 55.44 mm (σ = 26.92 mm) and from maximal negative to IED was 78.58 mm (σ = 26.88 mm). Cluster polarity was a significant main effect in the model ($p < .001$) with the maximal negative clusters being significantly farther from the IED contact than the maximal positive clusters ($p < .001$, Sidak corrected, Figure 3.3B).

Fifty-four Cluster-IED studies produced both positive and negative clusters. Within these studies, cluster polarity was a significant factor ($p = .032$) with the maximal positive clusters ($\bar{x}$ = 55.09 mm, σ = 26.88 mm) being significantly closer ($p = .032$, Sidak corrected) to the IED than the maximal negative clusters ($\bar{x}$ = 75.90 mm, σ = 26.52 mm, Figure 3.3C). Only 7 of these pairs met the criteria for high confidence. The average distance from the high confidence maximal negative clusters to the IED was 68.76 mm (σ = 28.66 mm) and for the high confidence maximal positive clusters 46.61 mm (σ = 37.72 mm). The high confidence maximal positive clusters were significantly closer ($p < .001$, Sidak corrected, Figure 3.3D), but IED type had to be removed as a model factor due to the limited sample size.

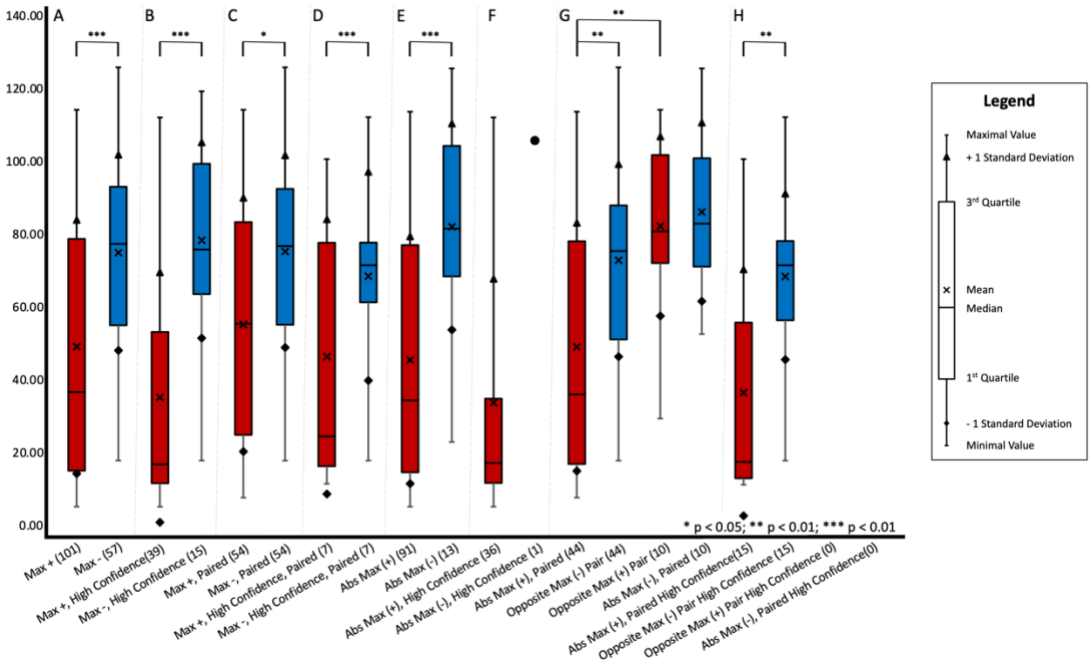

Figure 3.3: Distances from clusters to IED. Number of clusters in each group in brackets following the name, maximal positive clusters depicted in red, maximal negative in blue, + = positive, - = negative, Paired = IED generated a positive and a negative BOLD cluster. All distances are from the cluster to the respective IED recording electrode(s). The groups in each subpanel are: (A) All maximal positive and all maximal negative clusters. (B) High confidence maximal positive and maximal negative clusters. (C) All Cluster-IED studies that have a maximal positive and negative cluster. (D) Cluster-IED studies that have a high confidence positive and a high confidence negative cluster. (E) All absolute maximal (positive) and all absolute maximal (negative) clusters. (F) High confidence absolute maximal (positive) and high confidence absolute maximal (negative) clusters. (G) All absolute maximal (positive) that have a paired non-absolute maximal negative clusters, and all absolute maximal (negative) that have a paired non-absolute maximal positive clusters. (H) High confidence absolute maximal (positive) that have a paired non-absolute maximal negative clusters, and high confidence absolute maximal (negative) that have a paired non-absolute maximal positive clusters.

Fifty-four Cluster-IED studies produced both positive and negative clusters. Within these studies, cluster polarity was a significant factor (p = .032) with the maximal positive clusters ($\bar{x}$ = 55.09 mm, σ = 26.88 mm) being significantly closer (p = .032, Sidak corrected) to the IED than the maximal negative clusters ($\bar{x}$ = 75.90 mm, σ = 26.52 mm, Figure 3.3C). Only 7 of these pairs met the criteria for high confidence. The average distance from the high confidence maximal negative clusters to the IED was 68.76 mm (σ = 28.66 mm) and for the high confidence maximal positive clusters 46.61 mm (σ = 37.72 mm). The high confidence maximal positive clusters were

significantly closer ($p < .001$, Sidak corrected, Figure 3.3D), but IED type had to be removed as a model factor due to the limited sample size.

Of the 104 absolute maximal clusters, 91 were maximal positive clusters and 13 were maximal negative clusters. Both cluster polarity and IED type were significant main effects in the model ($p < .001$ and $p = .043$ respectively) but there was no interaction between these factors. The absolute maximal positive clusters ($\bar{x} = 45.71$ mm, $\sigma = 33.98$ mm) were significantly closer to the IED ($p < .001$, Sidak corrected) than the absolute maximal negative clusters ($\bar{x} = 82.36$ mm, $\sigma = 28.35$ mm, Figure 3.3E). When considering only high confidence maps, 36 absolute maximal positive clusters ($\bar{x} = 33.97$ mm, $\sigma = 34.04$ mm) and 1 absolute maximal negative cluster ($x = 105.94$ mm) met the criteria resulting in no statistical testing being performed for this pairing (Figure 3.3F).

To explore the selection of the absolute maximal cluster, comparisons were made between the absolute maximal clusters and their paired, non-absolute, opposite polarity maximal cluster. 54 studies were included and grouped into the following four groups: absolute maximal positive clusters, non-absolute maximal negative clusters, absolute maximal negative clusters, and non-absolute maximal positive clusters. It was determined that the absolute maximal positive clusters ($\bar{x} = 49.29$ mm, $\sigma = 34.11$ mm, $n = 44$) were significantly closer to the IED than both their paired negative clusters ($p = .003$, Sidak corrected; $\bar{x} = 73.09$ mm, $\sigma = 26.44$ mm) and the non-absolute maximal positive clusters paired with the absolute maximal negative clusters ($p = .004$ Sidak corrected; $\bar{x} = 82.47$ mm, $\sigma = 24.64$ mm, $n = 10$, Figure 3.3G). The absolute maximal negative cluster distances ($\bar{x} = 86.39$ mm, $\sigma = 24.51$ mm) were not significantly different from the other test groups. Fifteen absolute maximal positive clusters met the criteria for high confidence, while no absolute maximal negative clusters met the criteria. The absolute maximal positive clusters ($\bar{x} = 36.76$ mm, $\sigma = 33.86$ mm) were determined to be significantly closer to the IED ($p = .003$, Sidak corrected) than their paired non-absolute maximal negative clusters ($\bar{x} = 68.61$ mm, $\sigma = 22.81$ mm, Figure 3.3H), but IED type had to be removed from the model in order for the model to converge.

3.4.2.2 Cluster-SOZ analyses

Figure 3.4 summarizes the results of the BOLD cluster-IED analysis. A significant main effect of cluster polarity ($p < .001$) was found for maximal cluster to SOZ distances when considering all 127 clusters. The average distance from maximal positive cluster to SOZ was 42.56 mm ($\sigma = 29.58$ mm, $n = 80$) and from maximal negative cluster to SOZ was 71.59 mm ($\sigma = 27.76$ mm, $n = 47$). A post-hoc pairwise comparison determined that the maximal positive BOLD clusters were significantly closer to the SOZ than the negative clusters ($p = .017$, Sidak corrected, Figure 3.4A). This result ($p < .001$, Sidak corrected) was also observed when comparing only those studies which generated both a maximal positive and maximal negative cluster ($n = 45$; positive $\bar{x} = 59.25$ mm, $\sigma = 30.33$ mm; negative $\bar{x} = 73.78$ mm, $\sigma = 27.23$ mm, Figure 3.4B).

After application of the high confidence testing, 50 maximal positive and 37 maximal negative clusters were removed, leaving 40 clusters in the analysis. Cluster polarity remained a significant main effect ($p < .001$), with the maximal positive cluster to SOZ distances ($\bar{x} = 29.20$ mm, $\sigma = 23.76$ mm, $n = 30$), being significantly shorter ($p < .001$, Sidak corrected) than the maximal negative cluster to SOZ distances ($\bar{x} = 63.06$ mm, $\sigma = 21.82$ mm, $n = 10$, Figure 3.4C). Within the high confidence subset, 5 studies generated both a positive and a negative cluster. A clear and significant difference ($p < .001$, Sidak corrected) was seen between the maximal positive ($\bar{x} = 19.25$ mm, $\sigma = 12.57$ mm) and maximal negative ($\bar{x} = 56.96$ mm, $\sigma = 28.05$ mm, Figure 3.4D) to SOZ distances, however SOZ number had to be removed from the model for analysis to be completed.

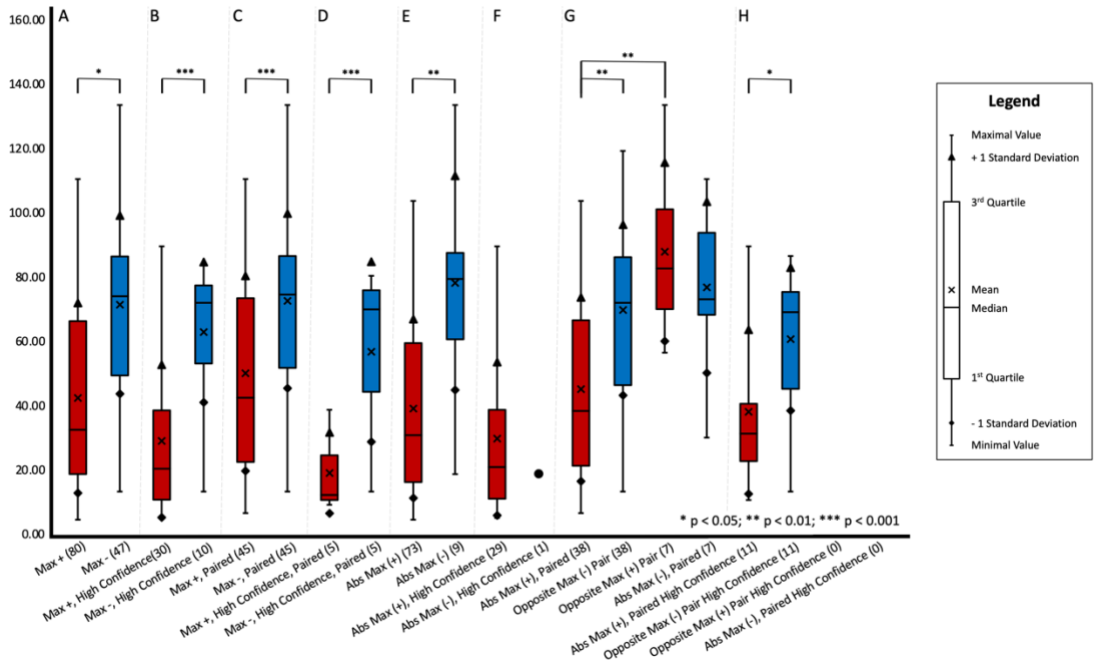

Figure 3.4: Distances from clusters to SOZ. Number of clusters in each group in brackets following the name, maximal positive clusters depicted in red, maximal negative in blue, + = positive, - = negative, Paired = IED generated a positive and a negative BOLD cluster. All distances are from the cluster to the respective SOZ electrode(s). The groups in each subpanel are: (A) All maximal positive and all maximal negative clusters. (B) High confidence maximal positive and maximal negative clusters. (C) All Cluster-IED studies that have a maximal positive and negative cluster. (D) Cluster-IED studies that have a high confidence positive and a high confidence negative cluster. (E) All absolute maximal (positive) and all absolute maximal (negative) clusters. (F) High confidence absolute maximal (positive) and high confidence absolute maximal (negative) clusters. (G) All absolute maximal (positive), that have a paired non-absolute maximal negative clusters, and all absolute maximal (negative) that have a paired non-absolute maximal positive clusters. (H) High confidence absolute maximal (positive), that have a paired non-absolute maximal negative clusters, and high confidence absolute maximal (negative) that have a paired non-absolute maximal positive clusters.

The absolute maximal BOLD cluster was determined to be a maximal positive cluster for 73 of the 82 Cluster-SOZ studies. Within the absolute maximal clusters, cluster polarity was a significant main effect on cluster distance to SOZ ($p = .007$), with absolute maximal positive clusters ($\bar{x} = 39.26$ mm, $\sigma = 27.83$ mm, $n = 73$) being significantly closer to the SOZ than absolute maximal negative clusters ($\bar{x} = 78.40$ mm, $\sigma = 33.32$ mm, $n = 9$, Figure 3.4E). After application of the high confidence criteria, 44 absolute maximal positive clusters and 8 maximal negative clusters were removed. With only 1 absolute maximal negative cluster (x = 18.89 mm) statistical

testing could not be performed but the application of the criteria did appear to restrict the absolute maximal positive clusters to those clusters closer to the SOZ ($\bar{x}$ = 29.92 mm, σ = 23.87 mm, *n* = 29, Figure 3.4F).

The large proportion of absolute clusters that were positive precluded direct comparison of the maximal positive cluster and the absolute maximal cluster. Thus, to test whether the absolute maximal cluster should have been chosen over the alternative maximal cluster, the distance from the absolute maximal cluster was compared to the alternative maximal cluster. For this reason, only the 45 Cluster-SOZ studies which generated both maximal positive and maximal negative clusters were included in these analyses. Of these paired absolute maximal clusters, 7 were maximal negative clusters. To compare these groups, all 4 were included in one model in which cluster type was a significant main effect (*p* = .002). In the pairwise comparisons, the absolute maximal positive clusters ($\bar{x}$ = 45.31 mm, σ = 45.31 mm, *n* = 38) were closer to the SOZ than both their maximal negative cluster counterparts (*p* = .001, Sidak corrected; $\bar{x}$ = 69.67 mm, σ = 26.54 mm, *n* = 38) and the maximal positive clusters paired with the absolute maximal negative clusters (*p* =.002, Sidak corrected; $\bar{x}$ = 88.04 mm, σ = 27.77 mm, *n* = 7, Figure 3.4G) but not the absolute maximal negative clusters (*p* =.057, Sidak corrected; $\bar{x}$ = 77.02 mm, σ = 26.66 mm, *n* = 7). Limited absolute maximal clusters met the high confidence of significance criteria, resulting in only 11 absolute maximal positive cluster pairs and no absolute maximal negative cluster pairs being included in the analysis. Between the absolute maximal positive clusters ($\bar{x}$ = 38.26 mm, σ = 25.53 mm, *n* = 11) and their maximal negative counterparts ($\bar{x}$ = 60.86 mm, σ = 22.24 mm, *n* = 11), cluster polarity was a significant main effect (*p* = .035), and the absolute maximal positive clusters were significantly closer to the SOZ (*p* = .035, Sidak corrected, Figure 3.4H).

3.5 Discussion

Emerging trends in the use of EEG-fMRI are often developed, verified, and implemented using scalp EEG-fMRI. While the general principles of data acquisition, processing, and utilization are the same, the nuances of the iEEG-fMRI make the datasets unique enough that the outright adoption of new methodology and practices should be done with caution. The use of intracranial

electrodes provides the potential for more precise recordings of IEDs, closer to their source. In addition, IEDs occurrence is typically much greater in intracranial EEG recordings compared to scalp EEG. In addition, iEEG offers the benefit of decreased movement and pulsatile artifacts. On the other hand, intracranial electrodes have the limitation that they are often implanted in the presumed SOZ, potentially causing BOLD signal loss in this region. With this in mind, the iEEG-fMRI data presented here do not support the use of the absolute maximal cluster as an indicator of the SOZ for iEEG-fMRI data.

3.5.1 Positive and negative clusters

The maximal positive cluster being closer to the target than the maximal negative cluster was a consistent finding regardless of the subgrouping of the dataset. Given that positive BOLD responses result from increases in activity, it is not unexpected that these clusters would be closer to suspected seizure generating tissue. Thus, our results provide further evidence that the maximal positive BOLD is more likely to indicate the location of the SOZ than the maximal negative BOLD. Likewise, a common finding in the literature is that maximal negative BOLD clusters are often not concordant with the SOZ but rather represent other clinically irrelevant regions [89,99,135–142], a finding supported by these results. While the general trend of the maximal positive BOLD cluster being close to the SOZ has found support in this data, this finding is not without exception. Subject 41 IED4, produced no positive BOLD clusters, but produced a maximal negative cluster proximal to both the IED and the SOZ, suggesting that the negative BOLD may be useful in isolated cases. The morphology of IED4 featured a complex consisting of three slow waves, rather than a spike or sharp wave as typically observed, with the EEG of the electrode being reminiscent of delta slowing. EEG of this morphology may suggest tonic inhibition[179] supporting the notion that the negative BOLD response is indicative of neuronal activity and may suggest that inhibition occurs proximal to the SOZ and IED generating regions.

3.5.2 Absolute maximal BOLD

The original concept was to determine which cluster would have the greatest utility in identifying the location of the SOZ: the maximal positive BOLD cluster or the absolute maximal BOLD cluster

(which included negative BOLD clusters). In approximately 90% of cases, the absolute maximal cluster was positive, and when the absolute maximal cluster was negative it was significantly further from the IED generator or SOZ (Figure 3.3E and 3.4E, respectively). These findings question the benefit of using the absolute maximal cluster and suggest that including the absolute maximal negative clusters makes it a much less reliable indicator of the IED generator or SOZ. Statistically, it was shown that the use of the absolute maximal cluster provides no added benefit over considering just the maximal positive cluster. One interesting finding that came out of the absolute maximal cluster exploration was the relationship between the absolute maximal positive clusters and the non-absolute maximal positive clusters. In both the Cluster-IED and Cluster-SOZ studies, these two groups were significantly different with the non-maximal positive clusters being further from the respective target (see figure 3.2G and figure 3.3G). In other words, when the absolute maximal cluster was negative, its corresponding non-absolute positive cluster was not closer to the target region. These findings may suggest that if the absolute maximal cluster is negative neither it nor the non-absolute positive cluster will be close enough to the presumed SOZ to be of clinical relevance.

3.5.3 High confidence of significance

Spurious results are a concern in all analyses but are of particular concern in data that will be translated into patient care. We therefore determined whether the set of criteria for high confidence applied to these data[125] could increase confidence in the assertion that a given cluster indicates the location of the SOZ. To this end, it was found that those clusters which passed the confidence test were closer to the target, be that the IED or the SOZ, suggesting that the test has utility for selecting those most clinically relevant clusters. Furthermore, the high confidence criteria removed all absolute maximal negative clusters, and the bulk of the maximal negative clusters, suggesting that the maximal negative cluster has limited reliability for clinical applications.

3.5.4 Limitations and future directions

A consideration that needs to be made in any iEEG-fMRI study is that the iEEG electrodes are placed in brain regions suspected to be the SOZ. This placement results in signal dropout in the brain regions BOLD responses are expected to occur which could reduce cluster size near electrodes or result in clusters not being generated in the suspected SOZ. This said, clusters are often proximal to the SOZ and the emergence of a BOLD response despite signal dropout strengthens the likelihood that a cluster proximal to an electrode is clinically meaningful.

A limiting factor in these analyses was the disproportionate generation of negative BOLD clusters. This restricted the comparisons that could be made and may also have contributed to the disproportionate number of absolute maximal clusters that were positive. Recent studies have identified negative BOLD specific hemodynamic response functions[151] and it is possible that the use of these functions may increase the yield of negative BOLD clusters.

As mentioned, the practices tested herein were developed using scalp EEG-fMRI. Thus, they may not translate directly to iEEG-fMRI, and emphasis should therefore be placed on developing similar methods and tests using iEEG-fMRI data that accommodates the unique concerns of intracranial electrodes.

The analyses presented herein was a higher-level exploration of the positive and negative BOLD response in iEEG-fMRI. Going forward, these analyses should be reframed to consider what factors may contribute to difference within the distances from cluster to SOZ or IED and between positive and negative BOLD differences. These analyses should consider factors such as TLE vs extra-TLE, seizure frequency, disease duration, or surgical outcome. One study that may be of particular interest is whether IED morphology is related to the BOLD response generated. Subject 41 IED4 was a 3 slow wave complex and generated only a negative BOLD response proximal to the SOZ. Perhaps similar phenomena are occurring with other participants. Finally, a comparison between the negative BOLD response and the resective cavity should be conductive in order to

determine percent overlap and whether resection of the negative BOLD response has any predictive power for seizure freedom.

3.6 Acknowledgements

I would like to thank all the kind, thoughtful, and selfless patients who generously agreed to participate in our research knowing it would help future generations. Additionally, this research is only possible with the help of our health care allies, including porters, EEG technologist, 3T MR technologists, nurses, fellows, and clinical assistants Drs. Rey Avendano, Mabel Cruz-Bagadiong, Salma Hanna, and Alma Retuta.

3.7 Funding sources

This research was supported by the Canadian Institutes of Health Research (MOP-230809).

3.8 Disclosure

None of the authors have any conflicts of interest to disclose.

3.9 Supplementary material

Supplementary Table 3.1: Participant demographics. Abbreviations: ASM anti-seizure medication, bFLE bilateral frontal lobe epilepsy, bmTLE bilateral mesial temporal lobe epilepsy, bTLE bilateral temporal lobe epilepsy, bTPE bilateral temporoparietal epilepsy, FA focal aware, FIA focal impaired awareness, FTBTC focal to bilateral tonic clonic, GTC generalized tonic clonic, LFLE left frontal lobe epilepsy, LHE left hemispherical epilepsy, LmTLE left mesial temporal lobe epilepsy, LTLE left temporal lobe epilepsy, LTPE left temporoparietal epilepsy, MFE multi-focal epilepsy, MO month, PID patient ID, RFLE right frontal lobe epilepsy, RFTE right frontotemporal epilepsy, RmTLE right mesial temporal lobe epilepsy, ROFE right orbitofrontal epilepsy, ROFTE right orbitofrontotemporal epilepsy, RTLE right temporal lobe epilepsy, SMA supplementary motor area.

PID	Age at Study	Sex	Handedness	Onset Age	Seizure Type	Seizure Frequency (MO)	Seizure Onset Zone	Diagnosis	Noted Lesion	Previous Surgery
02	29	Female	Right	24	FAS, FIAS, FTBTCS	8	Bilateral Temporal Lobes	bTLE	Yes	No
04	32	Female	Right	18	FIAS	0 when compliant with ASMs	Left Temporal Lobe	LmTLE	Yes	No
05	24	Male	Right	22	FAS, FIAS, FTBTCS	4	Bilateral Temporal Lobes	bTLE	No	No
07	27	Female	Left	22	FAS, FIAS, FTBTCS	20	Left Temporal Lobe	LFLE	Yes	No
10	21	Male	Right	11	FAS, FIAS, FTBTCS	1	Left Temporal Lobe	LTLE	No	No
11	56	Female	Left	3	FTBTCS	12	Bilateral Temporal Lobes	LTLE	Yes	No
12	53	Female	Right	28	FAS, FIAS, FTBTCS	2	Bilateral Temporal Lobes	bTLE	No	No
13	21	Male	Right	14	FAS, FIAS, FTBTCS	2	Left Temporal Lobe	LTLE	No	No
14	37	Male	Right	5	FAS, FIAS, FTBTCS	4	Right Temporal Lobe	bTLE	Yes	No
16	28	Male	Right	18	FAS, FIAS, FTBTCS	2	Left Temporal Lobe	LTLE	No	No
17	39	Male	Right	1	FAS, FIAS, FTBTCS	4	Right Temporal Lobe	RTLE	Yes	Yes
18	48	Male	Right	28	FAS, FIAS, FTBTCS	12	Right Hippocampus	RTLE	Yes	No
19	40	Male	Ambidextrous	9	FAS, FTBTCS	20	Left Parietal Lobe	bFLE	No	No
20	49	Male	Right	25	FAS, FIAS, FTBTCS	4	Left Temporal Lobe	LTLE	No	Yes
21	23	Female	Right	17	FIAS, FTBTCS	11	Left Orbitofrontal Lobe	LFLE	No	No
22	34	Male	Left	31	FIAS, FTBTCS	18	Bilateral Temporal Lobes	TPE	Yes	No
23	28	Male	Left	25	FTBTCS	4	Right Temporal Lobe	RTLE	No	No
24	42	Male	Right	19	FTBTCS	3	Left Insula	LTLE	No	No
27	53	Female	Right	25	FIAS, FTBTC	20	Left Temporal Lobe	LTLE	No	No

28	24	Female	Ambidextrous	14	FTBTCS	1	Left Mesial Frontal Lobe	LFLE	Yes	No
29	22	Male	Ambidextrous	11	FAS, FIAS, FTBTCS	37	Right Hippocampus	RmTLE	No	No
30	24	Female	Right	17	FIAS, FTBTCS	11	Left temporal, Orbitofrontal lobes	LFLE	No	No
31	24	Female	Right	11	FAS, FIAS, FTBTCS	30	Bilateral SMAs	bFLE	No	No
32	23	Male	Right	11	Absence, GTC	15	Left Temporal Lobe	LHE	No	No
33	22	Male	Right	12	FAS, FIAS, FTBTCS	50	Right Temporal Lobe	RTLE	No	No
34	30	Male	Right	0	FAS, FIAS, FTBTCS	5	Left Temporal Lobe	LTLE	No	No
35	30	Female	Right	16	FIAS, FTBTCS	18	Right Frontotemporal Lobe	RFLE	No	No
36	31	Male	Right	15	FAS, FIAS, FTBTCS	120	Right Temporal Lobe	ROFTE	Yes	No
37	28	Female	Left	13	FIAS, FTBTCS	4	Right Temporal Lobe	RmTLE	No	No
38	40	Male	Right	6	FIAS, FTBTCS	6	Left Hippocampus	bTLE	Yes	No
39	27	Female	Ambidextrous	13	FAS, FIAS, FGTC	4	Left Hippocampus	LTLE	Yes	No
40	37	Female	Right	18	FIAS, FTBTCS	6	Right Orbitofrontal Lobe	ROFE	Yes	No
41	52	Female	Right	46	FAS, FIAS, FTBTCS	10	Right Temporal Lobe	RTLE	Yes	Yes
42	34	Female	Right	8	FAS	42	Right Orbitofrontal Lobe	RFLE	No	No
43	46	Female	Right	27	FIAS, FTBTCS	2	Right Frontotemporal Lobe	RmTLE	Yes	No
44	55	Male	Right	8	FIAS, FTBTCS	0.5	Bilateral Temporal Lobes	bTLE	Yes	No
45	64	Male	Right	57	FAS, FIAS	16	Bilateral Hippocampi	bTLE	No	No
46	37	Female	Right	14	FAS, FIAS	6	Right Hippocampus	ROFTE	Yes	Yes
47	22	Male	Right	10	FAS, FIAS, FTBTCS	3.5	Bilateral Temporal Lobes	bTLE	No	No
48	58	Female	Right	8	FAS, FIAS, FTBTCS	2	Left Hippocampus	LmTLE	No	No
49	41	Male	Ambidextrous	26	FAS, FIAS, FTBTCS	10.5	Left Hippocampus	LmTLE	No	Yes
50	20	Male	Right	5	FAS	45	Left Insula	LTPE	No	No
51	23	Male	Right	12	FAS, FIAS, FTBTCS	210	Bilateral Frontotemporal Lobes	RFTE	No	Yes
53	55	Male	Right	52	FAS, FIAS	3	Left Hippocampus	LmTLE	No	No
54	26	Male	Right	11	FAS, FIAS, FTBTCS	1	Right Parietal Lobe	rTLE	Yes	Yes

55	22	Male	Right	18	FAS, FIAS, FTBTC	1.5	Bilateral Hippocampi	bTLE	No	No
56	25	Female	Right	21	FAS, FIAS	92.5	Bilateral Temporal Lobes	bTLE	Yes	No
57	33	Female	Right	10	FAS, FIAS	100	Right Temporal Lobe	RmTLE	No	No
58	31	Male	Right	14	FIAS	6	Bilateral Temporal Lobes	bmTLE	Yes	Yes
59	39	Male	Right	10	FIAS, BTCS	2	Bilateral Temporal Lobes	bHE	No	No
60	38	Female	Right	25	FAS, FIAS, FTBTCS	8	Right Temporal Lobe	RmTLE	No	No
62	32	Female	Right	21	FAS, FIAS, FTBTCS	12	Right Temporal Lobe	bTLE	No	No
63	32	Female	Right	16	FAS, FIAS, FTBTCS	1	Bilateral Cingulate Cortex, Left SMA	LFLE	No	No
64	38	Female	Right	17	FIAS, FTBTCS	1.5	Right Temporal Lobe	RmTLE	Yes	No
65	29	Female	Right	17	FIAS, FTBTCS	15.5	Left Hippocampus	LmTLE	No	No
66	63	Female	Right	13	FAS, FIAS, FTBTCS	14	Right Insula	RmTLE	No	No
69	40	Male	Right	26	FIAS, FTBTCS	0.334	Bilateral Frontotemporal Lobes	MFE	Yes	No
70	46	Male	Right	1	FAS, FIAS, FTBTCS	16	Right Temporal Lobe	RmTLE	Yes	Yes

Supplementary Table 3.2: IED and SOZ locations and distance results. ‡ = absolute maximal. Electrode prefixes: d depth, g grid, s strip, Abbreviations: IED interictal epileptiform discharge, LA left amygdala, LAD left amygdalar dysplasia, LaH left anterior hippocampus, LaIN left anterior insula, Lam left anterior mesial, LamTg left anterior mesial temporal gyrus, LaP left anterior parietal, LaR left anterior rolandic, LasT left anterior superior temporal; LaxH left axial hippocampus, LcOP left central operculum, LH left hippocampus, Li left inferior, LiOF left inferior orbitofrontal, LipmP left inferior posterior middle parietal, LiT left inferior temporal, LiTcv left inferior temporal convexity, LlT left lateral temporal, LM left primary motor area, LmC left middle cingulate, LmH left middle hippocampus, LmIN left middle insula, LmmTg left middle middle temporal gyrus, LmO left mesial occipital, LmOF left mesial orbitofrontal, LmsubT left mesial subtemporal, LmT left mesial temporal, Lpcv left posterior convexity, LpH left posterior hippocampus, LpIN left posterior insula, LPM left premotor, LpmTg left posterior middle temporal gyrus, LpR left posterior rolandic, LpT left posterior temporal, LpTP left posterior temporoparietal, Ls left superior, LSMA left supplementary motor area, LspmP left superior posterior mesial, PID patient ID, RA right amygdala, RaC right anterior cingulate, RaH right anterior hippocampus, RaIN right anterior insula, RasT right anterior superior temporal, RasTg right anterior superior temporal gyrus, RaxH right axial hippocampus, RC right cingulate, RFOP right frontal operculum, RH right hippocamus, Rl right atrial heterotopia, RiP right inferior parietal, RlmF right lateral middle frontal, RlOF right lateral orbitofrontal, RlsubT right lateral subtemporal, RmC right middle cingulate, RmF right mesial frontal, RmIN right middle insula, RmOF right mesial orbitofrontal, RmP right middle parietal, RmsT right middle superior temporal, RmsubT right mesial subtemporal, RmT right mesial temporal, RpC right posterior cingulate, RpH right posterior hippocampus, RpIN right posterior insula, RPOP right parietal operculum, RpsT right posterior superior temporal, RpT right posterior temporal, RSMA right supplementary motor area, RsO right superior occipital, RTcx right temporal neocortical, RTP right temporoparietal, RUmTg right uncus middle temporal gyrus, SMA supplementary motor area, SOZ seizure onset zone.

	Cluster-IED Studies									Cluster-SOZ Studies							
PID	**IED Type**	**# of IEDs**	**IED Contacts**	**IED Location**	**IED Elect-rode Type**	**Max Pos z-Score**	**Max Pos Dist-ance (mm)**	**Max Neg z-Score**	**Max Neg Dist-ance (mm)**	**SOZ #**	**SOZ Location**	**SOZ Contacts**	**SOZ Elect-rode Type**	**Max Pos z-Score**	**Max Pos Dist-ance (mm)**	**Max Neg z-Score**	**Max Neg Dist-ance (mm)**
02	1	148	sRmT3-4	Right temporal	Strip	7.36‡	25.1			2	Right temporal	sRmT2-4	Strip	7.36‡	27.7		
	2	199	sLmT4-5	Left temporal	Strip	5.31‡	22.4			1	Left temporal	sLmT5-6, sLlT4-5	Strip	5.31‡	19.3		
04	1	8	sLmT4-5, dLiTcv4-6	Left temporal	Strip, depth	5.04‡	66.9	4.94	111.60	1	Left temporal	sLmT4-5 dLiTcv4-6	Strip, depth	5.04‡	66.9	4.94	111.6
05	1	841	sLmT5	Left temporal	Strip	10.30‡	9.7			1	Left temporal	sLmT5-7	Strip	10.30‡	10.6		
07	1	1074	gL35	Left temporal	Grid	5.79‡	22.5			1	Left temporal	g55-54, g41-42	Grid	5.79‡	31.0		
10	1	1467	sLaP 6-8	Left parietal	Strip	5.14‡	98.8	3.93	118.35	1	Left temporal	sLmT5-6, sLiT1-2	Strip	5.14‡	60.5	3.93	119.5

11	1	36	sLmT5-6	Left temporal	Strip	4.56	80.8	5.23‡	81.81	1	Left temporal	sLmT3-5	Strip	4.56	67.5	5.23‡	82.9
12	1	390	sRmsubT5	Right temporal	Strip	6.20‡	18.4	4.20	81.99	1	Right temporal	sRmsubT3-5, sRlsubT6-7	Strip	6.20‡	22.7	4.20	78.1
	2	31	sLmsubT6	Left temporal	Strip	6.20‡	11.7			2	Left temporal	sLlT4-6, sLmsubT5-7	Strip	6.20‡	15.6		
13	1	630	gLiT5	Left temporal	Grid	4.79‡	95.6										
	2	274	dLH5	Left hippo-campus	Depth	8.54‡	21.0			1	Left hippo-campus	dLH1-2	Depth	8.54‡	10.6		
	3	135	sLpT1-4	Left temporal	Strip			4.52‡	105.94								
14	1	119	dLmT1-2	Left temporal	Depth	13.50‡	12.6	4.74	47.36								
	2	66	dRmT2-5	Right temporal	Depth	7.27‡	20.9			1	Right orbito-frontal	dRmOF1-2	Depth	7.27‡	45.1		
	3	1281	dRmIN1-3	Right insula	Depth	4.27	81.3	4.58‡	91.00								
	4	2487	dLpIN4	Left insula	Depth	4.29‡	79.0										
16	1	5	dLaH1, dLmH1	Left hippo-campus	Depth	4.48	108.1	4.55‡	119.16	1	Left temporal	dLpT2-3	Depth	4.48	104.1	4.55‡	133.7
17	1	242	dRH3-4	Right hippo-campus	Depth	4.96‡	88.0	3.83	76.07	1	Right temporal	dRpT1, dRH3	Depth	4.96‡	80.6	3.83	74.3
	2	448	dRpT1-2	Right temporal	Depth	4.26‡	31.7	4.26	79.52	2	Right insula	dRpIN3-4	Depth	4.26‡	25.6	4.26	97.5
18	1	693	dRA1-2, dRH1-3	Right amygdala hippo-campus	Depth	7.02‡	8.8			1	Right hippo-campus	dRH1-2	Depth	7.02‡	6.3		
	2	127	dLA1-3, dLH1-3, dLpH1-3	Left amygdala hippo-campus	Depth	10.10‡	5.4										
19	1	1966	sLipmP8, sLspmP8, sLpcv8	Left parietal	Strip			6.24‡	77.62	1	Left parietal	sLspmP5-7, sLipmP5-7	Strip			6.24‡	70.4
20	1	34	gLs9-10, gLi18-20	Left temporal	Grid	4.24‡	61.0	3.96	36.59	1	Left temporal	g1-4, g9-12	Grid	4.24‡	53.6	3.96	26.7
21	1	1216	sLiOF3	Left orbito-frontal	Strip	5.02‡	109.9	4.71	101.08	1	Left orbito-frontal	g5-7, sLiOF2-4	Strip, grid	5.02‡	92.1	4.71	104.6
	2	21	sLmT5	Left temporal	Strip	8.81‡	10.1										

22	1	209	dLA3, dLH2, dLAD2	Left amygdala hippo-campus, dysplasia	Depth	9.87‡	12.3			1	Left amygdala hippo-campus, dysplasia	dLA1-3 dLH1-3 LdAD1-3	Depth	9.87‡	11.2		
	2	190	dRA2, dRAH1-3	Right amygdala hippo-campus	Depth	9.34‡	12.6			2	Right hippo-campus	dRH1-3	Depth	9.34‡	11.3		
23	1	84	dRmsT5-6, dRpsT5-6	Right temporal	Depth	6.15‡	45.2			1	Right temporal	dRmsT3-4, dRpsT3-6	Depth	6.15‡	46.7		
24	1	21	dLpIN1-3	Left insula	Depth	4.88‡	98.9			1	Left insula	dLpIN2-4	Depth	4.88‡	99.2		
27	1	142	dLA7-8	Left insula	Depth	6.74‡	35.3			1	Left temporal	dLasT1-2	Depth	6.74‡	33.7		
28	1	520	dLaR1-2, dLpR4-6	Left rolandic cortex	Depth	3.84‡	88.1			1	Left mesial frontal (SMA)	sLam1-2, dLaR 2-3, dLpR1-2	Strip, depth	3.84‡	82.0		
	3	32	gL5-7		Depth	4.68‡	78.5										
29	1	293	dRaH1-4, dRpH1-3	Right hippo-campus	Depth	13.80‡	8.0			1	Right hippo-campus	dRaH3, dRpH2	Depth	13.80‡	9.9		
	2	42	dLaH1-3, dLA2-4	Left amygdala hippo-campus	Depth	3.77	70.3	3.97‡	52.83								
30	1	387	dLmOF1, dLaH1, dLaH7-8, dLpH1	Left orbito-frontal, amygdala hippo-campus	Depth	5.75‡	93.8	3.99	93.31	1	Left hippo-campus	dLaH1-2, dLpH1-2	Depth	5.75‡	80.9	3.99	84.1
31	1	65	dLSMA6-8	Left parietal	Depth	5.64‡	73.6	5.16	52.13	2	Left SMA	dLSMA6-8	Depth	5.64‡	73.6	5.16	52.1
	2	318	dLPM5-7	Left parietal	Depth	11.10‡	13.9	7.15	42.97	1	Right SMA	dRSMA6-8	Depth	11.10‡	42.7	7.15	43.2
32	1	132	gLiT28-31	Left temporal	Grid	6.47‡	24.3			1	Left temporal	sLpTP7-8, gLiT31-32, gLiT23-24	Strip, grid	6.47‡	20.1		
	2	109	sLpTP3-6	Left temporal	Strip	5.92‡	76.8	3.54	119.54								
33	1	1324	dRasTg 2-4, dRaIN 2-4	Right temporal insula	Depth	7.18‡	36.5			1	Right temporal	dRasT2-4	Depth	7.18‡	55.2		

34	1	363	dLA1-2, dLaH1-3	Left amygdala hippo-campus	Depth	6.49‡	9.1			1	Left amygdala hippo-campus	dLaH1-3, dLA1-3	Depth	6.49‡	17.7		
	2	13	dRaH1-2, dRA2-3	Right amygdala hippo-campus	Depth	3.77‡	108.5										
35	1	1682	dRmF3-4, dRH5-6, dRaIN1-4	Right frontal, hippo-campus, insula	Depth	7.05‡	27.8	6.10	55.87	1	Right fronto-temporal	dRmF2-4, dRaIN7-9, dRC9-10	Depth	7.05‡	22.6	6.10	64.8
36	1	48	dRpIN 1-5, dRaIN 1-5, dRH 1-3	Right hippo-campus, insula	Depth	8.90‡	29.0	6.73	67.64	1	Right hippo-campus, insula	dRH2, dRpIN2-4, dRaIN2-4	Depth	8.90‡	31.5	6.73	69.3
	2	30	dLH1-3	Left hippo-campus	Depth	6.19‡	14.2	5.42	93.86								
37	1	19	dRA2-4, dRaH1-3	Right amygdala hippo-campus	Depth	5.35‡	15.0	4.89	86.48	1	Right amygdala hippo-campus	dRA1-3, dRaH1-3	Depth	5.35‡	15.0	4.89	86.5
38	1	40	dLaH3-6, dLpH1-4	Left hippo-campus	Depth	6.71‡	7.9	6.50	48.97	1	Left hippo-campus	dLaH1-3	Depth	6.71‡	6.8	6.50	47.2
	2	249	dLmO7-10	Left occipital	Depth	5.87‡	50.3	4.79	48.53								
39	1	58	dLaxH3-6	Left hippo-campus	Depth	4.41‡	97.6	4.25	44.18	1	Left hippo-campus	dLaxH4-7, dLamTg5-10, dLmmTg5-10	Depth	4.41‡	100.3	4.25	42.3
	2	137	dLamTg7-9, dLmmTg7-10, dLpmTg5-8	Left temporal	Depth	5.63‡	38.6	4.34	126.11	2	Left hippo-campus	dLaxH1-8, dLmmTg1-3, dLpmTg1-3	Depth	5.63‡	40.3	4.34	103.1
40	1	1213	dRaH3-6, dRpH1-5	Right hippo-campus	Depth	6.50‡	36.9										
	2	254	dLaH3, dLA5	Left amygdala hippo-campus	Depth	9.64‡	17.1			1	Right orbito-frontal	dRmOF1-3	Depth	9.64‡	63.9		
	3	932	dRpIN2	Right insula	Depth	8.38‡	12.6	3.86	73.27								

41	1	2139	dRTcx4-6, dRTP4-6	Right temporal	Depth	4.85‡	65.9	4.24	105.17	1	Right temporal	dRTcx4-6	Depth	4.85‡	64.3	4.24	107.8
	2	2555	dRmP2-5, dRiP2-6	Right parietal	Depth			3.79‡	23.19	2	Right temporal	dRTP1-4	Depth			3.79‡	18.9
	3	851	dRPOP2-5	Right oper-culum	Depth	4.85‡	108.4						Depth				
	4	108	dRlOF3-6	Right orbito-frontal	Depth					3	Right temporal	dRpIN3-6	Depth	5.29‡	21.0		
42	1	241	dRpC6-8	Right cingulate cortex	Depth	10.40‡	82.9	5.02	82.94	1	Right orbito-frontal, cingulate	dRpC1-4, dRlOF4-9	Depth	10.40‡	81.1	5.02	86.8
	2	154	dRmC1-3, dRSMA1-3	Right parietal	Depth	4.42	78.4	5.20‡	79.40	2	Right cingulate cortex	dRmC1-4	Depth	4.42	73.3	5.20‡	79.6
	3	245	dRmC7-8, dRaC5-6	Right cingulate cortex	Depth	8.24‡	85.6	3.82	112.44								
	4	353	dRlOF8-10	Left orbito-frontal	Depth					3	Right orbito-frontal	dRlOF6-9	Depth	4.89‡	9.3	3.93	80.6
43	1	86	dRaH1-2	Right hippo-campus	Depth	8.80‡	11.4	4.08	64.18	1	Right hippo-campus	dRaH1-8, dRpH1-6	Depth	8.80‡	21.1	4.08	58.6
	2	236	dLaH1-2, dLA1-3, dLpH1-2	Right amygdala hippo-campus	Depth	9.84‡	15.2	4.41	97.14	2	Right orbito-frontal, amygdala	dRFOP2-5, dRlOF3-6, dRRaIN3-5	Depth	9.84‡	75.3	4.41	124.5
44	1	509	dRaH1-3	Right hippo-campus	Depth	9.63‡	11.7	4.13	71.76	3	Left hippo-campus, insula	dRpH1-4, dRaH1-3, dRaIN1-8	Depth	9.63‡	10.8	4.13	70.2
	2	251	dLaH1-2	Left hippo-campus	Depth	4.19‡	67.2			1	Left hippo-campus	dLaH1-2	Depth	4.19‡	67.2		
	3	545	dLpIN3-4	Left insula	Depth	7.56‡	73.6	4.09	57.34	2	Left insula	dLpIN1-6	Depth	7.56‡	73.7	4.09	57.4
45	1	557	dLaH1-3, dLpH1-2	Left hippo-campus	Depth	5.97‡	10.9			1	Left hippo-campus	dLaH2-6, dLpH2-6	Depth	5.97‡	21.8		
	2	571	dRA1-3, dRaH1-3	Right amygdala hippo-campus	Depth	9.59‡	24.7	4.60	75.24	2	Right hippo-campus	dRA1-4, dRaH1-4	Depth	9.59‡	24.8	4.60	76.1

46	1	138	dRUmTg2	Right uncus	Depth	5.38‡	26.3	4.14	38.69	1	Right hippo-campus, uncus	dRUmTg1-3, dRH1-7	Depth	5.38‡	20.3	4.14	42.4
	2	93	dRaIN2	Right insula	Depth	4.27‡	39.0	3.78	77.95	2	Right hippo-campus	dRaxH1-2	Depth	4.27‡	66.4	3.78	106.1
47	1	2596	dRAH1-3	Right hippo-campus	Depth	9.40‡	90.4	5.18	49.07	1	Right orbito-frontal, amygdala	dRaH1-4, dRA1-2	Depth	9.40‡	89.8	5.18	46.4
	2	604	dLpH1-3	Left hippo-campus	Depth	8.23‡	14.7			2	Left hippo-campus	dLaH1-4, dLpH1-3	Depth	8.23‡	5.3		
48	1	59	dLaH1-2, dLpH1-3	Left hippo-campus	Depth	5.82‡	94.0			1	Left hippo-campus	dLaH1-2, dLpH1-4	Depth	5.82‡	95.3		
49	1	36	dLA6-7, dLaH5-7, dLasT1-5	Left temporal	Depth	4.04‡	113.9	3.93	62.76				Depth				
	2	18	dLA6-7	Left amygdala	Depth	4.12	108.2	4.26‡	104.54				Depth				
	3	172	dLaH1-3, dLA1-2, dLpH1-3	Left amygdala hippo-campus	Depth	4.72	29.6	4.76‡	68.69	1	Left hippo-campus	dLaH1-3	Depth	4.72	30.3	4.76‡	60.8
50	1	45	dLM2-4, dLSMA3, dLcOP3, dLpIN1-6	Left temproparietal	Depth	5.73‡	42.2	4.76	37.74	1	Left insula	dLpIN4	Depth	5.73‡	55.8	4.76	36.93
51	1	1014	dRlmF4-8, dRaIN2-3	Right fronto-temporal	Depth	10.40‡	17.8	3.72	18.07	1	Right frontal, insula	dRlmF3-4, dRaIN1-4	Depth	10.40‡	12.4	3.72	13.5
53	1	169	dLaH1-3, dLpH2-3	Left hippo-campus	Depth	6.50‡	7.9			1	Left hippo-campus	dLaH1-2, dLpH1-3	Depth	6.50‡	4.7		
54	1	225	dRpsT5-6	Right temporal	Depth	4.37‡	21.9			1	Right parietal	dRiP7-12	Depth	4.37‡	35.6		
	2	138	dRiP5-6	Right parietal		3.40‡	112.4						Depth				
	3	363	dRpsT5-6 dRiP5-6	Right temporal		3.83‡	91.5						Depth				

55	1	330	dRaH1-4	Right hippo-campus	Depth	8.84‡	8.6			1	Right hippo-campus	dRaH1-5	Depth	8.84‡	10.5		
	2	16	dLaH1-2	Left hippo-campus	Depth	4.75‡	39.6			2	Left hippo-campus	dLpH1-2, dLaH1-2	Depth	4.75‡	32.4		
56	1	875	dLA6-7, dLaH5-7, dLasT1-5	Left temporal	Depth	4.87‡	13.1	4.64	35.36	1	Left amygdala hippo-campus, insula	dLA1-3, dLaH1-2, dLpH1-2, dLaIN1-2	Depth	4.87‡	20.1	4.64	44.0
	2	182	dRA1-2, dRaH1-2, dRpH1-2	Right amygdala hippo-campus	Depth	5.18‡	38.2			2	Right hippo-campus, insula	dRaIN1-2, dRaH1-3	Depth	5.18‡	33.0		
57	1	1419	dRaIN1-4	Right insula	Depth	6.49‡	29.9	4.14	83.44	1	Right insula	dRaIN1-4	Depth	6.49‡	29.9	4.14	83.4
	2	608	dLmOF5-9	Left orbito-frontal		6.36‡	57.7						Depth				
58	1	807	dLaH2-3, dLpH1-2, dLA1-3	Left amygdala hippo-campus	Depth	11.70‡	12.0			1	Left amygdala hippo-campus	dLaH1-2, dLA1-4	Depth	11.70‡	21.5		
59	1	1381	dRA5-9	Right amygdala	Depth	4.76‡	107.0	4.33	107.90								
	2	77	dRaH1-2, dRA1-2	Right amygdala hippo-campus	Depth	6.46‡	17.8	4.26	77.05	1	Right parietal oper-culum	dRPOP4-6	Depth	6.46‡	55.5	4.26	74.8
	3	480	dLA6-8	Left amygdala	Depth	3.80‡	78.7										
	4	207	dLA2-3	Left amygdala	Depth					2	Left insula	dLmIN1-3	Depth	9.73‡	38.9	4.40	44.5
60	1	282	dRA1-2, dRaH1-4, dRpH1-4	Right amygdala hippo-campus	Depth	13.40‡	7.9			1	Right amygdala hippo-campus	dRA1-2, dRaH1-3	Depth	13.40‡	7.7		

62	1	1236	dRaH1-2, dRA1-3, dRpIN4	Right amygdala hippo-campus, insula	Depth					1	Right amygdala hippo-campus	dRaH1-2, dRA1-2	Depth	10.40‡	29.7	5.90	75.1
	2	1044	dLaH2, dLA1-2, dLpIN1-2	Left amygdala hippo-campus, insula	Depth	4.94‡	53.1			2	Left amygdala	dLA1-2	Depth	4.94‡	58.7		
63	1	103	dLpH1-2, dLaH2-3	Left hippo-campus	Depth	5.41‡	67.6			1	Left mesial frontal (SMA), cingulate	dLSMA4-5, dLmC6-8	Depth	5.41‡	59.7		
	2	12	dLA1-2	Left amygdala	Depth	5.19‡	73.5	4.25	82.36	2	Left cingulate cortex	dLmC6-8	Depth	5.19‡	103.9	4.54	108.9
64	1	60	dRaH1-4	Right hippo-campus	Depth	4.12	83.8	4.54‡	84.51	1	Right atrial hetero-tropia, hippo-campus, occipital	dRl3-8, dRpH1-4, dRsO4-6	Depth	4.12	132.9	4.54‡	48.0
	2	26	dRsO5-8	Right Occipital	Depth	3.88	114.5	4.06‡	125.81	2	Right amygdala hippo-campus	dRaH1-4, dRA1-4, dRpH1-2	Depth	3.88	99.1	4.06‡	81.8
65	1	302	dLpH1-3, dLaH1-3	Left hippo-campus	Depth	6.78‡	12.7	5.64	33.84	1	Left hippo-campus	dLpH1-4, dLaH1-2	Depth	6.78‡	16.4	5.64	33.6
66	1	533	dRpIN1-3	Right insula	Depth	5.97‡	35.0			1	Right insula	dRpIN1-6	Depth	5.97‡	37.3		
	2	409	dRaH1-2, dRpH2	Right hippo-campus	Depth	8.36‡	100.9	4.34	80.71								
69	1	218	dRaH1-3, dRA1-2	Right amygdala hippo-campus, insula	Depth	4.47‡	33.9	4.03	55.25	1	Right hippo-campus	dRaH1-5	Depth	4.47‡	30.0	4.03	51.9
	2	238	dLaH1-2, dLA1-2	Left amygdala hippo-campus	Depth	4.49	69.7	4.63‡	56.15	2	Left insula	dLA1-3	Depth	4.49	69.5	4.63‡	56.7

70	1	489	dRPOP4-5	Right oper-culum	Depth	6.11‡	28.9	3.60	82.29	2	Right insula	dRpIN1-4	Depth	6.11‡	14.4	3.60	69.1
	2	347	dRasT3-5	Right temporal	Depth	4.69‡	77.8						Depth				
	3	532	dRaIN1-2	Right insula	Depth	5.37‡	29.3			1	Right temporal	dRasT1-2, dRpIN3-6	Depth	5.37‡	15.3		

4.0 General Discussion and Future Directions

4.1 Introduction

The ultimate goal of epilepsy treatment is complete seizure freedom. Approximately 30% of individuals living with epilepsy are said to be resistant to medication[180], thus seizure freedom for these individuals cannot be reached by the use of medication alone. In these cases, the best course of treatment is epilepsy surgery. The success rate of epilepsy surgery is low however[35], likely due in part to the incomplete removal of the seizure onset zone (SOZ) — the area of the brain that generates clinical seizures. More precise identification of the SOZ is critical to increase the success rate of epilepsy surgery and provide epilepsy freedom for these individuals.

The overall aim of this thesis was to extend upon and apply previously developed methods with the intention of increasing the specificity and reliability of the identification of the SOZ using intracranial EEG-fMRI (iEEG-fMRI). The majority of the research in EEG-fMRI is conducted using scalp EEG-fMRI as it is a non-invasive methodology and therefore easier to collect and have larger study cohorts. However, iEEG-fMRI presents unique challenges and benefits. **Chapter 2** addresses the most common challenge when working with EEG-fMRI datasets: the presence of gradient switching artifact which contaminates the EEG. This chapter demonstrates that this artifact can be successfully removed for both conventional frequency ranges (0.1-80 Hz) but also for higher frequency oscillations. In **Chapter 3**, an exploration of the use of the absolute maximal BOLD cluster to localize the SOZ was performed. The results of this chapter provide evidence that with respect to iEEG data, the maximal negative BOLD response is of limited clinical value.

4.2 Thesis Overview

Conceptually, this thesis is two individual studies with one unifying theme: improving the localization of the SOZ. In **Chapter 2,** I focused on ensuring that the best model was created for the generation of the interictal epileptiform discharge (IED)-related BOLD response whereas **Chapter 3** focused on determining if a new way of looking at the IED-related BOLD response would lead to better localization of the SOZ.

4.2.1 Chapter 2: FiPP

While the principal purpose of this thesis was to consider the IED-related BOLD response, the Federico Lab iEEG Processing Pipeline (FiPP) was not intended to serve only IED identification. In light of recent data, it has been suggested that the use of IEDs as the temporal marker in EEG-fMRI studies may not be the most accurate marker to use[181]. Other markers, such as high frequency oscillations (found in the frequency range of 80-500 Hz) have shown promise in this area[182]. Thus, FiPP was developed in collaboration with Dr. LeVan and Dr. Zhang to produce artifact free iEEG through the full frequency band of 0.1-500 Hz. This enterprise was successful, with the core novel component of the pipeline being developed by Dr. LeVan and Dr. Zhang and named the LeVan Gradient Artifact Remover (LeGARE). The supporting structure of the pipeline and its validation were coded by me and developed with Mr. Pittman and Dr. Wilson.

4.2.2 The Absolute BOLD Response to IEDs

Most IED-related BOLD response studies focus solely on the identification and use of the maximal positive BOLD response to IEDs[124–127]. The logic of this focus was that the region of the brain that is most active and therefore maximally positive in response to IEDs is where the IEDs (and seizures) originate[124]. Despite sound logic, as time progressed, this assumption came into question and alternative BOLD response selection methods were suggested. One of these methods abandons the exclusive use of the maximal positive BOLD response to IEDs in favor of the maximal BOLD response regardless of polarity[149,150]. This theory is not without detractors, some claim the negative BOLD response is only a vascular phenomenon with no clinical significance, others have shown that the negative BOLD response is most often concordant with nodes of resting state networks, particularly the default mode network[99,135–142,152,160]. In **Chapter 3** the results provide evidence that the negative BOLD response to IEDs is not of clinical value in terms of localizing the SOZ in iEEG-fMRI data.

4.3 Exploring Chapter 2 FiPP

Using the FiPP pipeline, **Chapter 2** focused on the issue of gradient switching artifact (GSA) that imbues the EEG when the fMRI slices are being collected. An important characteristic inherent to the GSA that is leveraged during artifact removal is that the GSA is repetitive and predictable in shape and time in each TR of an fMRI scan. This is the assumption that is made with the traditional method of GSA removal: average artifact subtraction (AAS)[109]. This assumption is only true if the GSA is collected using a phantom, a "stand-in" scientific device used in MRI to simulate scanning a person. GSA recorded during a simultaneous iEEG-fMRI scan, however, does not have the same morphology and temporal sequence and is not always identical from one TR to the next. This leads to imperfect artifact removal using AAS and potentially to datasets being discarded due to excessive noise. Despite the limitations of GSA removal using AAS, its use was largely unchallenged as the focus of iEEG-fMRI was IED-related BOLD responses. IEDs can be identified in channel data which had been cleaned with AAS if a sufficient low-pass filter (e.g., 70 Hz) is applied to the data[109]. When the focus of EEG-fMRI research shifted to high frequency oscillations (HFOs) however, the use of AAS alone was no longer acceptable as it did not allow for the clear identification of HFOs.

4.3.1 Subject-Specific GSA

If GSA is supposed to be a perfect replication from TR to TR, it's important to consider why the pipeline was needed at all. MR machines are highly reliable and precise; we can easily determine when each gradient switch occurs. In **Chapter 2** a phantom scan was performed to capture the true GSA in EEG data, but we could have just as easily found the characteristics of the GSA from the sequence itself. The differences come from the patients we put in the scanner. Each patient, and often each electrode of said patient, will have GSAs of different morphology and occasional temporal shifts in GSA spike timings which presents a problem for artifact removal. These GSA variations are likely caused by several factors that contribute to the variations that we see in the GSA between subjects.

As explored in **Chapter 1**, AAS alone does not remove all GSA[101,102,109,116,117], due to inhomogeneities in the GSA as a result of temporal desynchronization between the MR scanner and the EEG clocks[101], head movement[117,118], ballistocardiogram artifact[101,116,117,119], or equipment vibrations such as the helium pump artifact[107,120]. Another physiological factor that should be considered but is easily overlooked is the phenomenon we are trying to capture with the BOLD signal: we are anticipating that with each IED a canonical hemodynamic response function (HRF) will occur. Blood vessels will dilate, a large volume of blood will arrive at the brain region and then local inhibition will cause hyperpolarization that constricts these same blood vessels causing an undershoot. This will cause micromovements in the brain region of question which repeat every time an event occurs. iEEG electrodes are specifically placed in areas where these events are expected to originate so it's to be expected that all electrodes will have micromovements if they have been placed in regions that are truly relevant to the patient's epilepsy.

An additional consideration should also be made with regards to the interaction between the radiofrequency (RF) signal and the electrodes. As stated in **Chapter 1**, electrodes within a magnetic field are subject to both Faraday's law[102], and Ampere's laws[103]. In MRI, the assumption is that the scanner's magnetic fields are neatly kept along three orthogonal planes, however, electrodes could be in any configuration, which could introduce a non-orthogonal magnetic vector altering the GSA by altering more than one of the x, y, or z magnetic fields thereby introducing error in data recording.

Observed GSA variability is a result of the interaction of physiological and technological factors. This interaction results in minute differences in the GSA from TR to TR. Each micromovement moves the electrode, the induced currents, the induced magnetic fields and thus changes the GSA. Macro-movements occur as well; in our studies up to 1.5 mm was acceptable. With electrodes smaller than the acceptable movement threshold, it is entirely conceivable that a patient could drift enough to change which two electrodes are the most external electrodes, entirely changing the induced voltages and magnetic fields. Of course, head drift is to be

expected, which is why all traditional artifact removal methods, and FiPP, work on a sliding window. The interactions of movement, be that micro or macro, and induced currents and the resulting induced magnetic fields is likely the ultimate cause of GSA variability from electrode to electrode, patient to patient.

4.3.2 FiPP Development

When I started my thesis program, the script that became FiPP was a simple shell which read in EEG and sent it through LeGARE. LeGARE was meant to be a "black box" in the sense that the user inputs artifact-contaminated iEEG and it returns meaningful signal with reduced GSA without the user needing to know what is happening inside the code. The threshold and in some cases, the definition of "cleaned" or artifact free EEG differs from user to user. In signal processing, artifact free EEG is typically considered by decreases in standard deviations of the measures or decreases in residual noise. To a clinician, even with the majority of the artifact removed, if the residual artifact resembled epileptic discharges or obscured clinically significant events the cleaning was not sufficient. To circumvent these issues, additional methods were added to FiPP such as: (i) acceptance of an artifact free iEEG comparator used to determine if the spectra of the cleaned EEG approximated that of this comparator and was thus sufficiently clean and (ii) for the user to override the number of PCA components to be removed.

Developing a processing pipeline around a black box presented many challenges. The first was the developing language itself. Matlab is a large program on its own that consumes large amounts of RAM and CPU capacity. As more processes were added around LeGARE to aid in increased artifact removal, the amount of data being held by Matlab became unfeasible. Ideally, FiPP would have been re-developed in a language without the limitations inherent to Matlab. LeGARE, however, was written in Matlab and it proved more difficult to try to send data to a Matlab script from a different language than to simply make Matlab work and accept the limitations of the language.

Another issue with developing around a closed script was the inability to directly modify the aspects of signal cleaning within LeGARE directly. The ability to tweak and modify aspects of FiPP became crucial throughout development to account for the high degree of variability within the cohort of iEEG-fMRI datasets. In previous use of AAS alone to remove GSA the number of epochs used in the average might be changed dependent on the residual GSA in the EEG data. The ability to tweak the number of epochs used in AAS may have been useful for some datasets as would have direct input to development of LeGARE.

4.3.3 The Artifact Free Comparator

A large decrease in residual GSA was noted once LeGARE was modified to base PCA component removal on the spectral comparison of the artifact laden iEEG to an artifact free exemplar. There was speculation before the validation process began that the choice of a non-scan comparator was meaningful, but since FiPP was developed using scan iEEG there was no way to test whether providing LeGARE with a specific non-scan comparator had significant impact on output data quality. To determine if FiPP was robust to non-scan choice, initial validation used the same non-scan time window for all datasets. Should the specific content of the non-scan be irrelevant, all datasets should have limited residual GSA after processing. It was determined, however, that the content of the non-scan comparator mattered. Quiescent non-scan comparators were likely to cause marked decreased amplitude of IED in the trace iEEG. Conversely, if the non-scan comparator was too event laden IEDs would be amplified. Thus, a non-scan should have an event in it, but not an event that has much larger amplitude than the trace iEEG. If the non-scan has multiple events, there shouldn't be too many, or many of large amplitude. These restrictions have implications for the datasets in clinical settings as artificially dampening spikes could lead to under identifying events, and artificially inflating the spikes could lead to over identifying events. The ability to modify this aspect of the script could ensure GSA artifact is accurately removed without altering the underlying physiological signal. This aspect of the pipeline was housed in LeGARE; thus, we did not alter it despite the narrow margin of error in non-scan comparator selection.

4.3.4 Future Directions

The field of signal processing is a constantly evolving. There is no end to developing a pipeline such as FiPP and the person(s) who follow will have to consider improvements in the field of signal processing. Developing the pipeline in Python or another interpreted language would likely decrease run time and CPU and RAM demand.

The recent finding with the variable GSA removal based on choice of non-scan comparator suggests that LeGARE should be revisited to reduce these variations. While we could just instruct all users to select specific non-scan time windows, this requires each user to open the iEEG before processing which is not easy for everyone as there are limited access points for EEG viewers. Naturally, FiPP could also be altered to allow for the user to scroll the iEEG trace, but this still requires both the user to be knowledgeable in event identification and for an event to occur within the limited artifact free data before and after the fMRI portion of the run which doesn't always occur. Thus, creating a more robust non-scan comparison method would better serve the end user.

The final direction that should be considered is a deviation from the methods within LeGARE altogether. Newer methods in the field are moving away from AAS and PCAs in favor of attempting to regress GSA out of each iEEG channel. This is done by adding additional ground channels in various locations around the head during data acquisition[111]. The logic is that regressing out the closest ground channel will most accurately remove the GSA generated in that region. Even if a complete switch to this method is not adopted, a consideration and testing of this method should be performed to determine if better GSA removal can be achieved.

4.3.5 FiPP Significance

The development of FiPP represents the first complete and self-contained preprocessing pipeline developed specifically for iEEG data. Additionally, the pipeline was developed with consideration of the potential users. Generally, processing methods are difficult to apply and read. FiPP was built with the recognition that not all individuals who may need to preprocess iEEG data will be

well versed in the methods used or the development environment Matlab. This may make implementation difficult for some users or result in improper use of FiPP. Through a combination of pre-set threshold variables and user prompts, FiPP guides users through the pipeline to ensure the same preprocessing occurs for all iEEG datasets. Having a self-contained and user-friendly pipeline increases the reliability and replicability of the iEEG data cleaning process which in turn increases the reliability and replicability of all studies based on the iEEG data. Additionally, the improvements made to the methods within FiPP allowed for more accurate identification and removal of GSA resulting in iEEG data from simultaneous iEEG-fMRI scans which are comparable in quality to the clinical iEEG data collected as part of the pre-surgical workup. This allows for more accurate identification of clinically relevant events for use in BOLD studies. The primary focus of **Chapter 2** was determining if the use of FiPP would result in easier and potentially more accurate identification of IEDs, but it was also determined that the use of FiPP may allow for the detection of HFOs, specifically in datasets where HFOs could not previously be identified due to excessive residual GSA which could not be removed using AAS alone. The development and implementation of FiPP will allow for better event identification resulting in more reliable and replicable BOLD studies.

4.4 Exploring Chapter 3: The BOLD response to intracranially recorded interictal discharges

4.4.1 IED-Related BOLD

IED-related BOLD has been the primary research interest of iEEG-fMRI and within that interest the focus has been on maximal positive BOLD response[124–127]. As the field has developed, however, the use of only positive BOLD responses and the consideration of only the maximal BOLD response has been questioned. The study presented in **Chapter 3** reflects an attempt to address these two points.

4.4.2 Standardization of fMRI Processing

A recent criticism of EEG-fMRI research is the lack of standardized analysis methods[146]. This is a fair criticism as the varying methods make it difficult to replicate data and at times may leave readers questioning if results are truly comparable. Further, it was specifically pointed out that

the lack of standardization is why EEG-fMRI is unlikely to be used for clinical applications in the near future[146]. As a response to concerns such as these, attempts at standardization were made within this thesis. The first was FiPP, however it can only standardize GSA removal of iEEG. The second was a pipeline to standardize fMRI processing.

In collaboration with lab members, current methods in fMRI processing were explored. The process we adopted was out of the MNI [125,138,155,159,177,178]. This process used four hemodynamic response functions with times to peak of 3, 5, 7, and 9 seconds to generate statistically significant BOLD response maps. The four z-score threshold maps were then amalgamated into a single cluster map. To create this map, the highest z-score for each voxel location from amongst the four z-score maps was selected as that voxel location's z-score. While all fMRI processing was conducted using FSL[170–172], steps were taken to automate the process. Using the research gathered by myself and my lab mates, I created a fully automated and closed Matlab process to complete the fMRI processing. The decisions of making the process closed, automatic, and limited to specific file organization was to force all persons processing data to follow the exact same process each time fMRI data is processed. While this process is not strictly novel, it's a promising step toward standardization and unity within the field of EEG-fMRI research.

4.4.3 The Negative BOLD Response to IEDs

Recently, it has become more common in IED-related EEG-fMRI analyses to consider both positive and negative clusters in order to find the maximal cluster[149,150]. This consideration relies on the notion that negative BOLD may be a reflection of enhanced local inhibition, altered neurometabolic activity, or disruption of network activity as a result of IEDs[183]. Negative BOLD responses tend to be smaller in extent and in significance than positive BOLD responses. With lower significance, negative BOLD clusters are far less likely to meet cluster z or p significance thresholds than positive BOLD responses. This translates into fewer negative BOLD responses being generated and also makes it less likely for a negative BOLD response to be selected as the maximal response. It's possible that difference between the numbers of positive and negative clusters generated and the difference in the significance of these clusters that are generated is

due to previous studies and the study in **Chapter 3** not using hemodynamic response functions (HRFs) specifically designed for identifying the negative BOLD response. Not using specific HRFs could account for a portion of the differences between the positive and negative BOLD responses and why so few of the negative BOLD responses are proximal to the SOZ.

The research that supports the use of the absolute maximal BOLD response as the indicator of the SOZ was carried out using scalp EEG-fMRI [149,150]. It cannot be ignored that scalp and intracranial EEG face different challenges when recording IEDs and other events of clinical significance. iEEG records events more directly and can record from deeper substructures, whereas for an event to be recorded on scalp EEG it has to be large enough to get through the signal dispersion that occurs due to the skull and content with larger movement artifact like jaw clenching and eye blinking. It is possible that the limited negative BOLD responses relative to the positive BOLD responses observed in **Chapter 3** is a result of the difference between scalp and intracranial EEG data. Since scalp EEG is recorded further from the IED generator it is possible that fewer positive BOLD responses are generated and that these BOLD responses have lower significance levels making the positive and negative BOLD responses generated more similar and thus the use of an absolute maximal cluster of more utility for identifying the location of the SOZ. In the study presented in **Chapter 3** however, the absolute maximal BOLD response was rarely the maximal negative BOLD response and when the absolute maximal BOLD response was negative, it was not likely to be proximal to the SOZ. This made the use of the absolute maximal BOLD response of limited value within our dataset and likely intracranial data in general. This is not to say that negative BOLD responses to IEDs should not be considered in relation to iEEG data, but rather that a new framework should be developed specifically for iEEG that allows for the consideration of both positive and negative BOLD responses to IEDs in a manner that is meaningful specifically to iEEG and not to the norms or practices in the field.

4.4.4 High Confidence in Cluster Significance

It has been noted in the literature that the use of the maximal BOLD response to IEDs alone is not sufficient for the localization of the SOZ[125,149]. This notion was supported by the preliminary

results in **Chapter 3**. The use of the maximal cluster without consideration of its clinical value or relevance may lead to the selection of clusters that are of limited utility for localizing the SOZ and also cluster selection that does not serve the best interest of the patient whose data generated the clusters.

The criteria a cluster had to meet in order to be considered significant was problematic[125,149]. First, the focus is still on the most maximal cluster. While the cluster with the highest z-score does have the highest likelihood of being the central locus of the activity that gave rise to the BOLD response, all the clusters are significant. A bigger separation between the z-scores of the two highest correlated clusters does not necessarily mean the biggest z-score represents the origin of the event. If we consider TLE, a cluster with a much larger z-score in the hippocampus could mean that another task happened to be occurring at the same time. There is no way to know based on just one metric. Additionally, if only one cluster was generated, it was automatically considered to have high confidence. Even if the metric was an ideal measure only generating one cluster does not mean the cluster is real and perfect, just that one was generated and assuming otherwise may not actually lead to the selection of the best cluster when not choosing the cluster may have been a better choice. Lastly, one of the criteria was a significance threshold. No matter how well reasoned, the choice of a threshold is arbitrary. The threshold in the original study, and in **Chapter 3**, was z = 3.1, but z = 2.3 or 3.7 could also be justified and would have changed the results.

Like most practices in EEG-fMRI analyses, the inequality used in **Chapter 3** was developed using scalp EEG-fMRI. While similar in nature, given how much closer the electrodes are to the IED generators, clusters generated from iEEG data are likely more significant and numerous. A test based on values measured in a completely different manner is unlikely to accurately reflect a similar but very distinct data acquisition method.

4.4.5 The Use of Maximal BOLD Clusters

The use of the maximal BOLD response – be it positive, negative, or absolute – is not ideal. The maximal BOLD response is the highest correlated region and is likely to represent a large amount of metabolic activity. However, this does not mean there is not another smaller region that is the

origin of the epileptiform activity and from that origin the activity is being amplified as it propagates. There is a tendency in science to want a simple single answer. We want one cluster to be the perfect cluster and this cluster to be selected in an objective way, such as selecting the maximal cluster. It is possible, however, that all clusters generated during iEEG-fMRI analysis should be considered by an expert for those results that are the most meaningful for the patient. Alternatively, a middle ground could be reached where objective measures reduce the generated clusters to a "most likely to be relevant" set of clusters that could be subjectively considered.

Moving beyond maximal clusters and considering clusters based on relevance and meaning may allow for broader utility of the negative BOLD response to IEDs. A loss of inhibition around the SOZ may result in the spread of ictal activity[181]. Given that IED related studies occur without the development of seizures, it is reasonable to expect that an area of inhibition around the SOZ occurs in relation to IEDs. Theoretically, inhibition could also be occurring at other nodes along the epilepsy network also stopping the propagation of ictal activity. This inhibition as a result of IEDs may not be the maximal response, but it may be a useful identifier of the region(s) of the brain that are involved in stopping ictal activity from propagating. While speculative, there were negative BOLD responses identified that were proximal to the SOZ but did not have the highest z-score thus were overlooked in the current analysis. Consideration of these responses based on their potential meaning may reveal patterns in the data which could increase the utility of the negative BOLD response to IEDs.

4.4.6 Future Directions

In this thesis, the primary concern of using simultaneous iEEG-fMRI was addressed on the iEEG side of data acquisition with the development of FiPP to remove GSA. A similar issue however occurs on the fMRI side of data acquisition. iEEG electrodes create artifact in the fMRI data and currently nothing is being considered to address this artifact, it is accepted as a necessity of iEEG-fMRI data collection. There may, however, be a way to address this artifact. Around each electrode there is signal dropout due to susceptibility artifact[184]; a result of rapid dephasing. By adjusting the pulse sequence, it may be possible to account for this rapid dephasing allowing for

the recording of the BOLD signal closer to the electrode. This could be accomplished by using a shorter TE or using a sequence that attenuates specifically attenuates metal artifact. Changes to the sequence would have to be tested and validated however to ensure that they specifically attenuate the artifact from the electrode without impacting BOLD signal collection.

To better understand the utility of the negative BOLD cluster in localizing the SOZ, an exploration of negative BOLD-specific HRFs should be conducted. These HRFs may help better identify IED-related negative BOLD responses and increase their representation in the dataset regardless of the cluster selection criteria. Further, should a confidence ranking be considered moving forward, new criteria should be developed using iEEG data rather than relying on tests generated using data that is not identical to the data in this cohort. One additional avenue that should be explored is whether the negative BOLD response to IEDs has any utility other than that of SOZ localization. Previous research has indicated that the IED-related negative BOLD response is often concordant with nodes of the default mode network[152]. An exploration of this finding in iEEG could increase the understanding of how IEDs and resting state networks such as the default mode network interact.

Most methods currently employed for determining cluster SOZ or IED concordance follow a similar process. A subset of clusters, or a single cluster, are chosen as the clusters of interest using some criteria. To determine how close these clusters are to a proxy of the EZ, the distance from a single point in the cluster to a single point in the SOZ or IED is calculated. There are several ways in which this method could potentially be improved. First, the SOZ and the IED are three-dimensional, distance calculations should account not only for how close the cluster is to the centre of these targets but also to the edges, which could be interpolated from the contacts involved. Further, epilepsy is a network disorder making it difficult to know which clusters truly are clinically relevant. Building a processing that creates a weighted relevance value for each cluster based on factors such as proximity to the SOZ and IED, clinical factors, brain region, or functional connectivity may provide clinically relevant information beyond the potential location of the EZ.

4.4.7 IED-Related BOLD Summary

IED-related BOLD research continues to expand in scope and methods in research centres that use scalp EEG-fMRI. The methods developed out of these centres should be scrutinized before being applied to iEEG-fMRI data. While the principles of data collection are the same, the reality of how the data is collected is different. It would likely be a best practice to test these methods and then replicate the development method using iEEG-fMRI data rather than directly applying the methods to our data.

4.5 General Summary

The purpose of my thesis was to develop and extend methods to increase accuracy in localizing the SOZ. The development of FiPP goes a long way in helping this goal as it helps better identify events such as IEDs due to its superior artifact removal over AAS alone. Further, by attempting to extend research completed in scalp EEG-fMRI to iEEG-fMRI, areas were identified where more focus should be placed in developing methods and questions specific to iEEG-fMRI research.

4.6 Significance

The use of iEEG-fMRI in clinical practice may aid in the pre-surgical identification of the SOZ. Currently, the method is not included due to limitations in reliability and replicability of the BOLD results. A crucial first step in event related BOLD analyses is the use of accurate temporal markers. Before the development of FiPP, the identification of events in iEEG from simultaneous iEEG-fMRI data collection was marred by imperfect event identification due to incomplete removal of GSA. FiPP stands as a self-contained user-friendly process which allows for the removal of GSA such that the quality of the EEG trace of the resultant signal rivals that of clinical iEEG allowing for accurate and reliable identification of events for use in BOLD related analyses increasing the reliability and replicability of the results of these analyses. Expanding IED related BOLD analyses to consider more than just the maximal response without validation also allows for more accurate identification of the SOZ. While the results in **Chapter 3** did not select for clusters that were as close to the SOZ as were expected, the modifications therein did remove clusters that were more distal to the presumed SOZ. A few modifications to the methods of **Chapter 3** such as

those presented here would further increase the reliability of the BOLD response as an indicator of the location of the SOZ. Taken together, this thesis presented methods that will further increase the reliability of IED related BOLD analyses in identifying the SOZ, a step towards the inclusion of iEEG-fMRI in the pre-surgical workup; an inclusion which will increase the likeliness of seizure freedom following surgery.

References

1. Gilmour, H., Ramage-Mrin, P. & Wong, S. Epilepsy in Canada: Prevalence and Impact. *Health Rep* **27**, 24–30 (2016).
2. Patel, P. & Moshé, S. L. The evolution of the concepts of seizures and epilepsy: What's in a name? *Epilepsia Open* **5**, 22–35 (2020).
3. Sveinsson, O., Andersson, T., Mattsson, P., Carlsson, S. & Tomson, T. Clinical risk factors in SUDEP: A nationwide population-based case-control study. *Neurology* **94**, e419–e429 (2020).
4. Magiorkinis, E., Diamantis, A., Sidiropoulou, K. & Panteliadis, C. Highights in the History of Epilepsy: The Last 200 Years. *Epilepsy Res Treat* **2014**, 1–13 (2014).
5. Fisher, R. S. *et al.* Instruction manual for the ILAE 2017 operational classification of seizure types. *Epilepsia* **58**, 531–542 (2017).
6. Fisher, R. S. *et al.* ILAE Official Report: A practical clinical definition of epilepsy. *Epilepsia* **55**, 475–482 (2014).
7. Chauvière, L. *et al.* Changes in interictal spike features precede the onset of temporal lobe epilepsy. *Ann Neurol* **71**, 805–814 (2012).
8. Specchio, N. *et al.* International League Against Epilepsy classification and definition of epilepsy syndromes with onset in childhood: Position paper by the ILAE Task Force on Nosology and Definitions. *Epilepsia* **63**, 1398–1442 (2022).
9. Scheffer, I. E. *et al.* ILAE classification of the epilepsies: Position paper of the ILAE Commission for Classification and Terminology. *Epilepsia* **58**, 512–521 (2017).
10. Sultana, B. *et al.* Incidence and Prevalence of Drug-Resistant Epilepsy: A Systematic Review and Meta-analysis. *Neurology* **96**, 805–817 (2021).
11. Schmidt, D. Drug treatment of epilepsy: Options and limitations. *Epilepsy and Behavior* **15**, 56–65 (2009).
12. DiIorio, C. *et al.* Behavioral, social, and affective factors associated with self-efficacy for self-management among people with epilepsy. *Epilepsy and Behavior* **9**, 158–163 (2006).
13. Yildirim, M. S. & Yildiz, E. Determination of self-efficacy of patients diagnosed with epilepsy. *Neurological Sciences* **43**, 2709–2715 (2022).
14. Dilorio, C. & Faherty, B. Epilepsy self-management: Partial replication and extension. *Res Nurs Health* **17**, 167–174 (1994).
15. Aghakhani, Y. *et al.* Co-localization between the BOLD response and epileptiform discharges recorded by simultaneous intracranial EEG-fMRI at 3 T. *Neuroimage Clin* **7**, 755–763 (2015).
16. Pillai, J. & Sperling, M. R. Interictal EEG and the diagnosis of epilepsy. *Epilepsia* **47**, 14–22 (2006).
17. Diamond, J. M., Chapeton, J. I., Theodore, W. H., Inati, S. K. & Zaghloul, K. A. The seizure onset zone drives state-dependent epileptiform activity in susceptible brain regions. *Clinical Neurophysiology* **130**, 1628–1641 (2019).
18. Diamond, J. M. *et al.* Interictal discharges in the human brain are travelling waves arising from an epileptogenic source. *Brain* **146**, 1903–1915 (2023).

19. Staley, K. J., White, A. & Dudek, F. E. Interictal spikes: Harbingers or causes of epilepsy? *Neurosci Lett* **497**, 247–250 (2011).
20. Karoly, P. J. *et al.* Interictal spikes and epileptic seizures: Their relationship and underlying rhythmicity. *Brain* **139**, 1066–1078 (2016).
21. Smith, E. H. *et al.* Human interictal epileptiform discharges are bidirectional traveling waves echoing ictal discharges. *Elife* **11**, 1–20 (2022).
22. Luan, C., Miller, J., Sollars, C., Peng, J. & Singh, J. Stereo-Electroencephalography-Recorded Interictal Epileptiform Discharges : Activation Pattern and Its Relationship With Surgical Outcome. *Creus* **15**, 4–8 (2023).
23. White, H. S., Smith, M. D. & Wilcox, K. S. Mechanisms of Action of Antiepileptic Drugs. *Int Rev Neurobiol* **81**, 85–110 (2007).
24. Sills, G. J. & Rogawski, M. A. Mechanisms of action of currently used antiseizure drugs. *Neuropharmacology* **168**, 107966 (2020).
25. Rogawski, M. A., Löscher, W. & Rho, J. M. Mechanisms of action of Antiseizure Drugs and the Ketogenic diet. *Cold Spring Harb Perspect Med* **6**, 28 (2016).
26. D'Andrea Meira, I. *et al.* Ketogenic diet and epilepsy: What we know so far. *Front Neurosci* **13**, 1–8 (2019).
27. Zhu, Z. *et al.* Use of Integrative, Complementary, and Alternative Medicine in Children with Epilepsy: A Global Scoping Review. *Children* vol. 10 1–23 Preprint at https://doi.org/10.3390/children10040713 (2023).
28. Ngugi, A. K., Bottomley, C., Kleinschmidt, I., Sander, J. W. & Newton, C. R. Estimation of the burden of active and life-time epilepsy: A meta-analytic approach. *Epilepsia* **51**, 883–890 (2010).
29. Lee, J., Son, K., Hwang, G. & Kim, M. Effect and safety of shihogyejitang for drug resistant childhood epilepsy. *Evidence-based Complementary and Alternative Medicine* **2016**, (2016).
30. Zangooei pourfard, M. *et al.* Efficacy and tolerability of hydroalcoholic extract of Paeonia officinalis in children with intractable epilepsy: An open-label pilot study. *Epilepsy Res* **176**, 106735 (2021).
31. Perucca, E. Cannabinoids in the Treatment of Epilepsy: Hard Evidence at Last? *J Epilepsy Res* **7**, 61–76 (2017).
32. Pearl, P. L., Drillings, I. M. & Conry, J. A. Herbs in Epilepsy: Evidence for Efficacy, Toxicity, and Interactions. *Semin Pediatr Neurol* **18**, 203–208 (2011).
33. Lim, A., Cranswick, N. & South, M. Adverse events associated with the use of complementary and alternative medicine in children. *Arch Dis Child* **96**, 297–300 (2011).
34. Kaiboriboon, K., Guevara, M. & Alldredge, B. K. Understanding herb and dietary supplement use in patients with epilepsy. *Epilepsia* **50**, 1927–1932 (2009).
35. Noachtar, S. & Borggraefe, I. Epilepsy surgery: A critical review. *Epilepsy and Behavior* **15**, 66–72 (2009).
36. Kwan, P. *et al.* Definition of drug resistant epilepsy: Consensus proposal by the ad hoc Task Force of the ILAE Commission on Therapeutic Strategies. *Epilepsia* **51**, 1069–1077 (2010).
37. Morrell, F. Secondary Epileptogenesis in Man. *Arch Neurol* **42**, 318–335 (1985).

38. Beyenburg, S., Mitchell, A. J., Schmidt, D., Elger, C. E. & Reuber, M. Anxiety in patients with epilepsy: Systematic review and suggestions for clinical management. *Epilepsy and Behavior* **7**, 161–171 (2005).
39. de Souza, E. A. P. & Salgado, P. C. B. A psychosocial view of anxiety and depression in epilepsy. *Epilepsy and Behavior* **8**, 232–238 (2006).
40. Ochoa-Urrea, M. More than seizures: In people with epilepsy, social anxiety affects quality of life. *Epigraph* **21**, (2019).
41. Singh, T. & Goel, R. K. Epilepsy Associated Depression: An Update on Current Scenario, Suggested Mechanisms, and Opportunities. *Neurochem Res* **46**, 1305–1321 (2021).
42. Mesraoua, B. *et al.* Dramatic outcomes in epilepsy: depression, suicide, injuries, and mortality. *Curr Med Res Opin* **36**, 1473–1480 (2020).
43. Tombini, M. *et al.* Depressive symptoms and difficulties in emotion regulation in adult patients with epilepsy: Association with quality of life and stigma. *Epilepsy and Behavior* **107**, (2020).
44. Batchelor, R. & Taylor, M. D. Young adults with epilepsy: Relationships between psychosocial variables and anxiety, depression, and suicidality. *Epilepsy and Behavior* **118**, 107911 (2021).
45. Collard, S. S. & Ellis-Hill, C. 'I'd rather you didn't come': The impact of stigma on exercising with epilepsy. *J Health Psychol* **24**, 1345–1355 (2019).
46. Tedrus, G. M. A. S., Pereira, R. B. & Zoppi, M. Epilepsy, stigma, and family. *Epilepsy and Behavior* **78**, 265–268 (2018).
47. Bellon, M., Walker, C., Peterson, C. & Cookson, P. The 'E' word: epilepsy and perceptions of unfair treatment from the 2010 Australian Epilepsy Longitudinal Survey. *Epilepsy Behav* **27**, 251–256 (2013).
48. Langfitt, J. T. *et al.* Worsening of quality of life after epilepsy surgery: Effect of seizures and memory decline. *Neurology* **68**, 1988–1994 (2007).
49. Janecek, J. K. *et al.* Cognitive decline and quality of life after resective epilepsy surgery. *Epilepsy and Behavior* **138**, 109005 (2023).
50. Winslow, J., Hu, B., Tesar, G. & Jehi, L. Longitudinal trajectory of quality of life and psychological outcomes following epilepsy surgery. *Epilepsy and Behavior* **111**, (2020).
51. Sheikh, S. *et al.* (Re)Defining success in epilepsy surgery: The importance of relative seizure reduction in patient-reported quality of life. *Epilepsia* **60**, 2078–2085 (2019).
52. Rosenow, F. & Lüders, H. Presurgical evaluation of epilepsy. *Brain* **124**, 1683–1700 (2001).
53. Nabbout, R. *et al.* Epilepsy in tuberous sclerosis complex: Findings from the TOSCA Study. *Epilepsia Open* **4**, 73–84 (2019).
54. Khoo, H. M. *et al.* The spike onset zone. *Neurology* **91**, e666–e674 (2018).
55. Berg, A. T. *et al.* Revised terminology and concepts for organization of seizures and epilepsies: Report of the ILAE Commission on Classification and Terminology, 2005-2009. *Epilepsia* **51**, 676–685 (2010).
56. Kramer, M. A. & Cash, S. S. Epilepsy as a disorder of cortical network organization. *Neuroscientist* **18**, 360–372 (2012).
57. Lara Jehi. The Epileptogenic Zone: Concept and Definition. *Epilepsy Curr* **18**, 12–16 (2018).

58. Marino, A. C. *et al.* Resting state connectivity in neocortical epilepsy: The epilepsy network as a patient-specific biomarker. *Clinical Neurophysiology* **130**, 280–288 (2019).
59. Ramaraju, S. *et al.* Removal of Interictal MEG-Derived Network Hubs Is Associated With Postoperative Seizure Freedom. *Front Neurol* **11**, 1–9 (2020).
60. Mithani, K. *et al.* Lesion Network Localization of Seizure Freedom following MR-guided Laser Interstitial Thermal Ablation. *Sci Rep* **9**, 1–11 (2019).
61. Bartolomei, F. *et al.* From mesial temporal lobe to temporoperisylvian seizures: A quantified study of temporal lobe seizure networks. *Epilepsia* **51**, 2147–2158 (2010).
62. Boerwinkle, V. L. *et al.* Network-targeted approach and postoperative resting-state functional magnetic resonance imaging are associated with seizure outcome. *Ann Neurol* **86**, 344–356 (2019).
63. Neal, E. G., Maciver, S., Schoenberg, M. R. & Vale, F. L. Surgical disconnection of epilepsy network correlates with improved outcomes. *Seizure* **76**, 56–63 (2020).
64. Sinha, N. *et al.* Predicting neurosurgical outcomes in focal epilepsy patients using computational modelling. *Brain* **140**, 319–332 (2017).
65. Tsipouras, M. G. Spectral information of EEG signals with respect to epilepsy classification. *EURASIP J Adv Signal Process* **2019**, (2019).
66. Höller, P., Trinka, E. & Höller, Y. High-Frequency Oscillations in the Scalp Electroencephalogram: Mission Impossible without Computational Intelligence. *Comput Intell Neurosci* **2018**, (2018).
67. Olejniczak, P. Neurophysiologic basis of EEG. *Journal of Clinical Neurophysiology* **23**, 186–189 (2006).
68. Ahlfors, S. P., Han, J., Belliveau, J. W. & Hämäläinen, M. S. Sensitivity of MEG and EEG to source orientation. *Brain Topogr* **23**, 227–232 (2010).
69. Spencer, S. S. The Relative Contributions of MRI, SPECT, and PET Imaging in Epilepsy. *Epilepsia* **35**, S72–S89 (1994).
70. Nippert, Amy, R., Biesecker, Kyle, R. & Newman, Eric, A. Mechanisms Mediating Functional Hyperemia in the Brain. *Neuroscientist* **24**, 73–83 (2018).
71. la Fougère, C., Rominger, A., Förster, S., Geisler, J. & Bartenstein, P. PET and SPECT in epilepsy: A critical review. *Epilepsy and Behavior* **15**, 50–55 (2009).
72. Devous, M. D., Thisted, R. A., Morgan, G. F., Leroy, R. F. & Rowe, C. C. SPECT brain imaging in epilepsy: A meta-analysis. *Journal of Nuclear Medicine* **39**, 285–293 (1998).
73. Yang, H. *et al.* Glycolysis in energy metabolism during seizures. *Neural Regen Res* **8**, 1316–1326 (2013).
74. Andrew, E. R. Nuclear magnetic resonance and the brain. *Brain Topogr* **5**, 129–133 (1992).
75. Deichmann, R., Nöth, U. & Weiskopf, N. The Basics of Functional Magnetic Resonance Imaging. in *EEG–fMRI: Physiological Basis, Technique and Applications* (eds. Mulert, C. & Lemieux, L.) 39–57 (Springer, 2010).
76. Woermann, F. G. & Vollmar, C. Clinical MRI in children and adults with focal epilepsy: A critical review. *Epilepsy and Behavior* **15**, 40–49 (2009).
77. Uğurbil, K. *et al.* Magnetic resonance studies of brain function and neurochemistry. *Annu Rev Biomed Eng* **2**, 633–660 (2000).

78. Magistretti, P. J. & Allaman, I. A Cellular Perspective on Brain Energy Metabolism and Functional Imaging. *Neuron* **86**, 883–901 (2015).
79. Buxton, R. B., Uludağ, K., Dubowitz, D. J. & Liu, T. T. Modeling the hemodynamic response to brain activation. *Neuroimage* **23**, 220–233 (2004).
80. Hall, C. N., Klein-Flügge, M. C., Howarth, C. & Attwell, D. Oxidative phosphorylation, not glycolysis, powers presynaptic and postsynaptic mechanisms underlying brain information processing. *Journal of Neuroscience* **32**, 8940–8951 (2012).
81. Lauritzen, M. Reading vascular changes in brain imaging: Is dendritic calcium the key? *Nat Rev Neurosci* **6**, 77–85 (2005).
82. Chow, M. S., Wu, S. L., Webb, S. E., Gluskin, K. & Yew, D. Functional magnetic resonance imaging and the brain: A brief review. *World J Radiol* **9**, 5 (2017).
83. Fonzo, G. A. & Etkin, A. Fonzo 2017 - Neuroimaging GAD. *Dialogues Clin Neurosci* **19**, 169–180 (2017).
84. Hakkers, C. S. *et al.* Review of functional MRI in HIV: effects of aging and medication. *J Neurovirol* **23**, 20–32 (2017).
85. Jaworska, N., Yang, X. R., Knott, V. & Macqueen, G. A review of fMRI studies during visual emotive processing in major depressive disorder. *World Journal of Biological Psychiatry* **16**, 448–471 (2015).
86. Sten, S. *et al.* Neural inhibition can explain negative BOLD responses: A mechanistic modelling and fMRI study. *Neuroimage* **158**, 219–231 (2017).
87. Mullinger, K. J., Cherukara, M. T., Buxton, R. B., Francis, S. T. & Mayhew, S. D. Post-stimulus fMRI and EEG responses: Evidence for a neuronal origin hypothesised to be inhibitory. *Neuroimage* **157**, 388–399 (2017).
88. Mullinger, K. J., Mayhew, S. D., Bagshaw, A. P., Bowtell, R. & Francis, S. T. Evidence that the negative BOLD response is neuronal in origin: A simultaneous EEG-BOLD-CBF study in humans. *Neuroimage* **94**, 263–274 (2014).
89. Jacobs, J. *et al.* Negative BOLD in default-mode structures measured with EEG-MREG is larger in temporal than extra-temporal epileptic spikes. *Front Neurosci* **8**, 1–12 (2014).
90. Pasley, B. N., Inglis, B. A. & Freeman, R. D. Analysis of oxygen metabolism implies a neural origin for the negative BOLD response in human visual cortex. *Neuroimage* **36**, 269–276 (2007).
91. Wilson, R., Mullinger, K. J., Francis, S. T. & Mayhew, S. D. The relationship between negative BOLD responses and ERS and ERD of alpha/beta oscillations in visual and motor cortex. *Neuroimage* **199**, 635–650 (2019).
92. Sengupta, B., Laughlin, S. B. & Niven, J. E. Balanced Excitatory and Inhibitory Synaptic Currents Promote Efficient Coding and Metabolic Efficiency. *PLoS Comput Biol* **9**, (2013).
93. Koush, Y. *et al.* Metabolic underpinnings of activated and deactivated cortical areas in human brain. *Journal of Cerebral Blood Flow and Metabolism* (2021) doi:10.1177/0271678X21989186.
94. Dupret, D., Pleydell-Bouverie, B. & Csicsvari, J. Inhibitory interneurons and network oscillations. *Proc Natl Acad Sci U S A* **105**, 18079–18080 (2008).
95. Middleton, S. *et al.* NMDA receptor-dependent switching between different gamma rhythm-generating microcircuits in entorhinal cortex. *Proc Natl Acad Sci U S A* **105**, 18572–18577 (2008).

96. Vazquez, A. L., Fukuda, M. & Kim, S. G. Inhibitory Neuron Activity Contributions to Hemodynamic Responses and Metabolic Load Examined Using an Inhibitory Optogenetic Mouse Model. *Cerebral Cortex* **28**, 4105–4119 (2018).
97. Foucher, J. R., Otzenberger, H. & Gounot, D. The BOLD response and the gamma oscillations respond differently than evoked potentials: An interleaved EEG-fMRI study. *BMC Neurosci* **4**, 1–11 (2003).
98. Beltrán, D., Morera, Y., García-Marco, E. & De Vega, M. Brain inhibitory mechanisms are involved in the processing of sentential negation, regardless of its content. Evidence from EEG theta and beta rhythms. *Front Psychol* **10**, 1–14 (2019).
99. Benuzzi, F. *et al.* An EEG-fMRI study on the termination of generalized spike-and-wave discharges in absence epilepsy. *PLoS One* **10**, 1–16 (2015).
100. Shmuel, A. *et al.* Sustained negative BOLD, blood flow and oxygen consumption response and its coupling to the positive response in the human brain. *Neuron* **36**, 1195–1210 (2002).
101. Warbrick, T. Simultaneous EEG-fMRI: What Have We Learned and What Does the Future Hold? *Sensors* **22**, (2022).
102. Yan, W. X., Mullinger, K. J., Brookes, M. J. & Bowtell, R. Understanding gradient artefacts in simultaneous EEG/fMRI. *Neuroimage* **46**, 459–471 (2009).
103. Jog, M. *et al.* Concurrent Imaging of Markers of Current Flow and Neurophysiological Changes During tDCS. *Front Neurosci* **14**, 1–13 (2020).
104. Fujita, Y. *et al.* Evaluating the Safety of Simultaneous Intracranial Electroencephalography and Functional Magnetic Resonance Imaging Acquisition Using a 3 Tesla Magnetic Resonance Imaging Scanner. *Front Neurosci* **16**, 1–15 (2022).
105. Peedicail, J. S. *et al.* Clinical safety of intracranial EEG electrodes in MRI at 1.5 T and 3 T: a single-center experience and literature review. *Neuroradiology* **63**, 1669–1678 (2021).
106. Carmichael, D. W. *et al.* Safety of localizing epilepsy monitoring intracranial electroencephalograph electrodes using MRI: Radiofrequency-induced heating. *Journal of Magnetic Resonance Imaging* **28**, 1233–1244 (2008).
107. Steyrl, D. & Müller-Putz, G. R. Artifacts in EEG of simultaneous EEG-fMRI: Pulse artifact remainders in the gradient artifact template are a source of artifact residuals after average artifact subtraction. *J Neural Eng* **16**, (2019).
108. Anami, K. *et al.* Stepping stone sampling for retrieving artifact-free electroencephalogram during functional magnetic resonance imaging. *Neuroimage* **19**, 281–295 (2003).
109. Allen, P. J., Josephs, O. & Turner, R. A method for removing imaging artifact from continuous EEG recorded during functional MRI. *Neuroimage* **12**, 230–239 (2000).
110. Hoffmann, A. *et al.* Electroencephalography during functional echo-planar imaging: Detection of epileptic spikes using post-processing methods. *Magn Reson Med* **44**, 791–798 (2000).
111. Kraljič, A., Matkovič, A., Purg, N., Demšar, J. & Repovš, G. Evaluation and comparison of most prevalent artifact reduction methods for EEG acquired simultaneously with fMRI. *Frontiers in Neuroimaging* **1**, (2022).
112. Bullock, M., Jackson, G. D. & Abbott, D. F. Artifact Reduction in Simultaneous EEG-fMRI: A Systematic Review of Methods and Contemporary Usage. *Front Neurol* **12**, 1–21 (2021).

113. Warach, S. *et al.* EEG-triggered echo-planar functional MRI in epilepsy. *Neurology* **47**, 89–93 (1996).
114. Ives, J. R., Warach, S., Schmitt, F., Edelman, R. R. & Schomer, D. L. Monitoring the patient's EEG during echo planar MRI. *Electroencephalogr Clin Neurophysiol* **87**, 417–420 (1993).
115. Allen, P. J., Polizzi, G., Krakow, K., Fish, D. R. & Lemieux, L. Identification of EEG events in the MR scanner: The problem of pulse artifact and a method for its subtraction. *Neuroimage* **8**, 229–239 (1998).
116. Warbrick, T. & Bagshaw, A. P. Scanning strategies for simultaneous EEG-fMRI evoked potential studies at 3 T. *International Journal of Psychophysiology* **67**, 169–177 (2008).
117. Ritter, P., Becker, R., Graefe, C. & Villringer, A. Evaluating gradient artifact correction of EEG data acquired simultaneously with fMRI. *Magn Reson Imaging* **25**, 923–932 (2007).
118. Bénar, C. G. *et al.* Quality of EEG in simultaneous EEG-fMRI for epilepsy. *Clinical Neurophysiology* **114**, 569–580 (2003).
119. Rusiniak, M. *et al.* EEG-fMRI: Ballistocardiogram Artifact Reduction by Surrogate Method for Improved Source Localization. *Front Neurosci* **16**, 1–16 (2022).
120. Grouiller, F. *et al.* A comparative study of different artefact removal algorithms for EEG signals acquired during functional MRI. *Neuroimage* **38**, 124–137 (2007).
121. Ryali, S., Glover, G. H., Chang, C. & Menon, V. Development, validation, and comparison of ICA-based gradient artifact reduction algorithms for simultaneous EEG-spiral in/out and echo-planar fMRI recordings. *Neuroimage* **48**, 348–361 (2009).
122. Negishi, M., Abildgaard, M., Nixon, T. & Todd Constable, R. Removal of time-varying gradient artifacts from EEG data acquired during continuous fMRI. *Clinical Neurophysiology* **115**, 2181–2192 (2004).
123. Niazy, R. K., Beckmann, C. F., Iannetti, G. D., Brady, J. M. & Smith, S. M. Removal of FMRI environment artifacts from EEG data using optimal basis sets. *Neuroimage* **28**, 720–737 (2005).
124. Jacobs, J. *et al.* Hemodynamic responses to interictal epileptiform discharges in children with symptomatic epilepsy. *Epilepsia* **48**, 2068–2078 (2007).
125. Khoo, H. M. *et al.* The hemodynamic response to interictal epileptic discharges localizes the seizure-onset zone. *Epilepsia* **58**, 811–823 (2017).
126. Aghakhani, Y. *et al.* fMRI activation during spike and wave discharges in idiopathic generalized epilepsy. *Brain* **127**, 1127–1144 (2004).
127. Gotman, J. Epileptic networks studied with EEG-fMRI. *Epilepsia* **49**, 42–51 (2008).
128. Zijlmans, M. *et al.* EEG-fMRI in the preoperative work-up for epilepsy surgery. *Brain* **130**, 2343–2353 (2007).
129. Hufnagel, A., Dümpelmann, M., Zentner, J., Schijns, O. & Elger, C. E. Clinical relevance of quantified intracranial interictal spike activity in presurgical evaluation of epilepsy. *Epilepsia* **41**, 467–478 (2000).
130. JASPER, H. H., ARFEL-CAPDEVILLE, G. & RASMUSSEN, T. Evaluation of EEG and cortical electrographic studies for prognosis of seizures following surgical excision of epileptogenic lesions. *Epilepsia* **2**, 130–7 (1961).

131. Alarcon, G. *et al.* Origin and propagation of interictal discharges in the acute electrocorticogram. Implications for pathophysiology and surgical treatment of temporal lobe epilepsy. *Brain* **120**, 2259–2282 (1997).
132. Azeem, A. *et al.* Interictal spike networks predict surgical outcome in patients with drug-resistant focal epilepsy. *Ann Clin Transl Neurol* **8**, 1212–1223 (2021).
133. Matarrese, M. A. G. *et al.* Spike propagation mapping reveals effective connectivity and predicts surgical outcome in epilepsy. *Brain* (2023) doi:10.1093/brain/awad118.
134. Bartolini, E. *et al.* Abnormal response to photic stimulation in Juvenile Myoclonic Epilepsy: An EEG-fMRI study. *Epilepsia* **55**, 1038–1047 (2014).
135. Meletti, S., Vaudano, A. E., Tassi, L., Caruana, F. & Avanzini, P. Intracranial time-frequency correlates of seizure-related negative BOLD response in the sensory-motor network. *Clinical Neurophysiology* **126**, 847–849 (2015).
136. Ozelo, H. F. B. *et al.* Pattern changes of EEG oscillations and BOLD signals associated with temporal lobe epilepsy as revealed by a working memory task. *BMC Neurosci* **15**, 1–9 (2014).
137. Fahoum, F., Zelmann, R., Tyvaert, L., Dubeau, F. & Gotman, J. Epileptic Discharges Affect the Default Mode Network - fMRI and Intracerebral EEG Evidence. *PLoS One* **8**, (2013).
138. Fahoum, F., Lopes, R., Pittau, F., Dubeau, F. & Gotman, J. Widespread epileptic networks in focal epilepsies: EEG-fMRI study. *Epilepsia* **53**, 1618–1627 (2012).
139. McGill, M. L. *et al.* Default mode network abnormalities in idiopathic generalized epilepsy. *Epilepsy and Behavior* **23**, 353–359 (2012).
140. Danielson, N. B., Guo, J. N. & Blumenfeld, H. The default mode network and altered consciousness in epilepsy. *Behavioural Neurology* **24**, 55–65 (2011).
141. Laufs, H. *et al.* Temporal lobe interictal epileptic discharges affect cerebral activity in 'default mode' brain regions. *Hum Brain Mapp* **28**, 1023–1032 (2007).
142. Kobayashi, E., Bagshaw, A. P., Grova, C., Dubeau, F. & Gotman, J. Negative BOLD responses to epileptic spikes. *Hum Brain Mapp* **27**, 488–497 (2006).
143. Thornton, R. *et al.* EEG correlated functional MRI and postoperative outcome in focal epilepsy. *J Neurol Neurosurg Psychiatry* **81**, 922–927 (2010).
144. Kowalczyk, M. A. *et al.* Clinical benefit of presurgical EEG-fMRI in difficult-to-localize focal epilepsy: A single-institution retrospective review. *Epilepsia* **61**, 49–60 (2020).
145. Tehrani, N. *et al.* Localization of interictal discharge origin: A simultaneous intracranial electroencephalographic–functional magnetic resonance imaging study. *Epilepsia* **62**, 1105–1118 (2021).
146. Szaflarski, J. P. Not a Slam-Dunk: Assessing the Role of EEG/fMRI in the Presurgical Evaluation. *Epilepsy Curr* **22**, 100–102 (2022).
147. Grouiller, F. *et al.* With or without spikes: Localization of focal epileptic activity by simultaneous electroencephalography and functional magnetic resonance imaging. *Brain* **134**, 2867–2886 (2011).
148. Thornton, R. *et al.* Epileptic networks in focal cortical dysplasia revealed using electroencephalography-functional magnetic resonance imaging. *Ann Neurol* **70**, 822–837 (2011).
149. Koupparis, A. *et al.* Association of EEG-fMRI Responses and Outcome After Epilepsy Surgery. *Neurology* **97**, e1523–e1536 (2021).

150. Khoo, H. M. *et al.* The spike onset zone. *Neurology* **91**, e666 LP-e674 (2018).
151. Suarez, A. *et al.* Identification of Negative BOLD Responses in Epilepsy Using Windkessel Models. *Front Neurol* **12**, (2021).
152. Jacobs, J. *et al.* Negative BOLD in default-mode structures measured with EEG-MREG is larger in temporal than extra-temporal epileptic spikes. *Front Neurosci* **8**, 1–12 (2014).
153. Watanabe, S., Dubeau, F., Zazubovits, N. & Gotman, J. Temporal lobe spikes: EEG-fMRI contributions to the "mesial vs. lateral" debate. *Clinical Neurophysiology* **128**, 986–991 (2017).
154. An, D. *et al.* Electroencephalography/functional magnetic resonance imaging responses help predict surgical outcome in focal epilepsy. *Epilepsia* **54**, 2184–2194 (2013).
155. Bénar, C. G. *et al.* EEG-fMRI of epileptic spikes: Concordance with EEG source localization and intracranial EEG. *Neuroimage* **30**, 1161–1170 (2006).
156. Kobayashi, E. *et al.* Temporal and extratemporal BOLD responses to temporal lobe interictal spikes. *Epilepsia* **47**, 343–354 (2006).
157. Moeller, F. *et al.* EEG-fMRI: Adding to standard evaluations of patients with nonlesional frontal lobe epilepsy. *Neurology* **73**, 2023–2030 (2009).
158. Bagshaw, A. P. *et al.* EEG-fMRI of focal epileptic spikes: Analysis with multiple haemodynamic functions and comparison with gadolinium-enhanced MR angiograms. *Hum Brain Mapp* **22**, 179–192 (2004).
159. Bagshaw, A. P. *et al.* Analysis of the EEG-fMRI response to prolonged bursts of interictal epileptiform activity. *Neuroimage* **24**, 1099–1112 (2005).
160. Laufs, H., Lengler, U., Hamandi, K., Kleinschmidt, A. & Krakow, K. Linking generalized spike-and-wave discharges and resting state brain activity by using EEG/fMRI in a patient with absence seizures. *Epilepsia* **47**, 444–448 (2006).
161. Magiorkinis, E., Sidiropoulou, K. & Diamantis, A. Hallmarks in the history of epilepsy: Epilepsy in antiquity. *Epilepsy and Behavior* **17**, 103–108 (2010).
162. Parvizi, J. & Kastner, S. Promises and limitations of human intracranial electroencephalography. *Nat Neurosci* **21**, 474–483 (2018).
163. Teplan, M. FUNDAMENTALS OF EEG MEASUREMENT. *MEASUREMENT SCIENCE REVIEW,* **2**, 1–11 (2002).
164. de Cheveigné, A. & Nelken, I. Filters: When, Why, and How (Not) to Use Them. *Neuron* **102**, 280–293 (2019).
165. Zhang, S. ARTIFACTS DENOISING OF EEG ACQUIRED DURING SIMULTANEOUS EEG-FMRI. (University of Freiburg, 2019).
166. Da Costa, J. P. C. L. *et al.* Multidimensional prewhitening for enhanced signal reconstruction and parameter estimation in colored noise with Kronecker correlation structure. *Signal Processing* **93**, 3209–3226 (2013).
167. Shen, X. J. *et al.* A generalized least-squares approach regularized with graph embedding for dimensionality reduction. *Pattern Recognit* **98**, (2020).
168. Jayakar, P. *et al.* Diagnostic utility of invasive EEG for epilepsy surgery: Indications, modalities, and techniques. *Epilepsia* **57**, 1735–1747 (2016).
169. Arteaga, D. F. *et al.* The vascular steal phenomenon is an incomplete contributor to negative cerebrovascular reactivity in patients with symptomatic intracranial stenosis. *Journal of Cerebral Blood Flow and Metabolism* **34**, 1453–1462 (2014).

170. Woolrich, M. W. *et al.* Bayesian analysis of neuroimaging data in FSL. *Neuroimage* **45**, S173–S186 (2009).
171. Smith, S. M. *et al.* Advances in functional and structural MR image analysis and implementation as FSL. *Neuroimage* **23**, 208–219 (2004).
172. Jenkinson, M., Beckmann, C. F., Behrens, T. E. J., Woolrich, M. W. & Smith, S. M. FSL. *Neuroimage* **62**, 782–790 (2012).
173. Beckmann, C. F. & Smith, S. M. Probabilistic Independent Component Analysis for Functional Magnetic Resonance Imaging. *IEEE Trans Med Imaging* **23**, 137–152 (2004).
174. Griffanti, L. *et al.* Hand classification of fMRI ICA noise components. *Neuroimage* **154**, 188–205 (2017).
175. Woolrich, M. W., Ripley, B. D., Brady, M. & Smith, S. M. Temporal autocorrelation in univariate linear modeling of FMRI data. *Neuroimage* **14**, 1370–1386 (2001).
176. Beckmann, C. F., Jenkinson, M. & Smith, S. M. General multilevel linear modeling for group analysis in FMRI. *Neuroimage* **20**, 1052–1063 (2003).
177. An, D. *et al.* Electroencephalography/functional magnetic resonance imaging responses help predict surgical outcome in focal epilepsy. *Epilepsia* **54**, 2184–2194 (2013).
178. Saad, Z. S., Ropella, K. M., Cox, R. W. & DeYoe, E. A. Analysis and use of fMRI response delays. *Hum Brain Mapp* **13**, 74–93 (2001).
179. Pittau, F., Fahoum, F., Zelmann, R., Dubeau, F. & Gotman, J. Negative BOLD response to interictal epileptic discharges in focal epilepsy. *Brain Topogr* **26**, 627–640 (2013).
180. Sultana, B. *et al.* Incidence and Prevalence of Drug-Resistant Epilepsy: A Systematic Review and Meta-analysis. *Neurology* **96**, 805–817 (2021).
181. Bragin, A., Wilson, C. L., Almajano, J., Mody, I. & Engel, J. High-frequency oscillations after status epilepticus: Epileptogenesis and seizure genesis. *Epilepsia* **45**, 1017–1023 (2004).
182. Kerber, K. *et al.* Differentiation of specific ripple patterns helps to identify epileptogenic areas for surgical procedures. *Clinical Neurophysiology* **125**, 1339–1345 (2014).
183. Alves, P. N. *et al.* An improved neuroanatomical model of the default-mode network reconciles previous neuroimaging and neuropathological findings. *Commun Biol* **2**, 1–14 (2019).
184. Boucousis, S. M. *et al.* Feasibility of an intracranial EEG-fMRI protocol at 3T: Risk assessment and image quality. *Neuroimage* **63**, 1237–1248 (2012).